# Power flow optimization of a renewable energy production hub

---

*Author:*
Frederic Linde

*Supervisors:*
Dr. ir. Ronald Aarts
Dr. Thiago Batista Soeiro
Dr. ir. Jose Rueda Torres
Dr. Alessio Trivella

A report submitted in fulfilment
of the requirements for the degree of
Master of Engineering

Specialization of Robotics & Mechatronics
Program of Systems & Control
Faculty of Electrical Engineering Mathematics and Computer Science

University of Twente

University of Delft

Enschede, Netherlands

August 2024

Author:
Frederic Linde

Supervisors:
Dr. ir. Ronald Aarts[1]
Dr. Thiago Batista Soeiro[1]
Dr. ir. Jose Rueda Torres[2]
Dr. Alessio Trivella[1]

Institute:
University of Twente, Overijssel, Netherlands[1]
University of Delft, Zuidholland, Netherlands[2]

# CONTENTS

# LIST OF FIGURES

# ABSTRACT

A rapidly changing energy landscape gives rise to new means of energy generation. Wind turbines are gaining traction as a cost-efficient renewable energy source (RES). They present opportunities and challenges alike.

Naturally, a RES like wind power is uncontrollable. For large-scale utilization, energy delivery from such a source must be reliable. Large variations in production must be reshaped to fit an uncertain, dynamic demand.

The replacement of traditional means of energy generation by inverter-based technology is accompanied by dwindling grid inertia. Its deployment has the potential to increase grid stability. Key is the utilization of grid-forming inverters (GFMIs) that can actively stabilize the voltage and frequency on the grid. It can be combined with a control strategy like droop control, relating the grid stabilizing variables to the power flow.

This thesis combines a GFMI with droop control and an advanced control strategy to manage the power flow inside an energy hub. The goal is a stable power supply from an uncontrolled source. Proposed is a novel concept, combining the design of an energy production hub with a 3-stage hierarchical model predictive control (MPC) scheme. The hub's novelty is an integrated energy storage system (ESS), comprising an $H_2$ cycle, a battery unit, and a supercapacitor (SC). The control scheme complements the hub by leveraging forecasts to anticipate production-demand mismatch. It minimizes the mismatch by devising power and state of charge (SOC) setpoints, regulating the storage elements.

Detailed exploration focuses on the middle layer, the steady-state target optimization (SSTO) layer. It forms the link between the other two layers, aiming to diminish the mismatch between the plant and its model. Functionally, it manages the power flow between the turbine, ESS, and the grid via the inverter and a coupling reactance.

Contributed is a mathematical model of the SSTO layer with a quadratic objective function. Herein, equations describing the coupling reactance and droop control are reformulated into constraints. It is investigated whether their addition improves the setpoint synthetization in the SSTO layer.

Conducting a simulation study, an optimization and a plant model are set up. After formulating the optimization model, it is implemented on the plant model to determine how the plant's dynamics are affected.

The simulation shows that the RES power setpoint can be altered by considering the coupling reactance dynamics in the SSTO layer. Power flow changes due to frequency deviations can be adjusted with the droop control gain. With it, the MPC can fulfill grid-forming functions.

The results are significant because the power flow on the RES side provides power to the inverter. The flow changes in response to varying demands in active and reactive power and to fluctuations in voltage and frequency.

# STATEMENT OF AUTHORSHIP

I, Frederic Linde, born September 24, 1998 in Cologne, declare that this thesis titled *Power flow optimization of a renewable energy production hub* and the work presented in it are my own. I confirm that this work was done mainly while in candidature for a research degree at Twente University.

Except where reference is made in the text of the thesis, this thesis contains no material published elsewhere or extracted in whole or in part from a thesis accepted for the award of any other degree or diploma. No other person's work has been used without due acknowledgment in the main text of the thesis. This thesis has not been submitted for the award of any degree or diploma in any other tertiary institution.

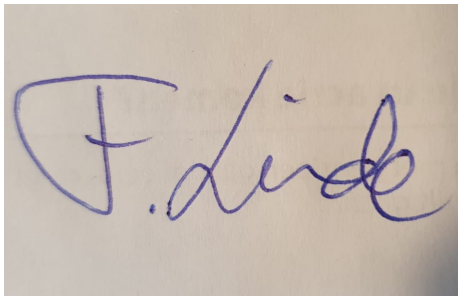

Frederic Linde August 22, 2024

# ACRONYMS

| | |
|---|---|
| **BESS** | Battery Energy Storage System |
| **DIBt** | Deutsches Institut Für Bautechnik |
| **DO** | Dynamic Optimization |
| **ECM** | Equivalent Circuit Model |
| **ESS** | Energy Storage System |
| **GFMI** | Grid-forming Inverter |
| **GNO** | Global Nonlinear Optimization |
| **KKT** | Karush-Kuhn-Tucker |
| **LPF** | Low-pass Filter |
| **MILP** | Mixed-integer Linear Programming |
| **MIMO** | Multiple-input-multiple-output |
| **MOST** | Matpower Optimal Scheduling Tool |
| **MPC** | Model Predictive Control |
| **NCO** | Necessary Condition Of Optimality |
| **OCV** | Open Circuit Voltage |
| **PCC** | Point Of Common Coupling |
| **QP** | Quadratic Programming |
| **RES** | Renewable Energy Sources |
| **RR** | Ramp-rate |
| **SC** | Supercapacitor |
| **SOC** | State Of Charge |
| **SSTO** | Steady-state Target Optimization |
| **TSO** | Transmission System Operator |

# 1 INTRODUCTION

The transition to sustainable energy sources demands fundamental change to the topology of our energy grid. Renewable energy sources are deployed on various scales and their production is decentralized. As their output cannot be planned, vast increases in production uncertainty can be observed.

## 1.1 BACKGROUND

Europe's electricity grid is unsuitable for future energy demand. Two major factors contribute to this circumstance. Firstly, almost half the grid is over 40 years old and cannot keep up with the ever-increasing demand. Secondly, the current grid topology is laid out for large-scale centralized production from fossil fuel sources, like coal and gas plants. They can be placed arbitrarily, allowing planned placement close to consumer centers and controlled energy production. [1, 2]

With their retirement, the general electricity grid is burdened with the challenges arising from the green energy transition. New connections of renewable energy sources (RESs) and long-range energy transmission drive the grid to its capacity limits, leading to local congestion. Large production peaks have the potential to overload transmission lines. Unregulated supply-demand mismatch can cause undesired power fluctuations that are detrimental to grid stability. They compromise equipment and possibly incite power outages. As a result of these issues, some already installed RESs cannot be connected to the grid. [3, 4]

## 1.2 PROBLEM STATEMENT

Today, the energy sector is approaching a turning point. The deployment of advanced control strategies has the potential to not only resolve issues but also overhaul traditional grid stabilizing measures. Their success heavily relies on providing reliable output from uncertain energy sources. However, their introduction brings its own set of challenges.

FORECAST As large uncertainty is associated with forecasting events, energy planning becomes less calculable. Yet, to better match supply and demand, it is desirable to make operational decisions based on statistically likely events. These future events are approxi-

mated through estimation. Commonly, computationally costly approximation techniques are employed to perform this task.

STABILITY Control implementations in physical applications must operate in real-time. They are required to make rapid adjustments to stabilize parameters like the grid's frequency. To compensate for disturbances and guarantee stable grid operation, such control signals must be calculated on the sub-second time scale. As computation time scales with computational complexity, costly estimation of future events is a severe limitation in the application of grid-tied RESs.

SYSTEM STATES Generally, this type of automated control utilizes measurements and estimations of the RES hub's variables and projects them into the future. The goal is to determine what control signals must be sent to steer the hub toward a desirable state. In other words, what action must be taken to, for example, sensibly change the power output from the hub to the grid while keeping the frequency stable?

To ensure safety, the hub or plant must be operated under consideration of various constraints. This could be a maximum power output according to component specifications. They can be implemented by constraining the plant's actions and states. Usually, the control unit is tasked with enforcing such limitations.

FEASIBILITY However, with uncertainty present, like in forecasting, maintaining limits becomes a non-trivial task. If the true value of a parameter is unknown, its estimation might differ from the one in the application. Situations occur where the true plant parameter runs into a physical limitation that does not correlate with the limitations implemented in the controller. Consequentially, a calculated control signal cannot be correctly executed on the physical application. Large discrepancies between the modeled and physical plant raise questions of feasibility.

Many more factors complicate the control signal calculation. Unforeseen changes in wind speed can affect estimations, and measurement noise can introduce parametric uncertainty.

## 1.3 RELEVANCE

In light of the present challenges associated with the green energy transition, major shifts in the energy landscape underline the necessity for innovative control structures. The deployment of advanced control strategies can be a cost-effective way to tackle the issues related to grid congestion, foregoing the need to renew infrastructure. With their introduction, it is possible to improve grid stability and further scale the penetration of RESs on the energy grid.

A term frequently used in this context is operational flexibility. High operational flexibility is the ability to appropriately match supply and demand in an uncertain environment.

Because energy production cannot be controlled, it is another important factor in providing reliable energy output.

Flexibility on the grid can be increased in several ways. Complementing control, some means are diversified energy production, improved forecasting techniques, and utilization of energy storage systems (ESS).

## 1.4 RESEARCH OBJECTIVE

This project focuses on the design of an ESS-integrated grid-tied RES hub, promoting its implementation at scale. The design of an RES energy hub should directly address the associated grid stability and flexibility issues. The introduction of advanced control strategies should be congruent with the hub design and further contribute to the successful deployment of RESs in light of the energy transition.

It will be investigated whether the introduction of an optimization-based control strategy can address these issues. It appears suitable because such control can incorporate forecast events.

CONTRIBUTIONS Contributed is a design that combines multiple energy storage elements with a wind turbine and grid-inverter into a comprehensive hub concept.

As a second contribution, this project proposes an overview of a novel 3-stage hierarchical MPC structure. The focus lies on incorporating active droop control into the problem formulation of the optimization algorithm. It is believed that this design addresses grid stability issues and will aid in increasing the grid's operational flexibility.

Subject to a simulation study, the developed controller is integrated into the designed energy hub. The controller should be able to reliably control the power flow of the RES hub, adhere to components' specified limits, and actively contribute to stabilizing the energy grid.

## 1.5 RESEARCH QUESTION

How can the design of an optimization-based control strategy be integrated with a decentralized RES hub to improve the power management and flow to the electricity grid without compromising its stability?

## 1.6 APPROACH

This project is set up to explore a new hierarchical MPC concept. The inductive approach aims to integrate the explored literature into a new, comprehensive structure. It combines elements from the theoretical research on MPC with practical implementations in the energy sector. Thus, the focus of the qualitative approach lies in the conceptual exploration of these structures in a new context. The goal is to provide proof of the concept by conducting a simulation study.

## 1.7 THESIS OUTLINE

The general goal of this project can be broken down into several parts. They were structured into according chapters:

**Chapter 2** provides insight into the challenges associated with the introduction of RES as an inverter-based technology. Explored are grid stability issues associated with the introduction of RESs and optimization-based control. It describes the theory necessary to frame these issues and proposes the hierarchical MPC as a suitable control strategy in the context of the explored challenges.

**Chapter 3** presents the conceptualization of a comprehensive design, comprising an energy hub with integrated energy storage and control strategy. As the control element, the MPC control strategy is developed to address the explored issues and complement the energy hub design.

**Chapter 4** sets up a computational model that captures mathematical descriptions of the plant's components. It entails the formulation of an optimization problem to improve the power flow in uncertain scenarios. Energy grid control elements are incorporated into this formulation.

**Chapter 5** translates the mathematical equations into a simulation model. This chapter details how the modeled plant and controller are implemented into a simulation. It describes what models are used to solve the optimization problem in a simulated environment.

**Chapters 6 and 7** show the simulation results and discuss the findings in the context of the thesis and their implications for the industry. They conclude upon the work and provide recommendations for further research.

# 2

# LITERATURE REVIEW

This chapter comprises five sections. Section 2.1 explores how increasing penetration of renewable energy sources reshapes the energy grid's landscape. Therein, stability concerns mediate a swing toward the smart grid.

Section 2.2 introduces the smart grid and clarifies its relevance for the changing energy infrastructure, exemplified by the struggles in the Dutch energy transition.

LITERATURE The next three sections describe three literature streams. They are depicted in Fig. 2.1.

Section 2.3 describes the theoretical fundament necessary to be able to parameterize the energy grid issues. General energy grid control concepts are introduced that allow stabilization of the grid with inverter-based technology.

The second literature stream (sec. 2.4) describes mitigation strategies to overcome challenges with uncertain energy production. First, forecasting techniques are explored to predict changes in energy production and demand. To leverage their potential, the energy storage system (ESS) is introduced. Here, it will be clarified how the MPC mitigates uncertainty, lending itself as a suitable control concept for the application of the energy hub.

The third literature steam describes a 3-stage MPC concept from a control theoretical perspective. This element highlights the issues associated with this type of control strategy.

The steams of Fig. 2.1 will be revisited and developed into a flowchart at the start of each chapter. They aim to point out the contributions of this thesis, converging the independent challenges of the energy grid control, production uncertainty, and MPC into a single comprehensive concept.

LIMITATION The observer (Fig. 2.1) is marked with dashed lines. It is briefly introduced in the literature review as a necessary component of the concept. However, to limit the scope of the work, it was not considered further.

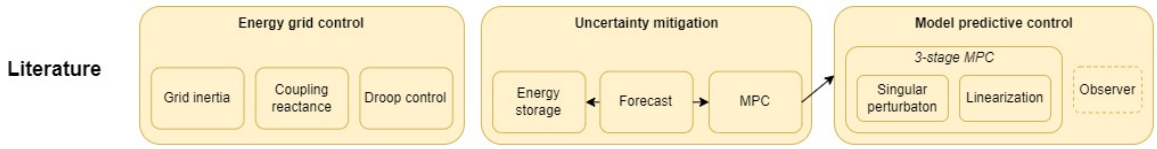


Figure 2.1: Literature review topics. Indicated in yellow are the topics that have been composed as a literature study.

## 2.1 THE GREEN ENERGY TRANSITION

Employing renewable energy resources commands change in the approach to energy production and distribution. It is necessary to relocate production to economically beneficial areas, which are, unfortunately, rarely adjacent to consumer centers. Furthermore, it is impossible to directly exert control over these resources. Their nature thus introduces a large production uncertainty. Now, production sites must be chosen with careful consideration of the local weather conditions. The Forschungszentrum Jülich ([5]) in Germany have identified three key challenges associated with the green energy transition:

PRODUCTION UNCERTAINTY This challenge refers to the very nature of renewable energy production. It is impossible to control the weather. As a result, the electricity grid experiences large power fluctuations. Sometimes the wind just will not blow and energy production cannot meet the demand. At other times, strong winds will peak production while demand is low. Both cases, if left unaddressed, will have detrimental effects on the grid, possibly damaging electrical equipment and causing power outages with extremely costly consequences. [5, 6]

ENERGY TRANSMISSION It is described by the long-range energy transmission. Bridging the gap between production and consumption centers begs potential grid congestion issues and large losses. Further factors like energy trading and cross-border energy transmission must be considered. It implies fundamental changes to the European power market and the associated energy pricing. [7]

DECENTRALIZATION Issues arise from decentralized energy production. Due to an increase in small-scale production units, e.g. on home rooftops and in smaller communities, the power flow becomes bidirectional. With centralized production, unidirectional power sufficed to distribute electricity to consumers. After the introduction of the prosumer, unifying the producer and consumer, former end users must be able to feed produced electricity into the grid. Their appearance vastly increases the number of grid-feeding voltage sources. An uncontrolled connection to the grid has the potential to cause significant current flows between sources. [6, 8, 9]

Compounding this conundrum is the fact that European energy demand is projected to rise by over 20% until 2030. [7] Further, predicted wind and solar energy production is estimated to provide 50% of the global energy demand by 2050. [10] For a successful green energy transition, significant technological advancements must be made to facilitate the integration of renewable energy resources into the energy infrastructure. One such technological advancement is the introduction of smart grids. [6]

## 2.2 THE SMART GRID

Smart grids are intelligent power systems that automatically regulate and optimize power flow. The focus herein lies on the automated control of production and demand in smaller, localized grids. Its nature aims at utilizing production diversification through the introduction of the prosumer and other renewable energy sources (RES). One important feature is the ability to operate a smart grid isolated from the main grid, so-called islanded mode. Local power management is believed to address transmission issues by reducing grid congestion. The smart grid's success hinges on a few key implementations. They comprise an advanced metering infrastructure, improved stability, and flexibility. It will be discussed how the latter two address the issues raised pertaining to the green energy transition.

### 2.2.1 *Grid stability*

Due to production decentralization and increased production uncertainty, grid stability is a major concern. The introduction of RES as well as the retirement of traditional means of energy production greatly affect grid stability. Thus, next to the efficient use of energy, this issue has received increasing attention. With a less robust grid, power fluctuations can be troublesome. Its effects on voltage stability may result in reverse power flow, damaging costly equipment. Thus, to protect these components and ensure proper operation, it is crucially important to maintain grid stability. [11, 12]

Section A.1.1 in the appendix will explore this issue further, describing the challenges of maintaining the grid's nominal frequency. Issues and opportunities that arise from renewable energy production are discussed in the following.

SYNTHETIC FREQUENCY GENERATION Most renewable energy is directly converted to electricity and fed into the grid with transformers. The transformers will synthesize the desired frequency to allow synchronization with the grid. The problem is that this method does not provide inertia to the grid as no synchronous generator buffers load changes. Thus these non-synchronous generators don't have any primary frequency response mechanisms. On a purely synthetically synchronized grid, large load changes could have detrimental effects on the grid's stability. [13, 14]

GRID-AWARE TECHNOLOGY Fortunately, modern inverter-based technology enables a "fast frequency response". It has a much faster response rate compared to the traditional primary frequency response, its nature is able to reduce the need for large grid inertia. The absence of the inertia allows the inverter to arbitrarily change the frequency. Active control mechanisms are necessary to participate in grid voltage and frequency stabilization, reducing the impact of power flickers due to changes in production and consumption. Such control is associated with so-called grid-forming inverter (GFMI). Their introduction is key in the green energy transition as they are able to replace the traditional frequency reference that the slack bus sets. Retiring its functionality allows the operation of smart grids on a

smaller scale. The GFMI can actively regulate the voltage and frequency on a localized grid. [15, 16]

### 2.2.2 *Grid flexibility*

Another important consideration for the grid operator is the increase in operational flexibility. Put plainly, power system flexibility means the ability to modify production and demand to be able to use the grid to its maximum potential. Increasing grid flexibility can be achieved in many ways. Katz *et al.* ([13]) touches upon a wide range of possibilities to steer demand and consumption. The demand side will not be described here as it is beyond the scope of this project. Contrarily, increasing operational grid flexibility from the production side is one of the goals of this assignment.

The Rijksoverheid relies on expanding the offshore power generation. They install large-scale wind turbines, aiming to generate 75% of all their electricity from a single source. Such a decision results in a dramatically low production diversification with potentially drastic consequences for the Dutch energy mix. [17] These issues are explored in detail in appendix A.1.2.

### 2.2.3 *Summary*

The green energy transition necessitates significant adaptions of the power grid. Therein, three key challenges have been identified. They can be summarized as the transition to uncertain energy production from diverse sources in remote locations. Particular to the Netherlands is the dire need to increase grid stability and flexibility. Due to its small size and relative geographic homogeneity, large-scale wind energy production has the caveat of low production diversification.

The appearance of smart grids tackles these issues by managing the power flow of uncontrolled energy sources. The transition to inverter-based energy grids is a challenge and an opportunity. The introduction of GFMIs has the potential to increase the stability and flexibility of the grid. It seems a crucial component in the transition to renewable energy generation. For their success, a sensor network, an understanding of the grid dynamics, and sensible control algorithms are required.

## 2.3 ENERGY GRID CONTROL

Most generally in AC networks, the requirement to contribute to the ancillary services consists of the delivery of active power (P) and reactive power (Q). Respectively, they compose the real and imaginary components of the apparent power (S). These grid variables and their interaction is discussed in appendix A.1.4.

### 2.3.1 *Grid-forming inverters*

Historically, inverter-based energy sources were designed to be load-following. They depend on another utility to regulate the grid's voltage and frequency. Some regard them as negative loads rather than sources as they solely provide real and reactive power. Incidentally, sudden changes in the grid loading result in voltage and frequency fluctuations. [3] Thus, to reliably provide energy, it is necessary to assert control over these grid parameters as well. Therefore, a GFMI aims to contribute to stabilizing the grid by locally altering the voltage and frequency of the grid. [9, 18]

The following paragraphs aim to provide insight into how the active and reactive power P and Q respectively, the grid voltage V, and grid frequency f are related to each other.

GRID INERTIA The fundamental equation of the grid frequency in the AC power system is given as

$$\frac{df}{dt} = \frac{P_{supply} - P_{demand}}{2H} \tag{2.1}$$

where H is the total system inertia. This inertia represents the system's rotating mass able to resist changes in frequency. Here, one can easily grasp the effect losses in rotating mass have on frequency fluctuations. As H tends to zero df/dt becomes infinite. Similarly, a supply-demand mismatch changes the grid frequency. It depends on the active power component and implicitly the voltage differential between the two voltage points. [16, 19]

GRID-TIED INVERTER Such issues are addressed by grid-tied inverters that form 3-phase HVAC power. Their design is extremely intricate as they must respond to sudden frequency changes, and generate high-quality power by minimizing harmonic distortion. Some recent advancements can be found in Xu *et al.* ([20, 21]), aiming to employ modern control techniques to achieve this goal. As the scope of this project is set on the system integration and control thereof, this component is much simplified. The challenge in here mainly lies in how changes in the energy grid can be compensated for by the control on the RES side.

RES VOLTAGE It appears that a stable DC link voltage (outer voltage loop) is crucial for inverter stability. [22] Frequency fluctuations have the potential to cause instability in the control loops, decreasing conversion efficiency. [23] Therefore, in inverter control, many assume a constant DC voltage supply, sometimes modulated with small ripples. [24] Meeting such requirements is quite challenging in the context of RES control because wind turbines inherently have poor grid stabilizing abilities. With a direct grid connection, the turbine output is strongly coupled to the grid dynamics. Due to the turbine's changing production levels, a weak grid (one with low inertia) can experience significant voltage oscillations, and steeply decaying system stability. [25]

Therefore, strong DC voltage control on the RES side is essential. To aid control, a number of things can be done. Firstly, it appears that leveraging predictions of reactive power

and voltage on the grid side could be useful in preempting changes and stabilizing the DC voltage on the RES side. Furthermore, it is highly desirable to decouple the wind energy production from the grid dynamics, limiting its influence on the stability of the grid. Next to the introduction of the ESS, a coupling reactance at the PCC has the potential to decouple the dynamics and ease control.

*Reactive power control*

Shifting the focus to the grid dynamics, not only the frequency fluctuations due to changes in active power are an issue, but also the voltage flickers due to reactive power flow. In the following, these interactions and their consequences are explored. [16]

REACTIVE CURRENT FLOW Reactive loads reflect power back into the grid which can be observed as reactive current. This circulating current is unable to perform work and strains the grid, contributing to transmission congestion. [3, 11]

In general, it is desirable to build transmission lines with low internal resistance to minimize power losses. Furthermore, voltage setpoints on different points of the grid change depending on the load. Consequentially, small voltage differentials can cause significant current flow and potential reverse power flow, affecting the operation of critical grid components. [12]

To prevent such undesirable interaction, sources must be carefully managed to ensure safe and reliable grid operation using inverter-based technology. To address this issue, control of reactive power flow and local voltage setpoints is crucial. This element adds to the active power control required of a GFMI. To facilitate the management of the grid, a coupling reactance is introduced between the inverter output and the PCC. [9, 18]

COUPLING REACTANCE Control of these four grid variables can be much facilitated by decoupling the interaction between the active and reactive power flow. This can be achieved by introducing a coupling reactance (Fig. 2.2). It also introduces a local voltage setpoint E which is separate from the grid voltage. This element is crucial in controlling the reactive current flow. [26]

Using the notation of Fig. 2.2, the active and reactive power flow can be captured by equation 2.2 [9].

$$\begin{aligned} P &= \frac{EV}{X_L} sin(\delta_P) \\ Q &= \frac{E(E-V)}{X_L} cos(\delta_P) \end{aligned} \tag{2.2}$$

where $\delta_P = \delta_E - \delta_V$ defines the power angle between the inverter and grid voltages and $X_L = 2\pi * f * L$ is the coupling inductance value. From these equations, it is possible to understand how the voltage and phase angle at the inverter output can be utilized to control the active and reactive power flow. Adding complexity to the control is the coupled interaction between these variables. As the power angle is a control variable, it is possible

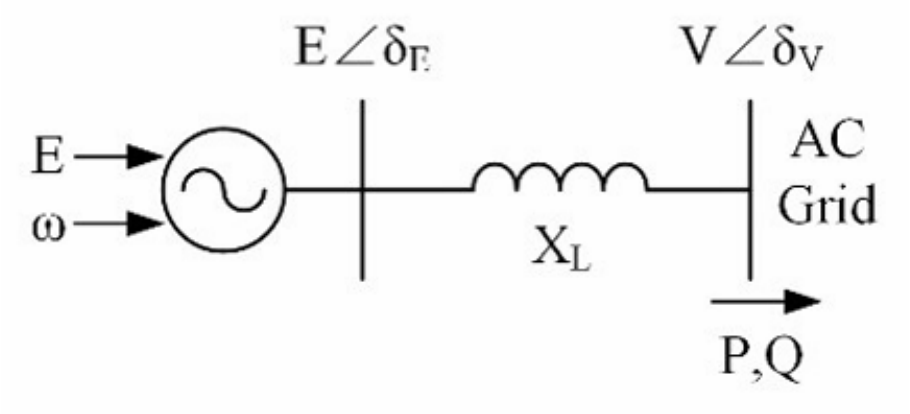


Figure 2.2: RES modeled as a voltage source, connected to the grid via a coupling reactance. The inverter output comprises voltage setpoint E at phase angle $\delta_E$ and the grid voltage V at phase angle $\delta_V$. $X_L$ is the coupling reactance. [9]

to limit its operational range. Properly sizing the coupling reactance can facilitate such limitation and enable the application of the small angle theory. [9, 27]

SMALL ANGLE THEORY Decoupling P and Q is achieved through linearization by way of the small angle approximation. As can be seen from figure 2.3, a power angle of $d_{P,max} = 30°$ allows operation in a quasi-linear region where the maximum angle provides an error of 4%. As a result, it is possible to approximate the power angle as $sin(\delta_P) \approx \delta_P$ and $cos(\delta_P) \approx 1$. Applying the theory to eq. 2.2 yields:

$$\begin{aligned} P &= \frac{EV}{X_L}\delta_P \\ Q &= \frac{E(E-V)}{X_L} \end{aligned} \tag{2.3}$$

*Decoupled power control*

With the linearized coupling reactance equations, the active power injection can be controlled with the power angle. The reactive power flow is controlled by setting the inverter voltage setpoint E relative to the grid voltage V. If $E > V$ the reactive power flow is positive, inductive reactive power can be compensated. The complementary is $E < V$ where the injected reactive power becomes negative. However, if only E is altered, the active and reactive power would change.

*Droop control*

Next to the local grid control, the concept of droop is crucial as its control allows RES to be introduced as GFMI on the grid. The reason is that droop control modifies the active

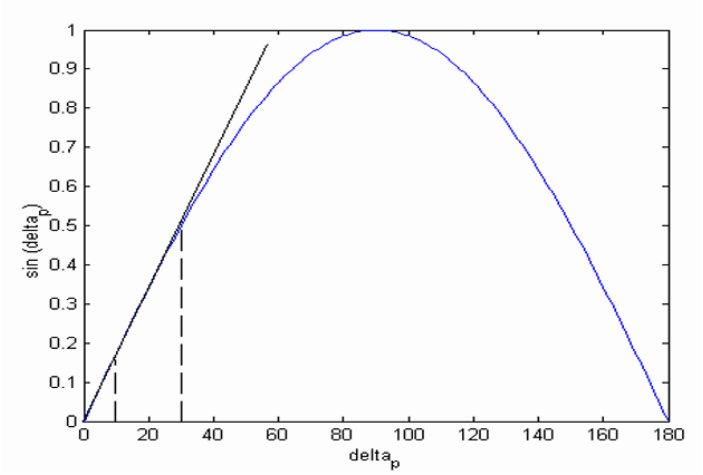


Figure 2.3: Linear approximation (black) of the power angle between the inverter voltage E and grid voltage V (blue). [27]

power setpoint based on frequency changes and the voltage setpoint based on reactive power flow.

The realization of the decoupling can best be explained with figure 2.4. Here, a change in reactive power flow is mediated through an adaption in the inverter voltage setpoint from E to E'. Now, by changing the power angle proportionally to the voltage magnitude, it is possible to keep the active power constant. Thus, the linearization enables decoupled active and reactive power control by altering the voltage magnitude and angle of the inverter output. [9, 26]

This concept is essential for connecting GFMIs to the general grid. It can be attributed to the careful management of active and reactive power flow as well as active stabilization of grid voltage and frequency. It enables the introduction of RES at scale, addressing the grid inertia loss issue through fast frequency response mechanisms. Adding this synchronicity element, droop control allows seamless integration with the grid. Further, droop control allows for greater redundancy and flexibility, contributing to overall grid resilience. Importantly, they can be implemented into an existing grid without any centralized control or exchange of information. [9, 28]

### 2.3.2 *Parameter prediction*

In the traditional power grid, the swing equation was used to predict frequency changes. With information on the rotational speed of the synchronous generator, electrical power output, and its inertia, frequency values could be obtained. [29]

With inverter-based technology and the introduction of virtual inertia, it is not straightforward to use the swing equation. The lack of physical inertia and the nonlinear nature of inverter control algorithms put its use in question. However, it is still highly desirable to be able to anticipate changes in grid frequency. Incorporating power prediction values into control algorithms could be a candidate solution. Before delving into the control, the role of forecasting is explored, and how it can support and stabilize the grid.

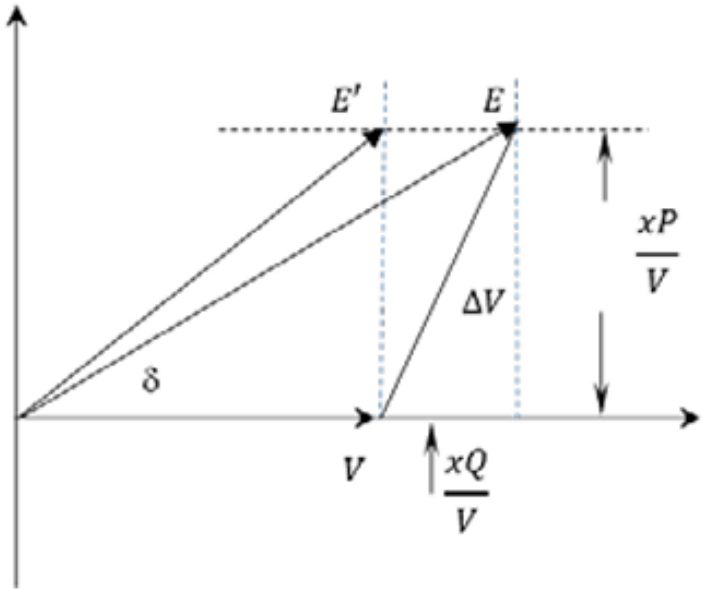


Figure 2.4: Change of inverter voltage setpoint from E to E′. The power angle changes while the active power setpoint stays constant. [9]

## 2.4 UNCERTAINTY MITIGATION

### 2.4.1 *Forecasting*

With the emergence of inverter-based energy generation, reliance on production and demand forecasting has much increased. Because accurate predictions decrease uncertainty, the ability to make system adjustments based on predicted energy generation and consumption is crucial. Making decisions based on likely future scenarios can improve both the stability and flexibility of the grid. [3, 13]

Variations in production and demand could best be compensated for if they were known in advance. Unfortunately, the future is always uncertain. Therefore, the next best approach is to rely on stochastic and statistical prediction techniques.

*Production forecast*

From a control perspective, a number of techniques are commonly employed. Regarding weather forecasts, they can be categorized into two classes, namely physical forecast, and persistence. [30, 31]

PHYSICAL FORECAST This method makes use of location-specific data to forecast weather parameters. Historic weather data is processed to anticipate trends and seasonal changes. In the context of wind energy production, it is especially important as the production varies significantly throughout the year. Climatological wind speed data shows seasonal as well as daily trends. Similar to the US (Fig. 2.5b), wind energy production in

the North Sea changes according to the sun and rises with larger air temperature differences. [1, 3]

Large weather variations ranging from seconds to months underline the importance of good forecasting. Local variations in wind speed have been observed to result in fluctuating wind turbine power generation levels (Fig. 2.5a). [3, 32] Kay *et al.* ([33]) have investigated wind droughts (doldrums) in the North Sea. They found that each winter has a more than 60% chance of experiencing wind droughts of one continuous week or more. The accuracy of production prediction can be further increased when including day-ahead forecasts as well as local sensor data. The former is commonly based on meteorological data. The latter, while not technically a forecast, could utilize data transmitted from nearby sensors. [30]

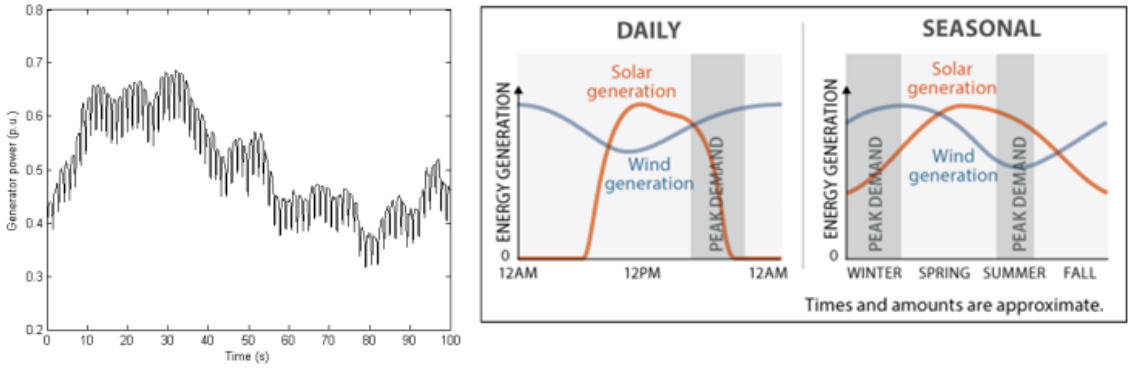


(a) Active power fluctuations of a 2MW wind turbine. [32]

(b) Daily and seasonal variations in wind energy production in California. [3]

Figure 2.5: Visualization of weather variations from short- to long-term.

*Demand forecast*

Similar to the production, demand can also be forecast. Historical data can provide insight into active and reactive power consumption. Next to that, information from local sensor data is particularly important. They enable the algorithm to take reactive control measures.

In more sophisticated approaches, dynamic energy pricing is considered. Such forecasting scenarios introduce further uncertainty factors. This issue is only explored very superficially as economic aspects of the energy market are beyond the scope of this project.

### 2.4.2 *Energy storage*

If production outmatches demand, energy is produced in excess. If the power is fed into the grid, it can cause congestion and instability. Due to the nature of RES, this scenario cannot be controlled. Alternatively, the energy can be let go to waste. Both cases are undesirable. [4]

Energy storage can help buffer production peaks. They store energy during excess production and release it when demand outpaces production. Both cases are important and

must be accounted for economic and stability. The low production diversity in the Netherlands. If predictions were perfect, it would be possible to balance the grid and optimally manage energy storage. Reserves can be shrunk as their utilization is performed with full certainty. Despite inaccuracies in the real world, storage sizing and management as well as grid stability strongly depend on accurate forecasting. [15]

The ESS as a capacitive element can decouple the power production from the energy grid. Herein, it is possible to actively manage the power flow. Only its addition provides the grounds for a GFMI to unfold its full potential. [34, 35]

Their introduction comes with its own set of challenges. Their complex dynamics are responsible for parametric uncertainty. As the control aims to take action based on uncertain events, it is of interest to efficiently manage these systems. Thus, compensating for large variations in supply and demand, their safety, and economic management is key.

Two key factors are the nonlinear dynamics of the ESS and parametric uncertainty from immeasurable system states. Their impact on the system behavior is explained in the app. A.1.3.

## 2.5 MODEL PREDICTIVE CONTROL

Societal ideological shifts and consequent policy changes have pushed industries to attune their process optimization to other objectives than cost minimization. In this context, next to power flow optimization, grid stability contributions are a core objective in the controlled process.

Such processes can be automated using MPC structures. They can run for extended amounts of time at high performance without the need for maintenance. Such an aspect is paramount concerning critical infrastructure, like the energy grid, as power outages are often extremely costly. [11, 36]

While the concept of MPC has been around for a while now, its increasingly frequent use can be attributed to several distinct features.

**MULTIVARIATE INTERACTION** Part of the MPC's popularity can be attributed to its simple way of handling large multiple-input-multiple-output (MIMO) systems. It can determine inputs' effects on various outputs and optimize for variables that cannot be directly measured or controlled. [37]

**OPERATIONAL CONSTRAINTS** Perhaps its greatest advantage over other control methods is its ability to explicitly handle input, state, and output constraints. For example, the state of charge (SOC) of an ESS can be limited to increase the lifespan of the component. As a state variable, the SOC can neither be directly controlled nor observed. Yet, it can be constrained. [38, 39]

**PREDICTION VALUES** Another powerful attribute of the MPC is its ability to make predictions about future system states. On their basis, an optimal control signal can be

calculated. A receding horizon scheme can leverage historical data or anticipated events, incorporating continuously updating information. Executing only the first small segment, it can adjust to disturbances and unexpected state changes. This way, it is also able to handle asynchronous or delayed sensor information. [37, 38]

In the context of power flow optimization, the forecast can be used to optimize energy storage based on anticipated energy production and demand. From the theory, it appears that reliance on forecasts in optimization has the potential to greatly improve operational efficiency. In that sense, accurate forecasts can be immensely helpful in stabilizing the grid. [15]

DISTURBANCE REJECTION Because MPC solves the formulated problem iteratively over a prediction horizon, it can account for measured disturbance. Prediction of and reactive recomputation due to disturbances facilitates the handling of unexpected state changes. This property is especially important in optimization with large uncertainty stemming from prediction errors and plant-model mismatch. [37, 40]

### 2.5.1 *Challenges*

Identified were several core challenges that must be addressed to facilitate the industrial application of the MPC. One factor is the cost associated with developing and updating the plant model. [41] It needs no further explanation. The other challenges are summarized in the following paragraphs:

UNMEASURED DISTURBANCE A significant challenge is unmeasured disturbances entering the system. They occur due to a lack of knowledge and can introduce large losses in optimality. The matter is complicated by heterogeneous disturbance dynamics of different variables. [41, 42]

PARAMETER UNCERTAINTY Similarly, parameter uncertainty induces a loss in optimality. They can originate from unmeasured disturbances but also from uncertainty through mismatching model structure. Both induce prediction errors. Since the plant behavior and the disturbances are dynamically changing, unobservable system states and erroneous plant models can be causal effects for losses in stability and optimality. [41–43]

DYNAMIC LIMITATIONS Due to the explicit enforcement of operational constraints on uncertain parameters, the controller can run into feasibility issues. For example, in the presence of unmeasured disturbances, hard constraints on output variables can potentially be violated. Especially ramping control variables suffer as they integrate errors. Differently, if the model structure mismatches reality, scenarios where the true system is unable to reach calculated setpoints arise. [41, 44]

LINEARIZATION If computation time is a major constraint, plant models are often linearized to address this issue. MPC with linear or quadratic objective functions can find solutions much more rapidly than controllers with complex objective function formulations can. In simplifying the dynamics, Pruitt *et al.* ([45]) demonstrate large gaps in optimality due to linearization.

Due to the highly nonlinear dynamics introduced by the storage elements, it is computationally very expensive to optimize an accurate plant model. When performing optimization on shorter time scales, this circumstance becomes problematic. Thus, linearization techniques are employed to simplify computations. The benefits and challenges associated with linearized control are described in appendix A.1.6.

### 2.5.2 *Dynamical range*

Adding complexity to the control of a renewable energy production hub are the vastly different time scales on which the plant parameters change. On a shorter scale are rapid changes in frequency and voltage that happen in a matter of milliseconds. Especially due to faults and outages. Power output adjustments must be made in seconds due to varying production and demand. [25]

SHORT SCALE In the context of the energy hub, Knechtges and Moser ([46]) have conducted a study on how grid frequency changes affect DC link energy levels. System splits induce large frequency gradients which must be compensated for by grid-forming control. Essentially, without active countermeasures, critical frequency limits (47.5Hz and 51.5Hz) are reached after roughly 2s. To stabilize the grid and prevent large-scale blackouts, the European TSO requires grid-tied power plants to reduce their active power output by 50% in the same time frame.

LONG SCALE Accurate modeling of nonlinear plant dynamics can become extremely costly and can render the MPC unfit for real-time use. Especially when stochasticity is introduced in forecasting, complex calculations are difficult to perform in such short time frames. Along those lines, Pruitt *et al.* ([45]) presents a dispatch problem of a 1-year mixed-integer nonlinear optimization that takes more than 10 hours to find a solution within 10% of the global optimum. It thus appears advantageous to introduce measures to reduce model complexity and computation time. [37, 47]

DISTURBANCES Similarly, a wide range of disturbances are expected to influence the operation of the plant. They can be introduced as sensor noise in the short term, for example measuring the frequency. Estimations of system states can suffer from parameter drift with significant errors appearing in a matter of hours. In the long term, factors like component degradation play a significant role in changing the control of the plant. [44]

### 2.5.3 *MPC decomposition*

To address the uncertainty issue, scientists have come up with various ways to limit the impact the linearization has on the solution. A promising approach can be found in the MPC decomposition. Its goal is to design multiple MPCs that share the scheduled tasks at hand and distribute the computational burden. Often, the split is done under consideration of time scales on which processes happen and the dynamics of the plant. These splits can be grouped into three general categories, namely the temporal, functional, and spatial decomposition. [37, 48]

One such innovative way of decomposing the classical MPC is the concept of the hierarchical MPC. Among others, it lends itself as a useful adaption for plant components that are located close to each other (high spatial density), enabling rapid exchange of information. Furthermore, it allows a combination of temporal and functional MPC decomposition. Therefore, the hierarchical MPC appears to be an interesting candidate as a control structure for a RES. To shed some light on this implementation, its nature will be explored further in the following section. [37, 48]

#### *Singularly perturbed system*

Oftentimes solutions to singularly perturbed problems evolve on disparate timescales. Due to the multi-timescale dynamics, the problem cannot be decomposed by the regular perturbation approach. The Poincaré expansion is insufficient because no uniform asymptotically approaching solution can be obtained. In singularly perturbed problems, small parameters multiply large operators, such that the former cannot be set to zero. [49]

This can be exemplified on the energy hub. Small parameter changes in demand or grid frequency mediate a response in the output of the power plant (operator). Neglecting these small perturbations would change the nature of the problem.

The singular perturbation theory is the fundamental basis for temporally decomposed MPC. Therewith, one can simplify a problem by tending to multiple discrete problems rather than a single full-scale one without discarding smaller perturbations. This can be especially advantageous if functional and temporal decomposition go hand-in-hand. [37, 48]

How the temporal decomposition can be used to divide tasks in a multi-stage MPC can be read up on in the app. A.1.8.

### 2.5.4 *Hierarchical MPC*

From the decomposition of the classic MPC follows the hierarchical MPC. Scattolini ([50]) reviews such control schemes where a global optimization scheme is combined with short-scale regulatory control. Here, the former aims to optimize the process and the latter is responsible for direct actuator control. The supervisory layer synthesizes setpoints from a nonlinear MPC and passes it to a linear MPC with simple dynamics for setpoint following. Together, they present the 2-timescale optimization scheme. Negenborn *et al.* ([51])

conclude their work by raising several issues surrounding this scheme. Pointing to further research, they recommend adding a penalty term to the cost function to guarantee closed-loop stability. Aiming to reduce model complexity, they intend to use a less detailed control layer to steer the lower control layer. Furthermore, issues directly about the control of power networks were mentioned. Notable are the vast number of network components resulting in large models and hybrid dynamics despite a multi-stage control approach.

Due to their mismatching model structure, concerns were expressed where variations in operating voltage would cause stability issues. They can arise from the difference in feasibility space in which the two control layers operate. Consequences are unreachable system states and setpoint offsets. [11, 52] These offsets manifest as suboptimal plant operation which has economic consequences. Pruitt *et al.* ([45]) showed that the power flow optimization with the application of a MILP routine resulted in a 15% estimation error in the operation of a distributed generation system. Minimizing these losses is of great economic interest.

### 2.5.5 *3-stage MPC*

The concept of the hierarchical MPC aims to integrate the MILP approaches with the top-layer supervisory control. The idea is the introduction of a third, intermediary layer between the full nonlinear upper layer and the lower linear dynamic setpoint tracking layer. Its goal is the mismatch minimization and determination of setpoints that can feasibly be tracked with a linear system model. [51]

The theoretical approach is inspired by the well-established structure presented in Fig. 2.6. It temporally decomposes a full-scale dynamic model into a hierarchical one with three layers. Therein, the plant dynamics as well as the disturbance dynamics are decomposed in accordance with the singular perturbation theory.

#### *Global nonlinear optimization*

The added benefits in terms of control of the global layer are twofold. Firstly, the nonlinear representation can capture the plant dynamics more accurately, and secondly, improve the predictions made by the following layer. This layer shall be referred to as the global nonlinear optimization (GNO) layer. It solves a nonlinear steady-state problem over a horizon of weeks or months. Its consideration can aid in improving storage level management. Due to the long prediction horizon, it can predict long-term process changes and adjust for slowly changing system parameters.

Here, the focus lies in the optimization of plant-wide processes under consideration of various factors. Many implement this layer as an economic one. Shifting away from operational considerations, it is used to predict profit margins. One would employ informed stochastic models to pinpoint times for buying and selling energy to maximize profit. Frequently, these nonlinear problems are non-convex and very costly to solve. [52, 53]

How these two layers are aligned to minimize modeling uncertainty is explained in appendix A.1.5.

*Steady-state target optimization*

This middle layer's main responsibility is the determination of future system states. It must synthesize setpoints that can be reached by the system. Some have deemed this layer especially useful in cases with large plant-model mismatches where active constraints are present. Thus, this layer is especially important when using linearized models as it is able to address the feasibility issue inherent to linearization. Essentially, it mediates between a large-scale nonlinear and a short-term linear optimization [41, 48, 54]

The addition of the SSTO layer also addresses the dynamic limitations issue raised by Qin and Badgwell ([44]), expressing feasibility concerns with enforcing explicit constraints on integrating control variables.

*Dynamic optimization*

The lowest layer is tasked with the DO of received setpoints. It should determine the trajectory that optimally tracks the given setpoint under consideration of operational constraints. Due to its short computation time, this layer is tasked with compensating quickly varying disturbances.

To perform in industrial applications, the solution of this objective function must be computed in real-time and execute drastic output changes in under 2s. This layer must find a fast and efficient solution that can reach the present setpoint. As the layer is tasked with direct process control and direct access to the system's input variables, its priority is high-frequency setpoint tracking. To maximize computational speed, the problem is formulated with a linear cost function and constraints. [48, 54, 55]

### 2.5.6 *State observer*

The state observer is an important component for multiple reasons. With estimation, it can reconstruct unobservable system states. It can also update system parameters in the optimization functions based on measurements. In essence, taking measurements and consecutive automatic model updating can reduce model uncertainty. [41, 56, 57] Its addition can mitigate the impact of unmodeled structural uncertainty and unmeasured disturbance on optimality. [43, 56] Its relevance and function is elaborated on in appendix A.1.7.

#### SUMMARY

With diminishing grid inertia, the way power is fed into the energy grid must change. Next to active and reactive power flow, grid stability contributions become increasingly important. Innovative solutions of GFMIs with fast-frequency response appear to be promising.

With the introduction of the 3-stage MPC, this thesis intends to address the stability issues arising from linear process control. The implementation of inverter-based technology locally stabilizes the grid, permitting its connection with decentralized RES. To accomplish this feat, the droop control was reformulated to fit into an MPC control structure.

Automated control structures like MPC can optimize the use of ESSs. Generalizing their application, they are deployed to control dynamic processes while satisfying a set of constraints. Here, it could be the ESS's SOC under consideration of its limits.

Further, the deployment forecasting techniques improve the energy management of intermediate energy storage. Their successful integration can vastly improve energy flexibility because it can buffer energy generated at an uncontrolled source, imposing control on the power flowing to the grid.

Based on a process or plant model, the MPC can predict how changes in independent variables can influence system states. For example, how the power flow in and out of the ESS affects the SOC. Leveraging these predictions can determine how the independent variables can be altered to steer the process to a desired state. In this case, it entails determining an optimal power flow to arrive at a desired SOC without violating the imposed limits.

Within the control structure, the addition of the SSTO layer aims to reduce the plant-model mismatch. It bridges the gap between the GNO layer, optimizing long-term processes, and the DO layer that is directly in charge of the components.

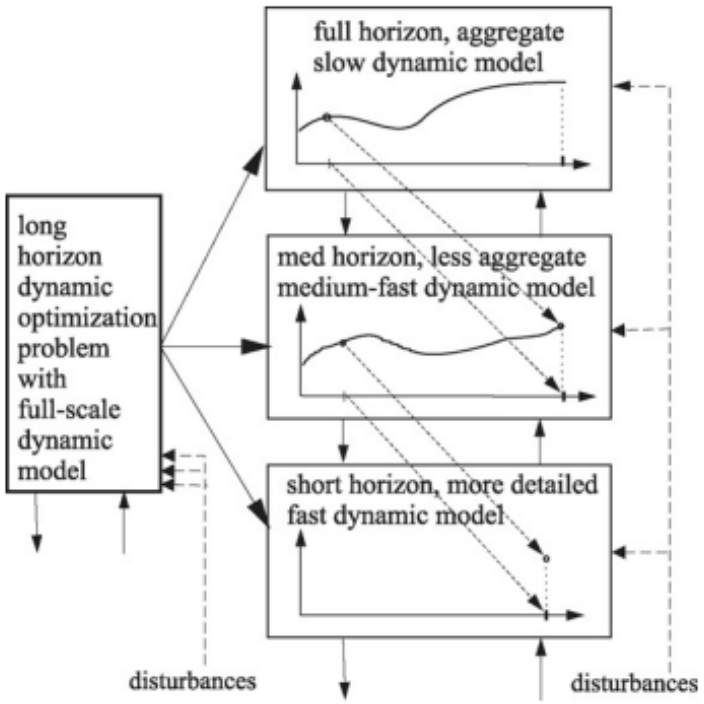


Figure 2.6: Temporal decomposition with a hierarchical structure. [48]

# 3

# CONCEPT

This chapter ties the visited issues of the RES implementation in the energy grid to the application of MPC control. The introduction of a 3-stage hierarchical MPC intends to address the raised issues in the literature by presenting an integrated controller-hub concept. To the author's knowledge, no 3-stage hierarchical MPC has been presented to optimize power flow in a RES production hub.

Building on the three literature streams of chapter 2 (Fig. 2.1), this chapter will present the conceptual design of the energy hub and 3-stage hierarchical MPC. An overview is given in Fig. 3.1.

The integrated hub design is shown first (sec. 3.1), describing the shown components. It is followed by the application of the control theory to the energy hub. Here, section 3.2 reveals how the structure of a 3-stage MPC will be applied as an exploratory design and how it is able to address specific issues associated with RES control.

LIMITATION At this point, it should be mentioned that the concept introduced here will describe the control structure in its entirety, integrating all aspects of the controller that were theoretically explored in chapter 2. Due to the expansive nature of this concept, it was deemed unrealistic to implement the entire design as part of the simulation. Keeping the time allocated for this project in mind, this choice set the focus on the theoretical exploration and the simulation of the SSTO layer on the energy hub. It was chosen because it acts as the connective piece between the other two layers, the turbine and the grid.

Due to the limited scope of the simulation, special attention was paid to embedding the conceptual design in existing literature. Because the presented components in this

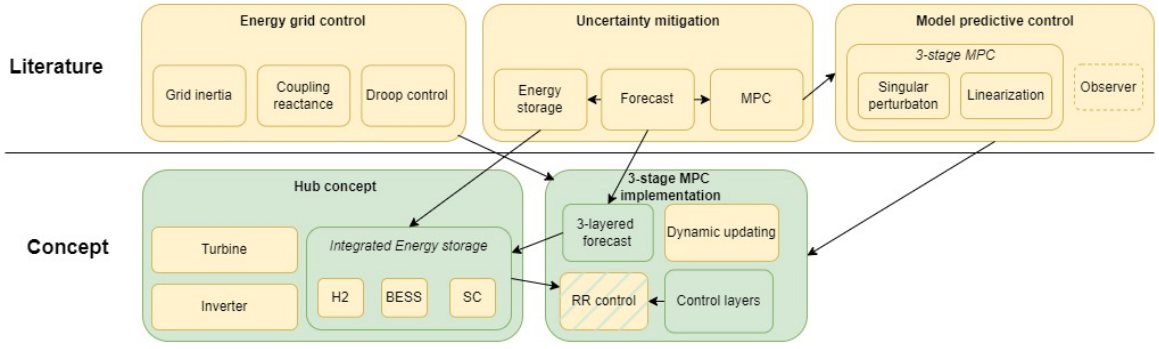


Figure 3.1: Conceptual contributions based on the literature review. Indicated in yellow are the topics that have been composed as a literature study. Indicated in green are contributions as an extension to the literature.

design are well-established, the author intends to provide as much literature context as possible. The goal is to increase the validity of the conceptual design, highlighting the novel assembly in the context of the energy hub as a contribution. This can be observed in Fig. 3.1, showing how the components of the concept are part of the literature study. However, they are introduced here after providing the reader with further context.

## 3.1 HUB CONCEPT

The purpose of the designed hub is to increase the reliability and stability of the power delivered to the grid. In total, three different storage mediums have been included, complementing the functionality of each presented control layer. The hub design connects each component through a transformer to the main RES bus (Fig. 3.2).

The RES model comprises components that are either used for energy generation, storage, or delivery to the grid. Here, the generation unit is a wind turbine. It acts as the prime mover of the system, injecting energy from an uncontrolled source. The unit is connected to the general electricity grid with the grid-forming inverter (GFMI). It is responsible for converting the power on the RES side to 3-phase HVAC power, fit to be synchronized with the grid. Further, different ESS are installed to buffer supply-demand mismatches. The following sections will describe what each component contributes to the concept.

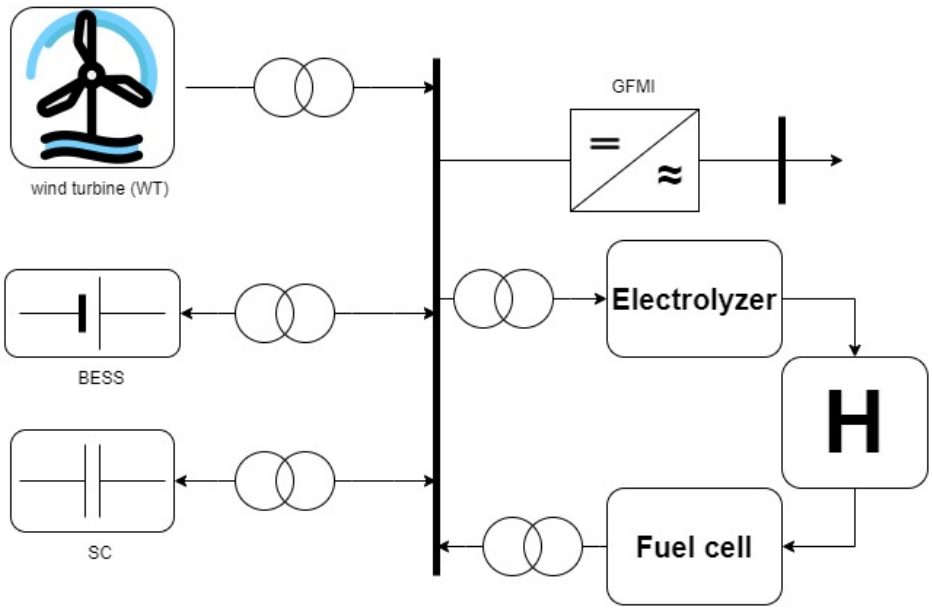


Figure 3.2: Schematic layout of the hub design.

### 3.1.1 *Storage solutions*

Research on storage technologies has grown quite extensively. Nowadays, there are countless ways to store energy. The following paragraphs will describe the three technologies chosen for this design and briefly argue why they are important.

BATTERIES The battery energy storage system (BESS) is popular due to its high cyclic life and efficiency as well as energy density. However, they have two shortcomings. Firstly, their power density is relatively low. Increased current rates significantly degrade a battery's lifespan. Degradation of a Li-ion battery is accelerated 1.5-2x at 1C and as much as 4.5x for a 2C discharge rate. Similar degradation problems occur with deep SOC battery cycles.

CAPACITORS One solution to compensate for the low power density of a battery is the introduction of a supercapacitor (SC). It permits a much higher current rate without significant loss of cycle life. Furthermore, its comparatively high cyclic efficiency renders it useful as a fast response mechanism to sudden power flow changes. A low energy density means that its output cannot be sustained for an extended period. The battery can compensate for this so these two components complement each other well.

The SC's fast response time could be especially powerful in the introduction of virtual grid inertia and in terms of frequency stability. Various sources (e.g. [29, 47]) use a first-order low-pass filter to smoothen the power output, emulating the inertial response of a synchronous generator. The high-frequency response capabilities would be particularly important in DC voltage control.

HYDROGEN The second shortcoming of the BESS is its limited capacity and lossy long-term storage. One flourishing storage solution is large-scale hydrogen tanks. Liquefied hydrogen can be stored in high-pressure tanks for extended amounts of time with relatively low storage losses. Here, a combination of electrolyzer and hydrogen fuel cell can manage the storage system. The former can convert electricity and water to hydrogen and store it in a pressurized tank. The latter reverts the process and generates electricity with water as a by-product. To guarantee long-term storage capacity, the $H_2$ storage tank is a stabilizing solution as it could compensate for seasonal variations in energy production.

Given the probable scenario of wind droughts, BESS are unfit to respond to such large production gaps. Conventionally, these cases are addressed by supplementing the power output with diesel generators. The $H_2$ cycle would be able to mitigate such non-renewable power production. In essence, the $H_2$ setup can buffer long-term mismatches. It can cover both cases, excess production and excess demand, minimizing energy curtailment and generator use.

## 3.2 CONTROL CONCEPT

The MPC structure that intends to control the designed hub is presented in fig. 3.3. As already explored, this concept comprises the three MPC layers, the GNO, SSTO, and DO. In the following, each component is briefly touched upon to place it within the context of the energy hub concept. The goal is to highlight their interaction specific to the energy hub application.

LIMITATIONS The scope of each layer has been reduced to maintain relevance to the topic and limit the workload.

Firstly, the GNO layer, which is frequently geared towards economic optimization is only briefly described to discuss its benefit for the designed hub.

Secondly, the SSTO layer will be the research focus in the optimization. The reason is that its addition is rather novel in the context of the energy hub. Most implementations directly connect the GNO and DO layers. Further, the inclusion of the coupling reactance into this layer is investigated. The according equations will be derived in chapter 4.

Lastly, in subsection 3.2.2, a small contribution to the concept of ramp-rate (RR) control is made. To the author's knowledge, RR has not been applied to an ESS with three elements. It is a necessary part of the control concept and will be supplemented with additional sources. It is marked with a hatched line in Fig. 3.1.

### 3.2.1 *3-layered forecast*

The hub concept intends to incorporate various forecasting methods into its control, tying them into all layers with regard to their purpose. Incorporating forecast data of all timescales into a prediction model would greatly improve the estimation accuracy and vastly decrease production and consumption uncertainty.

WEATHER As the GNO layer has the longest prediction horizon, the most sensible approach is to use historical weather data to anticipate production levels. Such climatological data should reflect long-term weather variations like seasonal trends.

Shorter into the future, such a time series can be updated with day-ahead forecasts, creating a more accurate picture of the expected weather conditions. As an element in the SSTO layer, more reliable medium-term predictions can be used to forecast production levels.

Finally, using transmitted data from sensors in close geographical proximity, measured data can be used to include live weather information in the control. Directly feeding into the DO layer, these measurements help anticipate short-term generation level changes. As this layer performs real-time optimization with a prediction horizon in the order of minutes, such data can be extremely useful and should be given large credibility values.

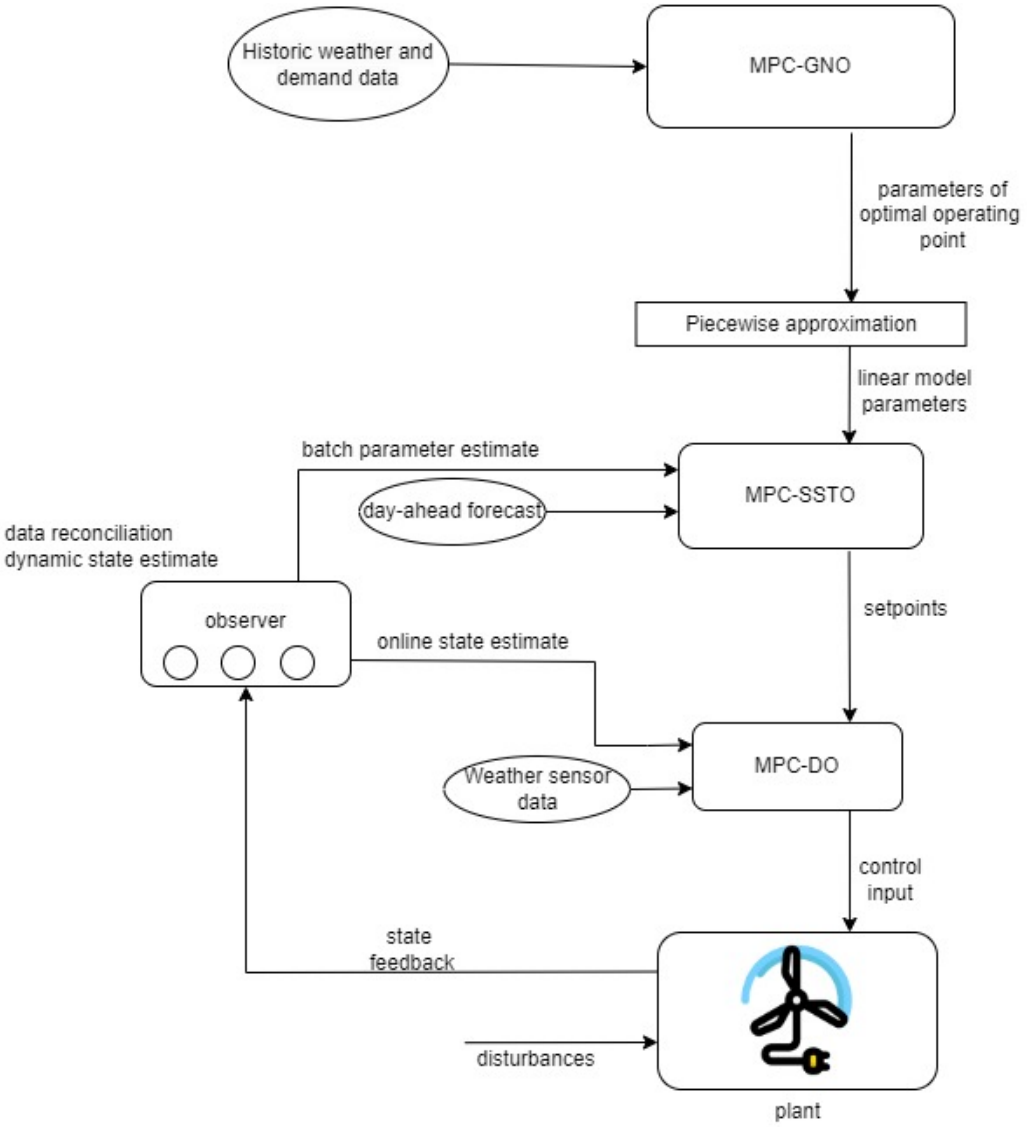


Figure 3.3: Schematic overview over the hierarchical control showing all control components.

DEMAND FORECAST Similar to the weather forecast, the demand prediction can be included. The same data scheme for all layers should be available from TSO companies, detailing consumption levels of active and reactive power.

Alike the production forecast, historical data is expected to provide long-term information about seasonal demand changes. They are processed by the GNO layer. The SSTO layer incorporates day-ahead consumption (and perhaps pricing) into its prediction, updating every hour as new information about the market becomes available. Similarly to production forecast, sensor feedback from the PCC is integral to the operation of the low-level controller.

It should be possible to derive information about frequency and voltage, potentially providing additional value.

### 3.2.2 *Control layers*

Given the symbiosis of the selected storage systems and forecasting, the MPC design aims to enable their implementation into the energy hub. They were carefully selected to match the timescales on which the hierarchical MPC operates.

The GNO integrates the seasonal changes and economic optimization with the management of the $H_2$ storage levels, passing a SOC and power setpoint.

The SSTO updates the prediction with a day-ahead forecast of production and consumption, managing the storage levels of the BESS to smoothen the power output over a single day. It also determines an optimal SOC and power setpoint.

Lastly, the DO must compensate for fast-acting disturbances, like sudden changes on the grid. The rapid response time of the SC is ideal to match such a requirement.

This section describes each of the layers in more detail and what their added value is.

*Global nonlinear optimization*

This layer intends to perform a global optimization of the full nonlinear plant model. Including historic weather and demand data, it can make predictions of production and consumption levels. Anticipation of such discrepancy would not only be a stability contribution but could yield considerable economic profits as well.

ECONOMY Due to its long prediction horizon, it can manage energy storage levels under consideration of long-term energy price changes. As the economic optimization layer, it aims to compute expected future scenarios based on stochastic approximations of uncertain forecasts. Therein, supply-demand mismatch should be reflected in dynamic energy prices on the market. It should be noted that due to their complexity, such estimations come at considerable computational cost.

STORAGE Especially, large seasonal variations in generation levels in regions with low production diversity risk energy shortages. If the layer can anticipate gaps in production caused by seasonal changes or events like prolonged wind droughts, large-scale reliance on RES would much increase.

Functionally, these process decisions can be implemented by leveraging the hydrogen infrastructure where the GNO layer manages its storage levels. Therewith, it is possible to minimize risks of energy curtailment and contingency scenarios. As long-term $H_2$ storage is quite energy efficient, it has the potential to fulfill the desired role. Particularly because $H_2$ storage tanks have been built at such scales and have been incorporated in on-shore wind turbine towers. In terms of storage sizing, the hydrogen infrastructure would permit reducing the size of other ESSs within the energy hub.

Furthermore, adequate storage capacity is necessary if the controller is equipped with a large prediction horizon. The $H_2$ storage caters to this need and provides the energy flexibility required to implement the optimization performed by the GNO.

OPERATING POINT The optimized control step of the GNO acts as the operating point for the other optimization layers below. Therefore, determining a feasible operating point under economic and stability considerations is crucial for efficiently operating an energy production hub. The piecewise linear approximation bridges the gap necessary for the interaction between these two layers.

IMPLEMENTATION In terms of economic plant optimization, vast literature exists treating the updating and optimization of this layer. Some identified issues and solution approaches are discussed in Ellis *et al.* ([52]) and Krishnamoorthy *et al.* ([41]), dealing with the dynamic optimization and linearization issues.

Unfortunately, the operations research component largely falls outside the scope of the project. For ease of implementation, it was decided to attach fixed energy rates to a deterministic optimization model and reoptimize to react to statistical uncertainty and prediction mismatches. However, with the object-oriented programming approach, it is entirely possible to develop a sophisticated price prediction model that can be woven into the general control structure. In such case, a prediction agent passes the anticipated pricing for the prediction horizon to the SSTO (or global) layer that is then able to optimize the operational aspects under economical considerations.

*Steady-state target optimization*

Obtaining an operating point, the objective of this layer is to solve an optimal control problem whose solution a combined BESS power and SOC setpoint is. Such a solution is determined by minimizing the energetic losses formulated in its objective function.

This main responsibility of the supervisory control layer can be broken down into several aspects.

PREDICTION Accounting for day-ahead demand forecast by the TSO, it can improve the prediction accuracy from the GNO layer. With daily production values from wind profiles driven by the diurnal cycle, it aims to shift mismatched peaks and valleys. This feature improves the prediction of volatile energy prices.

POWER BALANCE One major task of the SSTO is balancing power between the turbine, storage, and the grid. Setting setpoints that compromise between these components is a task vital to the efficient operation of the plant.

STORAGE The BESS has been explored as an ideal medium to manage intra-day demand changes. It is equipped with a high cycle life and geared towards low current discharge. Its abilities are symbiotic with the requirements an SSTO layer must fulfill.

LINEARIZATION Similarly to the BESS bridging the gap functionality of the hub components, the SSTO overcomes discrepancies between the GNO and DO layers. Piecewise linearization (sec. A.1.6), or in this case, quadratic approximation, of the operating point

minimizes model mismatches between the nonlinear optimization on the upper layer and linear optimization on the lower layer. With it, their operating spaces can be assimilated, checking for feasibility. The quadratic objective function form for this layer is described in detail in the App. A.2.1.

NCO TRACKING Here, the state observer design is of importance, controlling the actively constrained variables by tracking the Necessary Condition of Optimality (NCO). This condition ensures the local convexity of the problem function. It essentially underlies satisfying the Karush-Kuhn-Tucker (KKT) conditions which extends the Lagrangian for inequality constraints. It is handy in this project to enforce operational constraints. By tracking the NCO, the plant outputs can be adjusted to converge to a local minimum, i.e. a KKT point. [43, 54, 56]

OBSERVER It should be mentioned that each paper in the above analysis assumes observability of the active constraints. Such status can be achieved with a state observer. However, to limit the scope of the simulation, the observer design is not a direct part of the concept.

To mitigate the impact, the state observer was replaced with direct state feedback. Here, it was viable to obtain information on state variables that cannot be directly observed in the real world. With a higher degree of observability, uncertainty in the simulation environment was reduced. In the real application, a state observer is necessary as it is expected to function as a state estimator that can reconstruct unobservable system states.

*Dynamic optimization*

This layer is responsible for translating the setpoints synthesized in the SSTO layer into input variables that control the storage units. It is intended to determine the optimal reference trajectory, tracking the provided setpoint. With active control, the dynamics between the turbine and the grid can be decoupled.

Here, the components are managed by direct process control. Therein, the DO layer is responsible for governing the storage levels and operating their power flow. In this application case, the DO has direct control over the power flow in and out of the ESS assembly. The components comprise the $H_2$ system, the BESS, and the SC.

CONSTRAINTS An important aspect of storage control is the limitation of excessive input movement. Such a feat can be achieved by adding boundary constraints to the ESS ramp-rates. Such limits are further useful to guarantee the components' safety and longevity.

A relevant aspect in setting up the SSTO and DO layers is to consider what variables are constrained in which layer. Doubly constraining the same variables can lead to infeasibility. At the same time, it could be advantageous to hard constrain variables in steady-state but remove the limits for transient operation. It enables a larger feasibility space and the ability to better address large disturbances entering the system. [54]

In this application, the explicit RR control in the DO foregoes the implementation in the SSTO layer. Disturbances integrated in the SSTO layer have the potential to cause stability issues. Thus, removing the ramping constraint and imposing explicit control improves stability and efficiency.

TIMESCALE This layer must reject short-term disturbances and dynamic grid fluctuations. It must stabilize the DC link voltage and buffer changes in power fluctuations. Here, the effects felt from grid disturbances have been estimated to be around 10Hz. [25] Gathering information from investigations into a wind turbine and grid disturbance operation, significant adjustments (~0.5pu active power) from grid variations must be made within two seconds. [46] Similarly, on the production side, active power fluctuations of around 0.3pu from the wind turbine are expected to happen within 10 seconds. [32] Especially due to this high variability, it is recommended to resort to RR control. [58] Further, real-time computation necessitates finding a solution with a clock cycle. Such action is particularly relevant when quick reactive action is required.

RR control also enables the incorporation of national grid codes into the algorithm. For example, the Netherlands allows a maximum ramp rate of $10\% * P_{rated}/min$ for power plants. [58]

The RR limits and binary control components are implemented into an objective function determining the power flow due to the received setpoints. The problem formulation is given in the app. A.2.3.

VIRTUAL IMPEDANCE To utilize the SC as stability contributor towards DC link voltage, Zhang and Wei Li ([59]) propose the determination of the surge current due to load changes with equation 3.1.

$$i_o(s) = K * \frac{1}{\tau s + 1} \tag{3.1}$$

with

$$K = f(R_{load}, R_{SC}, C_{SC}, V_{ref})$$
$$\tau = f(R_{load}, R_{SC}, C_{SC})$$

where the gain K and time constant $\tau$ are functions of the load, capacitor resistance, and capacitance. The ESS parameters are obtained from the linearization performed in chapter 4. They conclude that this implementation can provide surge current compensation by introducing virtual impedance to the RES.

The supercapacitor is able to respond to these fluctuations, reducing high frequency deviations and dampen oscillations. Lasseter and Piagi ([27]) buffer this passively with rated energy storage on the DC bus. An actively controlled component would arguably improve the margins.

As the RR control consists of a multitude of LPFs, the format of the virtual impedance can be included in the formulation below.

*Ramp-rate control*

This type of control addresses the question of how the combined power setpoint $P_{ESS}$ can be split into three reference trajectories. Here, the DO must calculate a power reference trajectory which is then distributed among the ESS components.

The addition of a linear DO layer enables removing hard constraints and offloads ramping control from the SSTO layer. Here, the power of being able to constrain these two layers independently becomes clear.

The RR control is intended to regulate the rate of the power flow to each ESS component according to their purpose. Essentially, the larger the rate of change, the faster the response must be, utilizing the SC for such cases. Slower rates then make use of the BESS and $H_2$ storage. The following explores how the common setpoint $P_{ESS}$ is split.

In principle, this matter can be addressed with a combination of RR control and the introduction of low-pass filtering (app. A.2.2) and extend the design to incorporate the $H_2$ system. In that sense, below is a proposal for how these setpoints can be split using the RR approach that was designed for two components. A scheme of the approach is shown in Fig. 3.4. The design of the LPFs is briefly described in app. A.2.2.

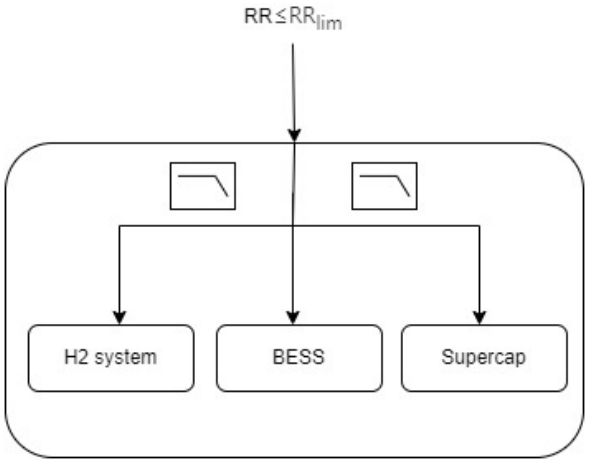


Figure 3.4: Doubly applied LPF to split the power reference among three storage elements.

This concept is then translated into objective function form to fit the frame of the MPC. The derivation and equations can be found in app. A.2.4. The proposed double LPF power splitting has the potential to provide virtual impedance to the grid, drastically increase voltage stability, and economic operation of the plant

### 3.2.3 *Update cycle*

The optimization horizon of each layer is not fixed and should be investigated in the specific application case. What is important is the congruence of the updates where the control step of the layer above spans the optimization horizon of the layer below (Fig. 3.5).

To include the economic benefit of day-ahead forecast and pricing announcements, the SSTO layer has been selected to have a 24h prediction horizon. With 1hr dynamic power

pricing intervals in the Netherlands ([60]), the SSTO layer receives new information every hour, hence the control step size.

It should be noted that the prediction horizon of each layer below is shorter than the control step above. That is intended to create some redundancy. If they were the same size, the update cycle of each layer is directly bound to the control step size of the layer below. It would imply that the SSTO must update every 0.1s, and the GNO every hour.

Due to the vastly different timescales present in this optimization problem, synchronicity between the three layers seems of importance. Therefore, section A.2.5 in the appendix has been dedicated to discussing this matter in more detail.

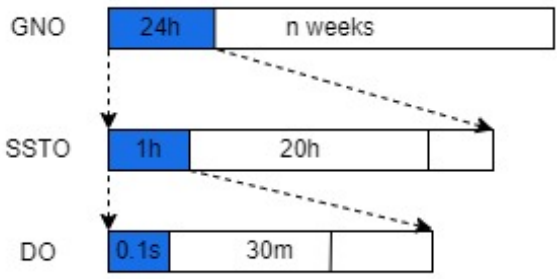


Figure 3.5: The update cycle for the respective MPC layers and their interaction.

#### VISUALIZATION

A small section in the appendix (App. A.2.6) is dedicated to the visualization of the plant design. It intends to give insight into how the assembly can be realized with market-available components, showing that its assembly is already possible to compose in the real-world.

## 3.3 SUMMARY

This section proposed a 3-layered MPC scheme, applied to an energy production hub. Highlighted are the contributions regarding integrated the controller-hub design.

Described were three MPC control layers, enabling the operational optimization on three timescales. Therein, synchronized production and demand predictions are leveraged to determine reference trajectories.

Three storage elements are incorporated into the hub design to unlock the MPCs' potential regarding power flow optimization. They provide the operational space for the controllers to perform their tasks.

RR control was introduced to manage the power setpoint splitting between the storage units. LPFs were utilized to split the signal according to each unit's capabilities. They enable disturbance compensation on vastly different time scales.

Piecewise quadratic approximation of the GNO operating point and parameter estimation from the observer update the SSTO layer. They minimized plant-model mismatch, improving operational efficiency.

# 4

# MATHEMATICAL MODEL

This chapter introduces the mathematical formulations that manifest the concept. As can be observed in Fig. 4.1, its structure follows that of chapter 3.

Two elements are contributed towards the hub model, namely the mathematical definition of the turbine and the BESS. Discussed in section 4.1, these two components were linearly approximated to permit their use in simple solvers.

The control element zooms in on the formulation of the SSTO layer. This layer has been chosen for the implementation as it synthesizes the common power setpoint while maintaining the power balance of the entire hub. Its role as a supervisory layer was deemed essential, acting as a cohesive element between the control layers on the software end and the wind turbine and the grid on the hardware end. A more elaborate discussion of the elimination process regarding the implementation choice can be found in app. A.3.2.

Highlighted is the contribution of the coupling reactance and droop control formulation (from sec. 2.3) in subsection 4.2.4. Part of the effort was the translation of the symbolic equations into objective function and constraint form. The results aim to combine components of anticipated and measured events to improve the optimization.

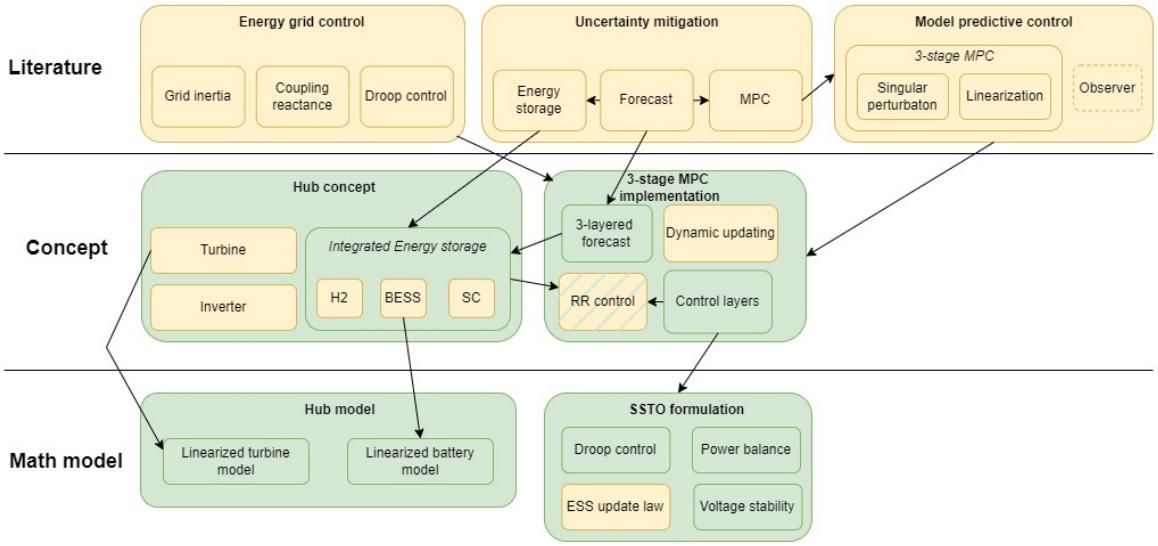


Figure 4.1: Development of the mathematical model for the explored concept. Indicated in yellow are the topics that were composed as a literature study. Indicated in green are contributions as an extension to the literature.

### 4.0.1 *Limitations*

Before being able to implement any form of control in a simulation environment, a plant model is necessary. Therefore, the first step in this work is the development of a plant model which underlies the control. However, as this project is intended to focus on the control aspect of such a setup, it is desired to build a simple, yet representative plant model. To achieve that, some simplifications were made.

TRANSFORMERS Firstly, all RES side transformers were discarded, assuming a common working voltage and no losses from AC/DC converting voltage or stepping it up and down. However, a general loss term was added to the objective function of the SSTO, enabling the incorporation of conversion loss functions.

ESS Due to the focus on the conceptualization and time constraints in the implementation, the scope of the simulation work is limited to the SSTO layer. As the SSTO layer determines a common power setpoint, the storage elements could be lumped into a unified ESS. It seemed sensible to only include the dynamics of the BESS because the layer does not yield information about the $H_2$ system nor the SC. In that sense, the properties of the SC, BESS, and $H_2$ cycle are integrated as seen by the SSTO.

SIZING Furthermore, little attention was paid to the realistic sizing of some components. Especially values of parameters like magnetization resistances and capacitances of transformers, shunt conductance, and susceptance of buses were not researched to match a realistic plant. Initial attempts revealed that this feat would require extensive work, outside the scope of this project. It appears that this aspect becomes particularly relevant when designing a plant for a specific application purpose. It is further believed that this effort would be fruitless as plants can vastly differ depending on their components. Consequentially, it is likely that a controller requires different tuning. Because component parameters constitute parts of the objective function and constraints, it is expected that the control structure remains the same.

OBJECT ORIENTATION The control aspect, implemented as the SSTO layer, is core to the structure as it connects all components and the top and bottom control layers. The goal is to provide clear in- and outputs that allow interaction with other control elements. It was deemed essential to clarify interfaces between components while paying special attention to the modularity, flexibility, and improved overview allows the continuous improvement of components without necessitating deep structural changes. This structure is especially relevant as it enables the introduction of concepts that can be augmented later on. For example, the determination of optimization steps from predictions using basic forecasting techniques. The forecasting could be augmented into a forecasting agent that integrates historical data, weather predictions, and sensor data into a stochastic model. Such an agent can be added without information or understanding of the optimization

algorithm. Similarly, using primarily local equations, it should be possible to add further components initially foregone from the implementation. The intention is to create a model predictive control (MPC) structure that is generalizable and adaptable without the need to understand the concept in its entirety.

## 4.1 HUB MODEL

Before attempting to control an autonomous system, it is of crucial importance to create an accurate model of the plant. The model intends to capture the dynamic behavior of the system. Generally, that can be achieved by incorporating three types of variables into the system equations, namely decision, state, and measurement variables. An explanation can be found in the App. A.3.1.

Per the linearized approach on the lower level control, it was necessary to linearize the production and storage units. The detailed workflow of the process is provided in app. A.3.3 and A.3.4.

With a limited focus set on the component parameters, it was chosen to detail their determination in a structured process. The goal is to achieve replicability such that new parameter values can be processed when more test data is available. This is particularly important in battery storage systems because every battery has a different chemical composition, necessitating individual testing.

### 4.1.1 *Grid variables*

It seems sensible to leverage the prediction capabilities of the MPC for the anticipation of grid variables. Accounting for changes in voltage, frequency, and active and reactive power over the prediction horizon could be beneficial in minimizing the uncertainty associated with these quantities.

MEASUREMENTS To enable the decentralized operation of the hubs, local measurements were used exclusively. The controller does not need wider system or sensor information when contributing to stabilizing the grid. The sensor information is vital to enable reactive optimization.

In the following, the elements of the objective function in the SSTO layer are presented. They aim to incorporate prediction values by combining the reactance term and droop control with the anticipated changes in the grid variables.

## 4.2 SSTO FORMULATION

This section details all mathematical formulations that have been added to the SSTO objective function and constraints. Their purpose is to incentivize efficient plant operation by penalizing sensible plant variables, and minimizing deviations.

After the initial formulation, the power balance equation, ESS update law, droop control law, and voltage stability equation are described. They compose the mathematical SSTO formulation.

LIMITATION It should be mentioned that concessions were made to fit the scope of the project to the allocated time. Herein, the SSTO layer seemed most fundamental as it contained the power balance equation with the connection to the grid. It acts as a mediator between the GNO and DO layers and could be regarded as the connective centerpiece to the control structure.

*Initial formulation*

The first element in the formulation of the optimization problem minimizes the error between a desired inverter setpoint $P_{inv,des}$ and the according optimization variable $P_{inv}$.

$$\begin{aligned} min \quad & w_1 * |P_{inv,des} - P_{inv}| + w_2 * (P_{inv,des} - P_{inv})^2 \\ s.t. \quad & P_{inv,des} = \lambda * P_{inv,meas} + (1 - \lambda) * P_{inv,pred} \end{aligned} \tag{4.1}$$

Firstly, the absolute value linear term intends to penalize small deviations between the power setpoint and the actual power delivered at the inverter terminal, restricting control action over the prediction horizon.

Secondly, the square term allows heavier penalization of larger deviations from the reference. It balances accurate tracking and disturbance rejection.

Further, the setpoint can be tuned by values of $\lambda \in [0, 1]$ to favor prediction or measurement, depending on their reliability. Lastly, the prediction of the inverter setpoint is based on long-term grid load predictions passed as operating point values by the GNO.

DISCRETIZATION Discretization of the optimization function is done in line with the update cycle described in section 3.2.3.

The time steps are discretized into hours of the day with $k = [0, 20]$ and the final value K=20.

### 4.2.1 *Power balance*

The load balance equation is implemented in the SSTO layer as a hard constraint. It equates to the produced, stored, and consumed power.

With power continuity, it is assumed that the power on the main RES bus is the same as on the output of the inverter after some loss, such that $\eta * P_{RES} = P_{inv}$. This way, the inverter setpoint on the AC side can be controlled by ESS power flow on the DC side.

To this end, part of the objective function constraints are described as

$$\begin{aligned} P_w - P_{ESS} - P_{loss} &= P_{RES} \\ \eta * P_{RES} &= P_{inv} \end{aligned} \tag{4.2}$$

Special attention must be paid to the sign convention of the ESS. Here, a positive value of $P_{ESS}$ charges the battery, so it takes a negative value in the load balance.

Losses, such as the battery loss term, can be included in the $P_{loss}$ variable. Further losses, such as conversion from transformers or transmission, could be added here.

### 4.2.2 *ESS update law*

This formulation manages the charging and discharging of the ESS and controls the SOC, minimizing fluctuations and enforcing component limitations. It also relates the power flow to the SOC of the ESS.

$$\begin{aligned} min \quad & w_{SOC} * (SOC_{ESS} - SOC_{ESS,des})^2 \\ & + w_{SOC,final} * (SOC_{ESS}(K) - SOC_{ESS,init})^2 \\ s.t. \quad & SOC_{ESS}(k+1) = SOC_{ESS}(k) + P_{ESS}(k) \\ & SOC_{ESS}^L \leq SOC_{ESS} \leq SOC_{ESS}^U \end{aligned} \tag{4.3}$$

Mathematically, the square term in the objective function implements the minimization of deviations from the target SOC. It is possible to parameterize the target value, to make it dynamic. Here, the simplified approach with a static target value of 70% SOC was chosen. The weight $w_{SOC}$ enables tuning the setpoint tracking.

A final constraint term incentives returning to the initial SOC, enabling the use of the same initial conditions.

The first constraint embodies the update law as it was implemented in the model. Positive values of $P_{ESS}$ charge the battery and negative ones discharge it. The power balance of the main DC bus considers the ESS charging as an outflow with an according negative value.

Lastly, the inequality equation limits the SOC of the ESS preventing it from discharging lower than 10% SOC and charging to more than 90% SOC.

### 4.2.3 *Voltage stability*

The penalty term was added to the SSTO objective function to minimize voltage fluctuations.

$$\begin{aligned} min \quad & w_{V,fluc} * (V_{DC,nom} - V_{DC})^2 \\ & V_{DC}^L \leq V_{DC} \leq V_{DC}^U \end{aligned} \tag{4.4}$$

It establishes $V_nom$ as a constant reference voltage and V as the optimization variable. The error function can be tuned with $w_{V,fluc}$. System limitations for the voltage are enforced with the inequality equation.

### 4.2.4 *Droop control*

Introduction of droop control into the MPC problem is deemed essential to the power setpoint synthesis of the SSTO layer. The speculation is that, based on historic active and reactive power production and consumption data, it should be possible to anticipate frequency and voltage changes.

CONTRIBUTION This section derives an optimization problem formulation for the SSTO layer in the modeled energy hub. Based on the sources below, it presents an estimation for the power variations in the coupling reactance. The contribution is their implementation in an optimization function, fitting the objective function form and constraints.

Provided the relative power angle remains in its linear range, s.t. $d_{P,max} = 30°$, the small angle theory from section 2.3.1 can be applied to split the control of the active and reactive power.

*Active power droop control*

In this formulation, the prediction term of the inverter setpoint is extended for the small signal variation $\Delta P$, aiming to capture power changes in the coupling reactance due to variations in power and frequency on the grid.

$$\begin{aligned} min \quad & w_1 * |P_{inv,des} - P_{inv}| + w_2 * (P_{inv,des} - P_{inv})^2 \\ s.t. \quad & P_{inv,des} = \lambda * P_{inv,meas} + (1-\lambda) * P_{inv,pred} \\ & P_{inv,pred} = P_{load,pred} + \Delta P \end{aligned} \tag{4.5}$$

$\Delta P$ is then intended to account for the reactance dynamics, altering the requested power based on frequency changes. Here, $\Delta P$ can essentially be regarded as small signal variations around the operating point. This step was taken to avoid integration of the angular velocity to determine the voltage angle. The derivative reactance relationship is implemented by Moritz *et al.* ([29]) in their work, directly using the angular speed, such that equation 2.3 becomes

$$\Delta P = \frac{EV}{X_L} * \Delta\delta \tag{4.6}$$

where E and V are the inverter and grid voltages respectively and $X_L = 2\pi f L$ is the reactance value. Implementing this relationship allows two things. Firstly, to constrain the relative voltage angle $\Delta\delta \in [0, 30°]$, and secondly, the incorporation of the droop control law from section 2.3.1. With $\Delta\delta = \omega_{inv} - \omega_{grid}$, the droop control law $\omega_{inv} = \omega_0 + m_P * (P_{set} - P_{meas})$ with a proportional error gain can be implemented in the

optimization function. Moritz *et al.* ([29]) split $P_{set} = P_{0,set} + dP_{set}$ and obtain $P_{0,set}$ from the economic optimization, here it is determined by the GNO layer. Further, $P_{0,set} = P_{load,pred}$ because the droop control should determine the frequency changes based on the same load prediction. $dP_{set}$ would reflect production-demand mismatch, accounting for their influence on frequency fluctuations. Lastly, $P_{meas}$ is passed as a batch variable from the observer. The power setpoint deviation due to frequency fluctuations becomes:

$$\Delta P = \frac{EV}{X_L} * (\omega_0 - \omega_{grid} + m_P * (P_{load,pred} + dP_{set} - P_{meas})) \tag{4.7}$$

*Reactive power droop control*

Thanks to the power control decoupling, it is possible to use the same principle for reactive power. The droop control law for the reactive power is implemented with

$$\Delta V = m_Q * (Q_{pred} - Q_{meas})$$

where

$$Q_{pred} = \frac{V_{inv}(V_{inv} - V_{load})}{X_L}$$

The voltage variation $\Delta V$ is supplemented with the $Q_{pred}$ term. The exact derivation of this relationship is shown in app. A.3.7.

*Parameter settings*

To quantify the droop gain, authors used droop settings of 5% for $m_P$, aiming to cause a 0.5Hz droop per 1pu of power error. The same gain drops 5% voltage for the reactive power. [9, 26]. Others emphasize the importance of the sizing of the coupling reactance. Balancing DC bus voltage ratings and the power angle linearization, they recommend its value to be around $X_L \approx 0.2pu$. [27, 61]

Further variations of $\Delta P$ and $\Delta V$ have not been investigated. They could be grouped as an extension under these terms.

*McCormick envelope*

Normally, the electrical power equation $P = VI$ relates the power flow to the voltage and current allowing their explicit handling in function form. However, their relation is nonlinear from which convergence issues occur. The McCormick envelope can approximate this relationship with a sum of linear terms (app. A.3.8).

# 5

# SIMULATION MODEL

This chapter investigates the application of the devised control concept to an energy hub model. The presented simulation model aims to implement the control structure, optimizing the storage levels and power flow based on predictions of production and uncertain consumption. It combines the presented control concept and the mathematical formulations particular to the SSTO layer with the linearized plant components. They are visualized in Fig. 5.1, depicting the three models that have been considered in this work.

The Matpower model is shown in a dashed box because it was developed before it was sufficiently clear that the program does not cater to the control implementation.

The plant model implementation has hatched lines because the basis of the model was developed by LeSage ([62]).

OUTLINE Part of the project consists of creating a suitable plant model on which a controller could be applied. To this end, the chapter discusses the explored plant models with their strengths and limitations. Highlighted are the plant model implemented in matpower as a contribution for further work and the composition of the SSTO objective function considering uncertain predictions and their anticipated effects on the grid dynamics.

MODEL STRUCTURE Essential to the model is the replication of the system dynamics and how the coupled grid dynamics interact with the hub. Within the scope of the simulation model is the investigation of the active power flow control following the production from the wind turbine.

ASSUMPTIONS Next to the linearized component dynamics, the some key assumptions about the environment were made. Isotherm conditions were modeled not to influence electrical component values and the density of air.

SIMPLIFICATIONS Regarding the inverter, a detailed component modeling is foregone in the simulation. The power flow between the RES bus and the grid is related with a constant efficiency term.

Due to the absence of measurements in the optimization model, a constant grid voltage is assumed. Furthermore, the grid frequency is obtained from time series data, determining changes from power variations from the mean, utilizing eq. 2.1. These changes are summed with the nominal grid frequency.

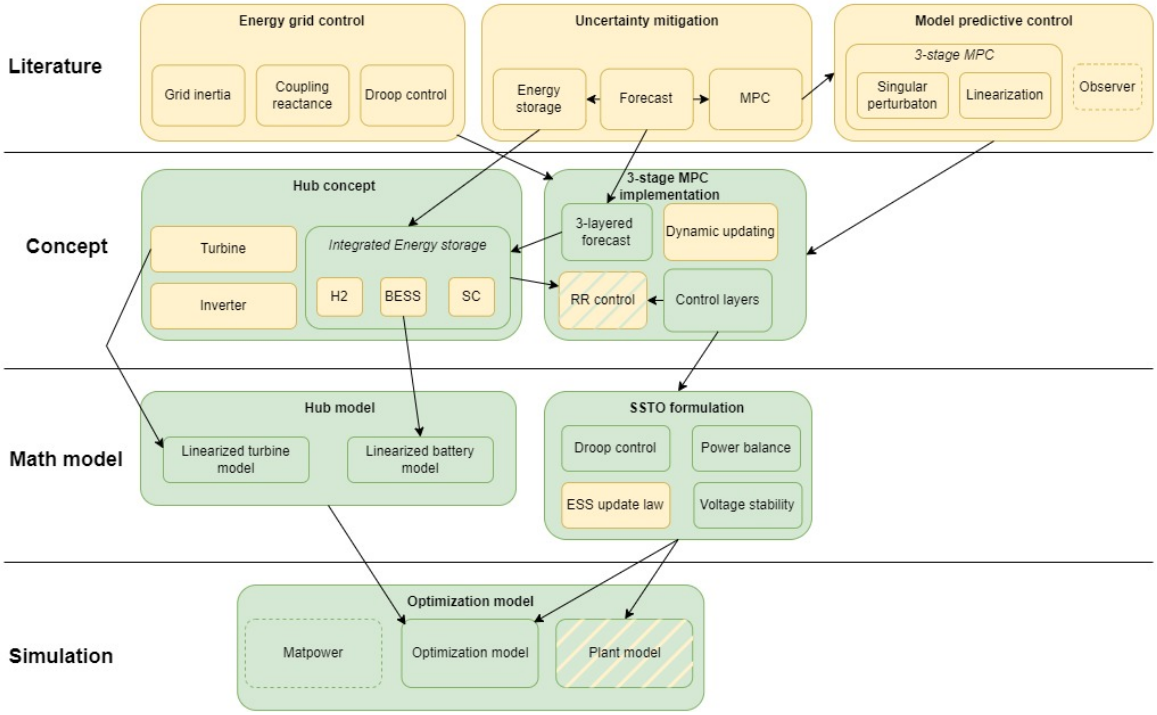


Figure 5.1: Development of the different simulation models based on the mathematical descriptions. Indicated in yellow are the topics that have been composed as a literature study. Indicated in green are contributions as an extension to the literature.

Further simplification was achieved by omitting the modeling of any transformers between ESS elements, the turbine, and the grid. Implied is the assumption of a common operating voltage for all components. Their cumulative losses are accounted for in the power balance equation as $P_{loss}$.

Storage losses are not accounted for in the optimization. There are vast differences between the storage technologies. With their addition, it is expected that the power flow optimization will change to minimize those losses.

Regarding the ESS, the modeled component was composed of measurement data, stemming from different tests. They don't represent a particular battery type. Further, most of the tests were performed on small-scale batteries, insufficient in size for the application. There are industrial methods to scaling the battery parameters. They have not been employed because they themselves rely on further tests to determine a battery scaling factor.

DATA SOURCES The wind profile was modeled using a statistical wind profile with a Gaussian distribution around the mean. Wind speeds typical for the North sea were taken as reference for the wind profile.

The consumption was modeled using data collected by Bendík ([63]) who sourced data on active and reactive power consumption of 1000 households in a single year. The data was further processed to characterize the mean hourly consumption of a single day. This time series data was used to modulate a constant consumption that modeled a base grid load.

The hub's component dynamics are thus shaped by empirical data, introducing some qualitative element to the project.

SOFTWARE To implement the simulation model, it was decided to use Matlab in conjunction with its Simulink and optimization toolboxes. The former is able to model complex grid dynamics and the latter provides solvers for formulated optimization problems. Further, the matpower toolbox invented by Zimmerman and Murillo-Sanchez ([64]) was utilized to generate a plant model. As this software is able to model complex grid dynamics and solve optimization problems, it was deemed appropriate for the project.

## 5.1 MATPOWER MODEL

The first implementation of the plant was undertaken using the Matpower toolbox ([64]). The toolbox was chosen because it can perform power flow optimization with out of the box components. Here, it is possible to customize them by defining a range of parameters. Furthermore, utilizing the Matpower Optimal Scheduling Tool (MOST) extension, components like wind generators and ESSs could be included. The Matpower model created for this project is in accordance with the scheme presented in figure 5.2 and congruent with the supplementary code.

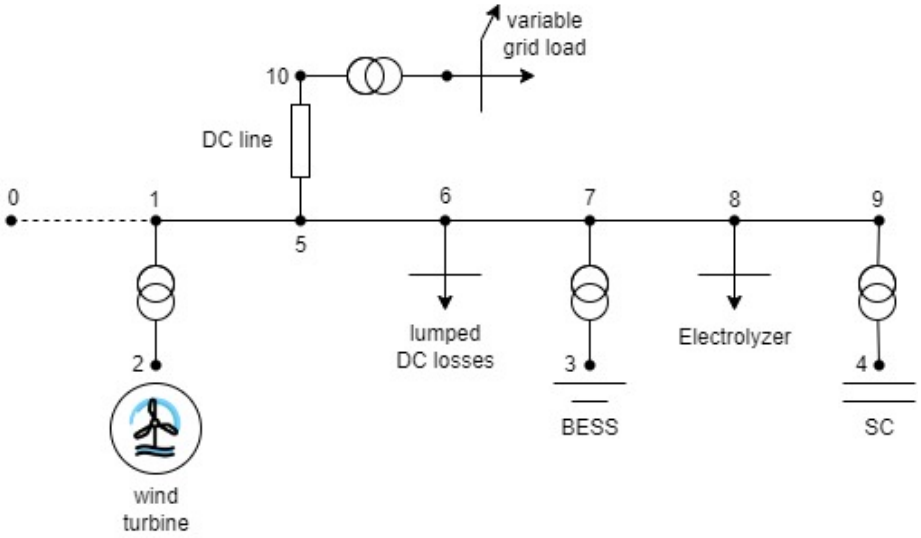


Figure 5.2: Schematic overview over the model implemented in Matpower. The dashed line represents the slack bus.

This model was not further used in the control implementation due to the absence of frequency dynamics in Matpower's optimization routine. Hence, no grid-forming technology could be integrated. A detailed discussion of the model is presented in app. B.1.1.

Despite the possible simplifications for the SSTO control layer, it was decided to first create a full scale model of the energy hub. It includes all production and storage components, as well as the consumption and losses to the environment.

## 5.2 OPTIMIZATION MODEL

Two takeaways from the Matpower model were the importance of the SSTO design in power flow optimization and the variety of timescales that influence the control layer. It prompted a shift of focus away from the plant modeling to the composition of an initial control design that could be transferred to and tested on a plant model.

The new approach consisted of two parts. In the first part, an optimization problem is formulated and solved. Its performance was analyzed as a sort of test design, optimizing over the prediction horizon for a single iteration.

In the second part, the designed algorithm is exported to run on a plant model which is able to provide sensor feedback on the plant dynamics. Tracking its behavior enables analysis of the controller performance on a simulated plant.

### 5.2.1 *Optimization model*

This setup was designed to solve an implicit optimization scheme. Due to the absence of the plant dynamics, information had to be known a-priori. Here, the sourced production and consumption time series data played a key role in fixing dynamic quantities that, in the simulation, depend on the grid dynamics.

The optimization was performed using the sourced data over a horizon of 24h. The control time step was taken to be 1h to be congruent with the data. Because a-priori information was required to model the predicted and actual consumption, data from different days was used. Its difference introduced a first element of uncertainty.

The intention of this implementation is the establishment of a working basis for the iterative optimization. Most adaptions of the objective function can be done here, showing their impact on the calculated solution.

### 5.2.2 *Plant model*

This part of the simulation combined a modeled plant with the control structure imported from the testing setup. In the first step, a plant model had to be constructed that fit the requirements of the designed energy hub. The second step consisted of the control implementation. Here, the imported controller was tied to sensor feedback from the plant and adapted to run over a rolling horizon scheme.

The plant model was required to contain an ESS model that can be controlled by changing the power setpoint. Underlying must be a structure that enables iterative solving of a formulated MPC problem. Most important is the modeling of the grid dynamics. Active and reactive power flow with according frequency and voltage changes is necessary. It should be possible to control these variables with a grid-tied inverter.

*Plant setup*

Various Simulink models provided by Mathworks ([65]) were considered on the quest of finding a suitable basis. In the database, it appeared that almost all models featured a 3-phase AC main bus on the RES side. Upon review, the model meeting the requirements and resembling the designed plant is provided by LeSage ([62]). It contained all the necessary elements, except that, alike the other models, the RES bus was 3-phase HVAC. Furthermore, the ESS model was integrated into a single component. The SSTO passes its power setpoint and SOC target value to the DO which splits the power point and generates the reference trajectory.

In the next step, the model was augmented to include a variable PQ load on the grid side, a coupling reactance, and a wind turbine as prime mover. The final plant design as basis for the SSTO optimization can be seen in Fig. 5.3. With such a model, it is possible to perform optimization under consideration of the grid dynamics, simulating changes in frequency, voltage, active, and reactive power.

System values, particularly the operating voltages, were kept the same as in the initial model.

SENSOR PLACEMENT The voltage, current, and power were measured at five different instances in the simulation. The first two are at the outputs of the wind turbine and ESS respectively. The third one is placed on the RES side before the inverter. The fourth sensor set is installed between the inverter and the coupling reactance. The last sensor can be found on the PCC, just after the coupling reactance. They will provide the data for the plots in the plant model optimization.

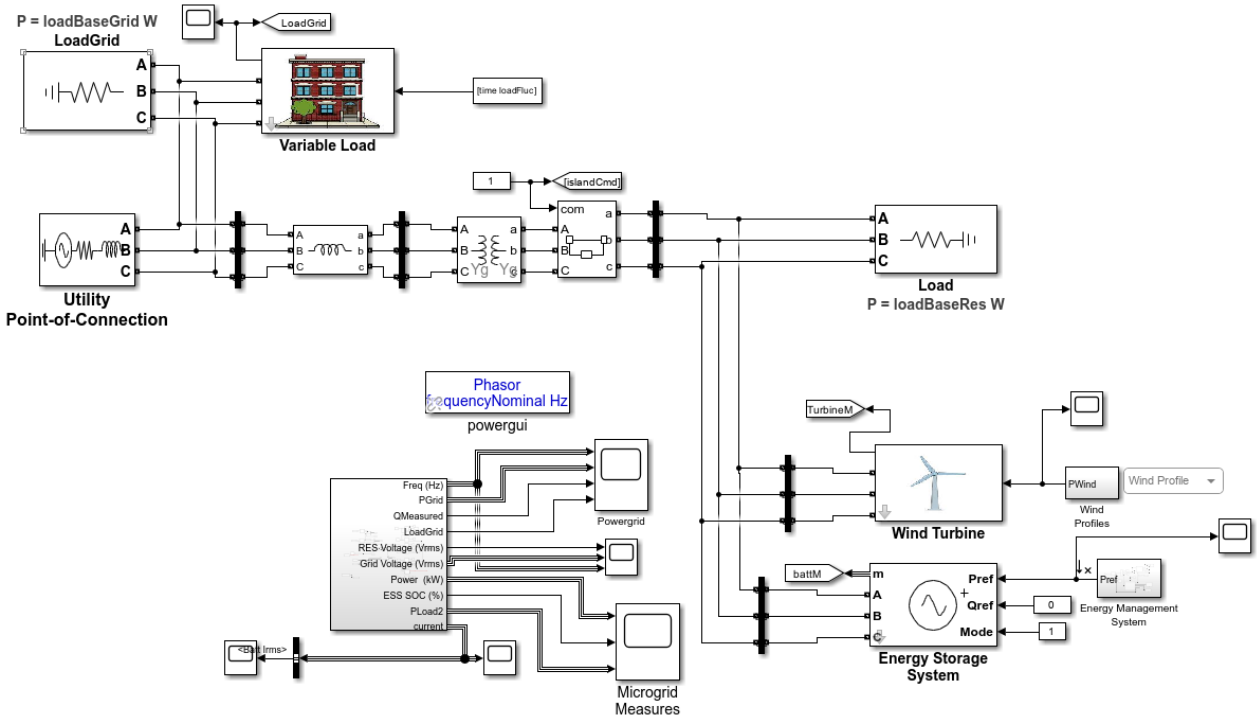


Figure 5.3: Screenshot of the Simulink model plant in the optimization.

# 6

# RESULTS AND DISCUSSION

The results and discussion chapter consists of three main bodies. First, the results section presents the key findings of each optimization and simulation model. Then, the implications of the results are discussed. Herein, the simulation findings are interpreted within the context of the design concept. Lastly, the limitations of the models are stated. They mainly pertain to the differences between the conceptualized plant and the implementation.

## 6.1 RESULTS

The results and implications are structured to present the optimization model first, pointing out the main findings. The findings are referenced to a more detailed description of these results and a detailed discussion in appendix B.2. Afterward, the simulation model is shown. It implements the optimization model following the same structure.

Due to a detailed discussion given in the appendix, it was chosen to include a more concise implications section. It briefly touched upon the most important aspects of the discussion.

### 6.1.1 *Key findings*

*Optimization model*

INITIAL FORMULATION The first form of the optimization model comprises the power balance equation (eq. 4.2), the ESS update law (eq. 4.3), and the voltage stability equation (eq. 4.4). The prediction and consumption values were taken from a predetermined time series.

This implementation provides the following insight. Firstly, the ESS update law successfully manages the storage levels, tracking the SOC (Fig. 6.1c). Secondly, SSTO's power balance equation can direct the power flow between the components, responding to demand variations. Thirdly, the voltage penalty term, added alongside the electrical power equation, can mostly maintain the nominal voltage and incentivize varying the power via current flow (Fig. 6.1b).

Disparate prediction and consumption values result in feasibility problems. This issue directly relates to the problem formulation with the single optimization variable $P_{ESS}$. It was found that one mitigation strategy is to increase the capacity of the ESS.

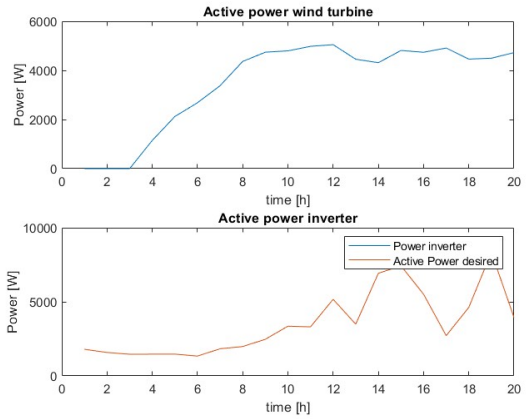


(a) Production and consumption quantities, top and bottom respectively.

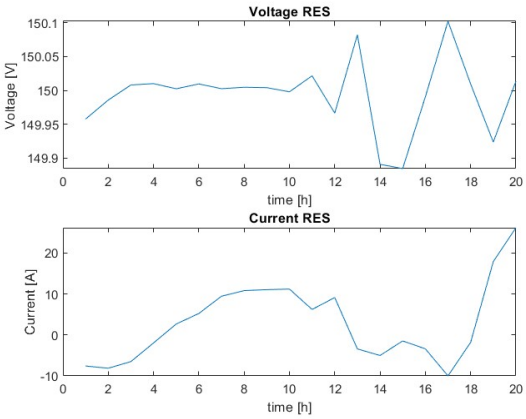


(b) Current and voltage plots.

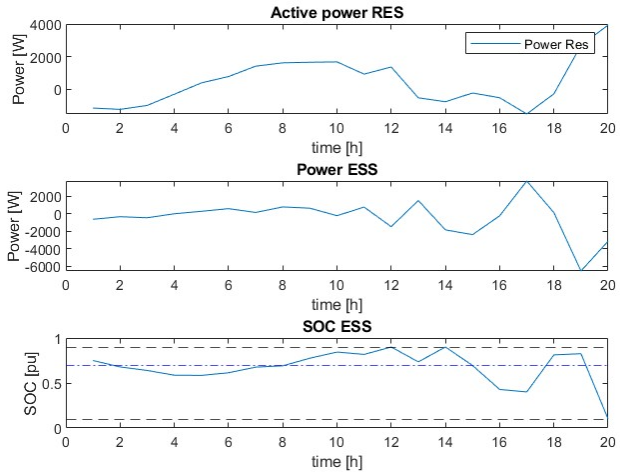


(c) Power flow and SOC of the ESS.

Figure 6.1: Plotted results of the initial optimization, where the prediction and consumption are the same.

The problem formulation, the expectation of the outcome, and some plotted solutions are discussed in detail in app. B.2.1.

POWER SETPOINT SHIFT This intermediary step shifts the setpoint of the initial formulation to enable its placement on the grid side. It aims to increase the controller's decision space. Introduction of the adjustment variable $P_{adj}$ strives to loosen the relationship between the fixed quantities and the decision variable $P_{ESS}$ and shift power peaks by penalizing large production-demand mismatches.

The results show that storage management is much facilitated, reducing the feasibility issues. However, it did not manage to shift said peaks. Further, without physical attribution, it was difficult to interpret the results. The relevant plots and discussion thereof can be found in app. B.2.2.

COUPLING REACTANCE This step augments the previous formulation to include the prediction term into the setpoint determination at the inverter (eq. 4.5) as well as the small-signal variation of the coupling reactance (eq. 4.6). With the addition of the relative power angle, the frequency at the inverter $f_{inv}$ complements the optimization variable $P_{ESS}$. Its goal is to attribute a physical quantity to the optimization variable, framing it with the coupling reactance equation.

Fig. 6.2 depicts the frequency deviations from the nominal value of 50Hz due to changes in power flow from the RES to the grid. These deviations buffer supply-demand discrepancies and enable accurate setpoint tracking.

The main takeaway from this augmentation pertains to the dynamics of the coupling reactance. The frequency term $f_{inv}$ can squander all previously experienced feasibility issues. Its incorporation by way of the coupling reactance seems essential to the optimization. However, in the absence of grid dynamics, the frequency variable is insufficiently constrained. Because its value directly changes with the power flow on the grid, it can buffer any discrepancy between production and demand. Detailed results of the optimization are presented in app. B.2.3.

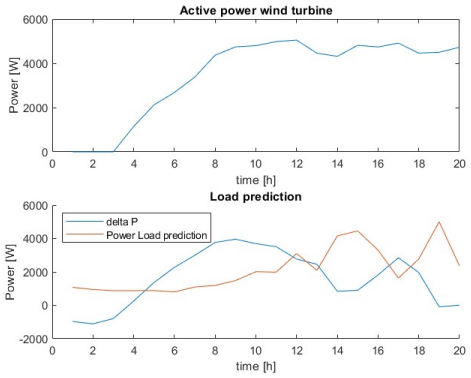


(a) Power production and prediction of the load as well as the adjustment due to the reactance.

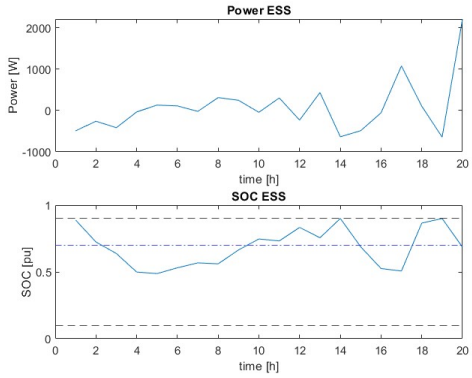


(b) Power flow and SOC of the ESS.

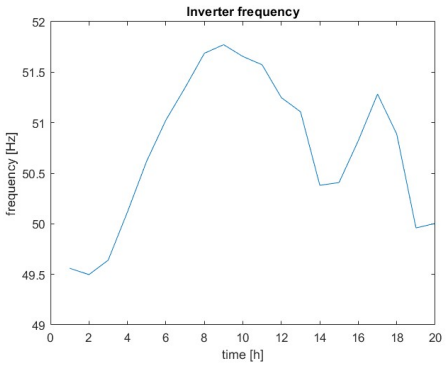


(c) Frequency at the inverter.

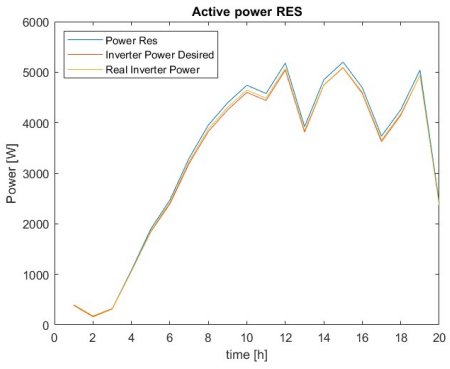


(d) Active power flow on the RES and inverter along with the setpoint at the inverter.

Figure 6.2: Plotted are the results of the optimization with a frequency optimization variable included.

DROOP CONTROL Finalizing the implementation of the mathematical model, the power angle extended by the droop gain formulation (eq. 4.7). This variation removes $f_{inv}$ as an optimization variable and estimates the frequency variations based on power fluctuations.

The results of Fig. 6.3 display the significance of the droop gain. The literature values did not seem to affect the solution. Increasing the droop gain changes the power flow at the inverter and across the reactance. It shows that the frequency term and droop gain in the problem formulation can influence the power flow across the inverter. A more elaborate description of these results can be found in app. B.2.4.

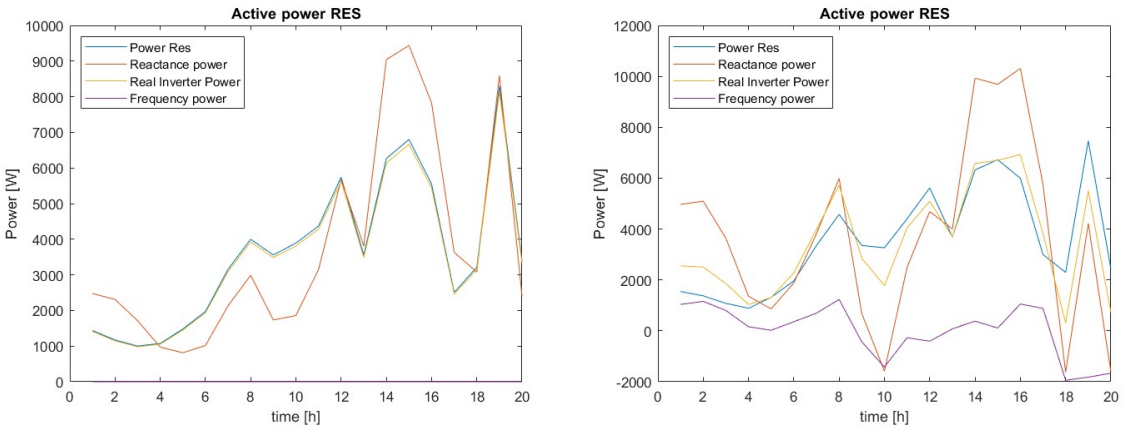


(a) Power flow from the RES to the grid with an explicit display of the power flow due to frequency fluctuations.

(b) Power flow from the RES to the grid with an explicit display of the power flow due to frequency fluctuations.

Figure 6.3: The plots compare the power flow for variations of the droop gain. The theoretical gain $m_P = 1\%$ (left) and its increased value of $m_P = 10^4\%$ (right).

GENERAL REMARKS Throughout the optimization, the NCO and the absolute function value at the end of each optimization were tracked. They supported estimating the quality of the solution approximation.

To establish the power voltage relationship and penalize voltage deviations, the electric power relationship P=VI was used. Consequentially, a nonlinear solver (Matlab's fmincon) was applied to the problem formulation. It was not investigated how the solution changes due to it.

*Plant model*

Results of the different versions of the optimization model on the plant are briefly shown here. The optimization routine is performed over a horizon of 20h with 30 min control steps, iteratively determining optimal ESS power and SOC setpoints. Additional observations of the optimization model are presented here. Detailed exhibition thereof can be found in app. B.3.

INITIAL FORMULATION Investigation of this version is performed on the simulation model before the coupling reactance component is added to the plant setup.

The power setpoint synthesized by the SSTO is passed to the ESS. With it, the power flow can be controlled, directing power to the grid, and influencing its behavior (Fig. 6.4a). Due to excess demand, the ESS is discharged until its lower limit. Fig. 6.4b shows that the hard constraints are successfully maintained by the algorithm as the ESS ceases to output power.

Storage management could be influenced by changing the optimization weights. Introducing soft constraints enables more accurate control over the SOC, disincentivizing deviations from the SOC reference. Differently, raising the weight of the inverter reference came at the expense of SOC tracking, degrading setpoint maintenance due to a lower relative weight. The detailed examination of these results is discussed in app. B.3.1.

COUPLING REACTANCE The physical coupling reactance is included into the plant model along with its equational pendant from the optimization. Its aim, is the dynamic decoupling of the hub and the grid. With the goal of voltage control, the electrical power law is reintroduced to penalize voltage deviations from the nominal value. It was deemed necessary as a complementary component to the coupling reactance equation.

Gauging from the plots of Fig. 6.5, the addition of the coupling reactance achieves some dynamic decoupling between the hub and the grid. It was observed that larger inductance values decrease the coupling. Frequency spikes occurring due to power setpoint changes can be seen to disappear on the grid side. It becomes especially clear as the ESS reaches its lower limit. Here, the negative frequency spike is attenuated on the grid.

Approximation of the electric power law with the McCormick envelope did not have the desired effect. Penalizing voltage deviations in the optimization function had no visible impact on the grid voltage. The detailed result section is shown in app. B.3.2.

MEASUREMENT It is desirable to use measurements from the PCC to improve the estimation accuracy of the optimization algorithm. To find the desired inverter setpoint, eq. 4.5 was implemented to. It balances the composition of the setpoint, sharing between a measurement and a prediction term.

This iteration successfully incorporates plant feedback into the optimization algorithm. Variations of the balancing variable $\lambda$ show that the power flow can be altered, showing the best results for $\lambda = 0.65$. Still, frequency spikes can be observed to occur at every ESS setpoint change. App. B.3.3 delivers a detailed review of the results.

SMALL ANGLE APPROXIMATION Finally, the droop control law of eq. 4.7 made it into the simulation environment. Due to the nonlinearity stemming from the reactance term, its small angle approximation was taken. The approximation step was undertaken because the solver could not find a solution to the formulated problem.

Observations of the grid behavior show different frequency fluctuations compared to previously (Fig. 6.6a). That is mostly due to lower setpoint fluctuations. The frequency spikes correlate with the zero power output from the ESS reference. This occurred because

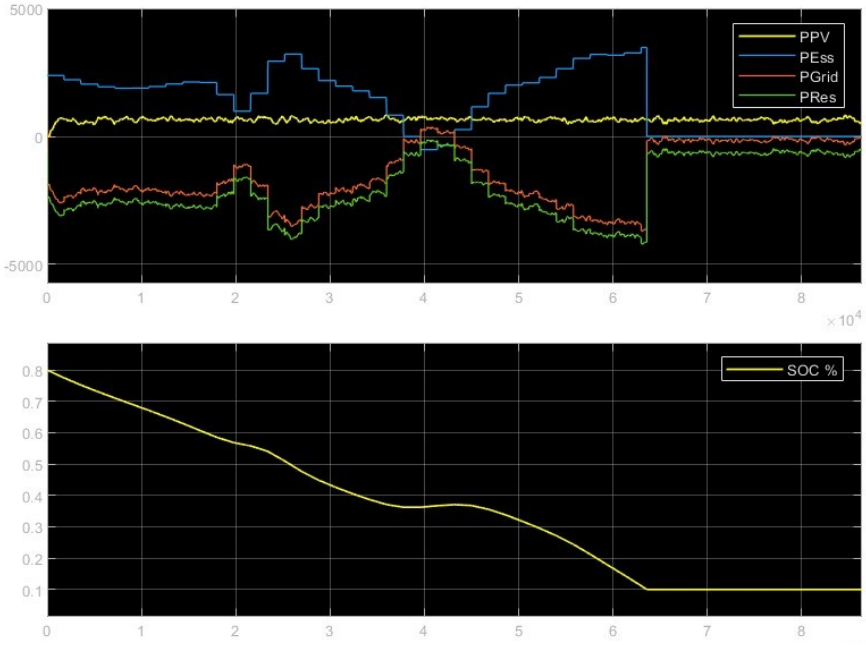


(a) Power flow through the different measurement points and SOC.

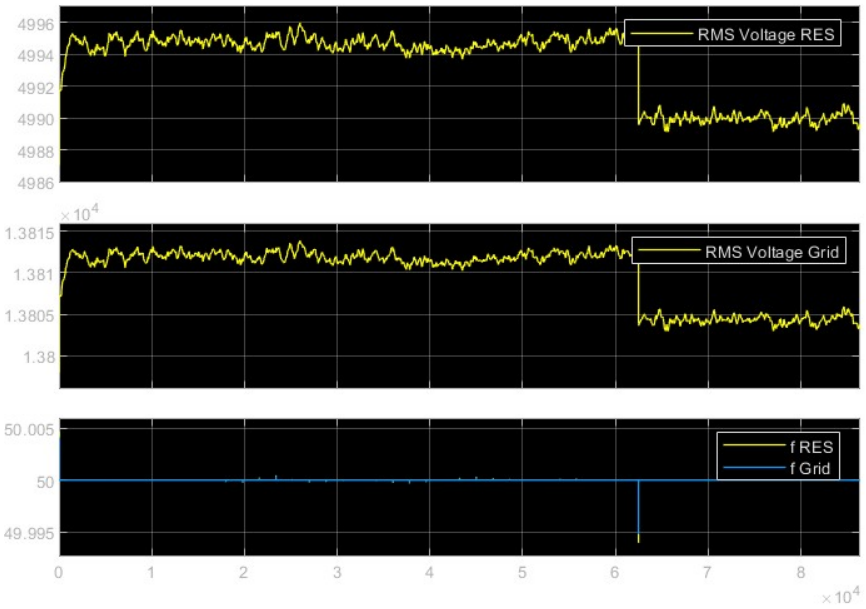


(b) Voltage and frequency plots on the RES and grid.

Figure 6.4: Model-based optimization

the solver could not find a timely solution in this iteration (Fig. 6.6b). Once again, a detailed showing of the results is added to app. B.3.4.

GENERAL REMARKS There are two differences between the designed and simulated plant model. They both pertain to the power transfer from the ESS to the grid.

The first difference is the fact that the RES side in the simulation was operated with AC power. Due to that, the inverter did not newly synthesize the 3-phase power on the grid side. The component did not allow explicit control of the power angle to vary the ratio between the active and reactive power.

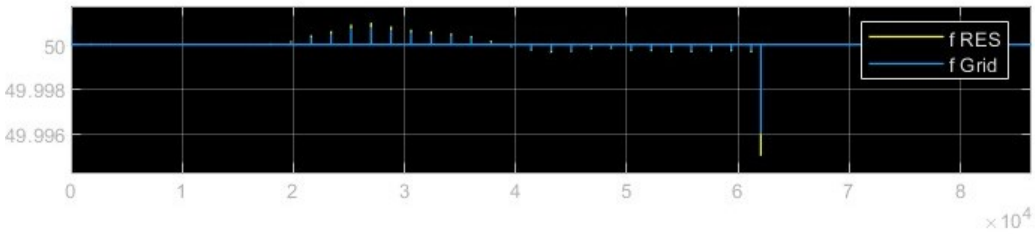


(a) Frequency spikes for an inductance value of L=0.0002H.

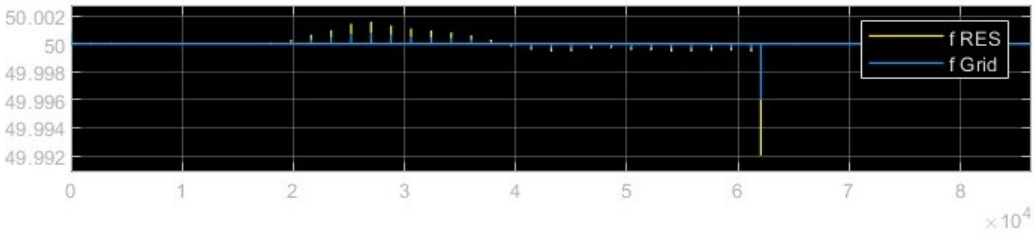


(b) Frequency spikes for an inductance value of L=0.002H.

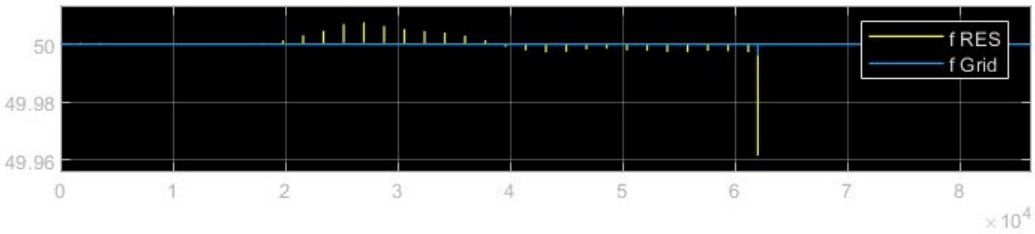


(c) Frequency spikes for an inductance value of L=0.02H.

Figure 6.5: Frequency spikes due to ESS setpoint changes.

The other difference lies in the ESS itself. It could be controlled in two modes: grid-forming and -following. The desire to stabilize the grid would suggest operating the ESS in grid-forming mode. However, the mode discards any power setpoint input so it was not possible to use it in conjunction with an optimization scheme. The grid-following mode does not contribute towards voltage or frequency stability.

## 6.2 IMPLICATIONS

This section is intended to discuss the results' implications for the concept, application, and context. The order is grouped by theme.

*Feasibility*

Some of the findings have implications for the feasibility of the optimization. It is apparent that in a small feasibility space, as created by the initial optimization with $P_{ESS}$ and two fixed quantities, no solution could be found for some cases. They highly depend on the accuracy of the prediction.

As the ESS capacity is increased, more erroneous predictions still yield feasible solutions. Regarding the conceptual setup, the inclusion of the $H_2$ system would be beneficial as it can support a smaller BESS as well as the optimization.

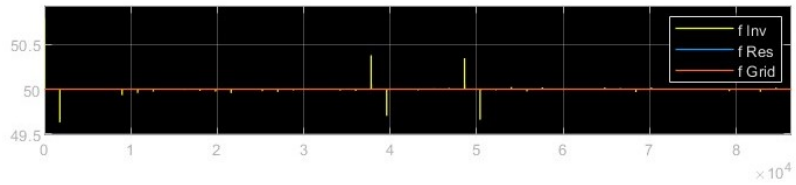


(a) Frequency plot of the RES and grid.

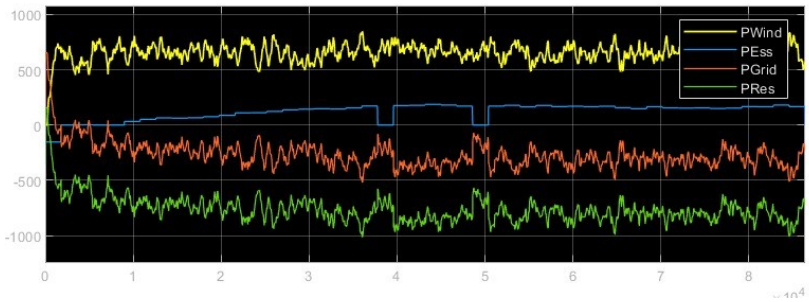


(b) Power plots on the RES and grid as well as ESS power setpoints.

Figure 6.6: Small angle approximation of the coupling reactance dynamics in the optimization function.

APPROXIMATION Both the McCormick envelope and the small angle approximation of the coupling reactance brought up their own set of challenges. Neither was able to fully solve the numerical issues associated with the nonlinear nature of the approximated equations. Their utilization in the simulation model was insufficient to reproduce the previous results seen in the optimization model. Lacking setpoint solutions, the system potentially operates under highly sub-optimal conditions.

MCCORMICK ENVELOPE The McCormick envelope would either not have any effect on the simulation plots or produce numerical issues. Loosely defined boundary conditions would result in the former and tight limits would amount to the latter. Essentially, the electric power law could not be applied in this context.

FUNCTION VALUES Tracking the NCO and absolute function value mainly confirmed that the optimization model was formulated too rigidly. The introduction of further optimization variables minimized those values by factor $10^4$.

The predictions used in the optimization also had a significant impact on the function values. It appeared as if they largely depended on the similarity between the production and prediction of consumption.

*Frequency fluctuations*

It was shown that the frequency variable in the optimization model behaves in accordance with the grid inertia law. However, with the introduction of grid dynamics, it was not possible to transfer the frequency control to the simulation model. ESS setpoint changes induce frequency spikes which were not counteracted by the optimization algorithm. Depending on their magnitude, they have the potential to be detrimental to grid stability.

Frequency fluctuations between setpoint changes were observed. They occur on a timescale too short for the SSTO to have any impact on them. It highlights the necessity for the DO layer for two reasons. Firstly, to attenuate these fluctuations, and secondly, to limit the ramping of the ESS output. The latter is believed to diminish the frequency spikes as a consequence of ESS setpoint changes.

It should be noted that the grid measurements used in the optimization were instantaneous. They relayed the last measured sample to the algorithm. This way, large variations can enter the optimization. In the concept, it was suggested to perform some form of batch optimization.

Finally, due to the limited availability of coherent grid measurements, optimization without modeled grid dynamics proved difficult. However, it should be possible to utilize the problem formulation in the state observer to improve the accuracy of the SSTO in the hierarchical model structure.

### 6.2.1 *Design concept*

Overall, the simulation delivered some proof of the necessity of the components presented as part of the concept. The simulation's findings are interpreted to argue what each of these elements contributes to the setup.

SSTO Judging from the simulation, the SSTO is able to balance the power flow between the hub components and synthesize a power and SOC setpoints. It executes these tasks by combining prediction and measurement quantities to alter power flow to the grid by way of controlling the ESS output.

GNO It has been shown that the accuracy of the solution has a dependency on the consumption prediction. Because the GNO is intended to integrate long-term predictions, it should be able to diminish the prediction error as part of the operating point determination.

HYDROGEN A different approach to increasing the feasibility of the solutions in the SSTO is an increase in storage capacity. Large-scale storage from the $H_2$ cycle can actively balance the BESS's SOC and help the solution finding.

DO The frequency fluctuations, especially those occurring between setpoint changes, should be attenuated in the DO layer. It was seen that these disturbances were present on such a short timescale that they can better be addressed by the DO in conjunction with a SC, equipped with quick ramping capabilities.

RR CONTROL In the simulation, drastic power setpoint changes induce frequency spikes. Limiting the RR of the storage minimizes these spikes. Although not shown in

the simulation, coordination of the three storage elements requires power and RR control. Especially to steer rapid power adjustments towards the SC.

OBSERVER As instantaneous measurements were taken, uncertainty is associated with the feedback from the plant to the optimization algorithm. The frequency of the measurements is much higher than that of the optimization so it is likely that batch optimization, enabled by the observer, would improve the quality of the feedback.

## 6.3 LIMITATIONS

A crucial aspect of scientific research is the acknowledgment of limitations to the expressiveness of one's work. It is important to recognize their value to interpret results and use them as an incentive for further research.

### 6.3.1 *Comparison*

Two major limitations were encountered in the process of comparing the two environments. Firstly, the comparability of the two models on the data used is limited. And secondly, the utilization of plant feedback influences the optimization.

DATA The production values for the wind turbine are drawn from the same statistical wind profile. However, they are not identical. Further, the load curves used in the models are not the same. This circumstance complicates the transfer between the two environments, limiting the added value of a direct comparison.

MEASUREMENTS Transfer to the model-based environment proved difficult for two reasons. At first instance, what was pointed out as a limitation in the optimization model, was the absence of grid dynamics and feedback thereof. Especially parameters, such as the grid frequency and voltage, limited the determination of the reactance dynamics. With nominal values replacing these parameters, some variables had a much higher correlation than anticipated.

To create some dynamic relationships, elements, like the electric power equation and the reactance itself, were added to the optimization environment. It prompted the use of a nonlinear solver, differing from the theory and implementation in the simulation environment. Its effect was not investigated within the scope of this thesis.

### 6.3.2 *Simulation design*

With a novel introduction to power electronics and power system modeling, some challenges are encountered in the simulation setup. It should be noted that the time allocated to plant modeling was considerable, yet insufficient, considering the focus on the control

aspect of the work. In the process, these reservations limit the scope of the results presented in this thesis.

STORAGE A shortcoming of the storage modeling was discovered. Here, the modeled ESS could be either set to grid-forming or grid-following mode. In the former case, the ESS, the unit compensates for active and reactive power flow without stabilizing the voltage and does not utilize the reference provided. The latter case prohibits active control of the power angle and voltage. Thus, neither variable can be actively stabilized by the devised droop control strategy.

INVERTER A further point of contention is the inverter component in the Simulink model. Since no DC to 3-phase HVAC conversion was done by the inverter, it was not possible to gain control over the power angle and the voltage magnitude at its terminal. This circumstance was found to be essential for the droop control to succeed.

REACTIVE POWER With time as a limited resource in this thesis, the reactive power control was not implemented in the simulation. Its addition would be greatly beneficial for the voltage stabilization on the grid. Fortunately, with the application of the small-angle theory (sec. 2.3.1), it was possible to decouple the active and reactive power control without major compromises.

PARAMETRIZATION The time-consuming task of accurate component parametrization and plant scaling was limited to determining core parameters that were deemed essential. Others were transferred from the initial plant model. As a result, the optimization and simulation environments don't operate on the same voltages and power magnitude. To accommodate these differences, production, storage, and consumption were scaled accordingly.

These limitations also extend to the system boundaries, often defined by the components' operating limits. When inaccurately parametrized, they vastly change the feasibility space, yielding cases with numerical issues. With clearly defined boundaries, mathematical formulations like the McCormick envelope might add more value.

# 7

# CONCLUSIONS AND RECOMMENDATIONS

## 7.1 CONCLUSION

As traditional means of energy generation become obsolete, research focus has shifted to the discovery of novel means to stabilize the electricity grid. In this thesis, an optimization-based strategy has been investigated to determine how its employment can optimize energy storage and power flow.

The first part of the work explored several key issues. They pertain to the energy grid and the control strategy.

Regarding energy generation and delivery to the grid, a RES poses several challenges. First, wind energy is uncontrollable and displays large variations throughout its dynamic range. Matching this kind of production with an uncertain demand becomes even more challenging than previously. Secondly, fluctuating production in conjunction with dwindling grid inertia can be detrimental to the stability of the energy grid.

A solution approach is the installation of ESSs. Such, intermediary storage must be actively regulated to fulfill its task of buffering excess production. For its control, it is necessary to capture its internal states and dynamics. However, modeling such nonlinear and immeasurable internal states introduces uncertainty. As a result, the modeled and real components do not match.

Combining an MPC structure with coupling reactance and droop control, this thesis addresses the challenges of reliable power delivery while stabilizing the local grid. This work investigated how these two concepts can be leveraged to manage the power of a designed energy hub.

### 7.1.1 *Highlights*

A novel 3-stage hierarchical MPC strategy with an integrated energy hub design has been proposed. Together, they incorporate three storage technologies. The assembly optimizes the power flow within the hub and to the grid. Therewith, it can meet active and reactive power demands in the short- and long-term while stabilizing the grid's voltage and frequency.

*Concept*

The design leverages the singular perturbation theory to achieve a separation of timescales. It achieves the disentanglement of plant and disturbance dynamics, ranging from fractions of seconds to several months. They are assigned to one of the three MPC stages, namely the global nonlinear optimization (GNO), the steady-state target optimization (SSTO), and the dynamic optimization (DO), responsible for long-, medium, and short-term optimization. Their respective control optimizes one of the three storage technologies: an $H_2$ setup, a BESS, and a SC. The hub's conceptual innovation lies in its combination. The main features are summarized as follows.

ENERGY STORAGE Each type of storage is required for a specific purpose. Due to its large capacity and slow dynamics, the $H_2$ setup is used to overcome prolonged wind droughts. Daily production and demand discrepancies are balanced by the BESS, distinguished by its high cyclic lifespan. The SC is installed to handle fast-acting disturbances, buffering split-second power flow changes.

EVENT FORECAST The 3-stage MPC design enables the utilization of production and demand forecasts to improve energy management. They minimize production-demand mismatch in the long-, medium-, and short-term. Predictions of seasonal trends, daily variations, and local sensor data aid storage optimization in the respective layer.

STEADY-STATE TARGET OPTIMIZATION This layer is novel in the context of the designed energy hub. It links the other control layers, the wider plant, and the grid. Tasked with maintaining the hub's power balance, it synthesizes static power setpoints for the DO to follow. Functionally, it optimizes the power flow to the grid and is thus subject to the simulation study.

CONGRUENCE The power of this control structure lies in the ability to refine complex, large-scale computations into simple setpoints. Firstly, the GNO layer optimizes an accurate plant model over a long prediction horizon, devising a trajectory for the plant to follow. With a control step length of 24h, this trajectory is used as an operating point for the SSTO layer. It quadratically approximates the setpoint, improves the prediction with day-ahead forecasts, and calculates the power and SOC setpoints. Consequently, the linear DO layer determines the optimal trajectory to follow these setpoints. Due to its simple formulation, it has a short computation time and can leverage sensor data to compensate for fast-acting disturbances with SC power flow.

RAMP-RATE CONTROL Integrating the novel assembly of storage components, a triple split ramp-rate (RR) control design is proposed. It details how the application of RR control splits a common power reference to optimize the power flow of each storage component. Therein, the power reference is passed through two LPFs, dissecting the moving average

of the power reference. The LPFs are designed to complement the storage components' dynamics and to provide virtual impedance, facilitating power sharing.

*Math model*

The mathematical formulation of the SSTO layer comprises a quadratic objective function and linear constraints. It mitigates uncertainty by diminishing modeling differences between the nonlinear GNO and the linear DO layers.

DROOP CONTROL Contributed is the mathematical formulation of the SSTO layer, integrating equations for the coupling reactance with droop control in objective function form. It enables the prediction of power flow variations due to changes in frequency. With it, compensatory action can taken by the MPC, adjusting the power flowing to the inverter. This way, frequency fluctuations can be minimized, stabilizing the grid.

*Simulation*

The main objective of the SSTO is the determination of optimal steady-state setpoints. As part of the simulation, this layer is modeled to investigate how the addition of the coupling reactance and droop control affects the power setpoint synthesis. Therein, the influence of the grid's frequency variations on the coupling reactance and the setpoint determination is investigated.

OPTIMIZATION MODEL This model provides insight into the system behavior without reliance on system dynamics. The formulation leverages equations describing the power balance and ESS power flow to determine setpoints in the SSTO layer.

With it, it was possible to implement the mathematical model, balancing prediction and measurement to synthesize the inverter power setpoint. With the application of the small angle theory, the active power setpoint on the RES side was synthesized. Simultaneously, the SSTO found a SOC reference. Altering the droop gain, magnitude adjustments of the power flow due to frequency fluctuations were achieved.

In the absence of a plant model, constraining the problem proved challenging. Especially, concerning the grid dynamics, the interaction between power, frequency, and voltage, could not be modeled accurately.

PLANT MODEL The formulated optimization problem was exported to the simulation model to test its interaction with the hub design and the influence of the grid dynamics. The optimization was performed iteratively, recalculating with new information available.

By incorporating prediction values and some degree of uncertainty, the objective function and constraints were tested for feasibility. Since the problem was newly set up and constrained, numerical issues could be eliminated in a controlled environment.

With the presence of the coupling reactance dynamics in the SSTO objective function, the RES setpoints were successfully altered. They were devised from a grid-side inverter reference which tracked a dynamic demand profile. Thus, the SSTO can leverage day-ahead

consumption forecasts and measurement data to synthesize power and SOC setpoints for the ESS.

Challenges arose due to the nonlinear nature of the coupling reactance. They were approached by employing various approximation techniques. With them, it was possible to fit the equation set into quadratic objective function form. The consequence was losses in accuracy.

### 7.1.2 *Significance*

SIMULATION The coupling reactance is crucial in diminishing the dynamic coupling of the RES and the grid. It permits control over the grid's active and reactive power, as well as the frequency and voltage. The SSTO can adjust the RES power flow, not only due to active power demand but also due to frequency fluctuations. Although not proven in the simulation, the mathematical model suggests the same for the reactive power and voltage. By actively regulating these four grid parameters, it is possible to respond to a dynamic demand while contributing towards stabilizing the grid. The simulation was a first step in showing the functionality of droop control in an MPC structure.

In the simulation, feasibility issues due to limited storage capacity were observed. Further, the BESS could not sufficiently suppress frequency fluctuations. The integrated ESS storage concept with RR control can address these challenges with limited storage capacity and power density. With it, long-term production-demand discrepancies are overcome. It also responds to short-term fluctuations on the grid, stabilizing the RES voltage by rapidly adjusting the power output. The $H_2$ cycle and the SC can address these respective issues.

Essentially, the simulation provided proof for all conceptualized components. The examination and interpretation of its limitations showed that the operational flexibility, grid stability, and hub longevity are improved by the proposed controller-hub design.

CONCEPT The 3-stage MPC effectively minimizes plant-model mismatch at the lowest layer without compromising stability from increased computation time, making it fit for real-time implementation. Because the upper two layers optimize longer-term targets, they can ensure a stable power supply from an uncertain energy source.

Together, they make a crucial contribution towards reducing grid congestion by balancing supply and demand. Increased energy flexibility permits more RESs to connect to the general electricity grid. An active stability contribution promotes the implementation of decentralized RES at an industrial scale.

The application of droop control has been described as an important element in facilitating the large-scale deployment of inverter-based technology on the grid. It relies exclusively on local measurements and foregoes the need for communication with the wider network. This way, it constructively contributes to locally stabilizing the grid while meeting a given power demand. Its inclusion in the control structure enables the RES hub to be connected to the grid without compromising stability.

This control structure permits installed energy hubs to be integrated with existing infrastructure. Its implementation in offshore energy production can help the Netherlands advance its green goals towards a low-cost, emission-free energy landscape.

## 7.2 RECOMMENDATIONS

Provided are some recommendations for further research. Their investigation could help bring the design closer to reality.

**SIMULATION MODEL** Due to the relatively long control step, the SSTO could not effectively eliminate frequency fluctuations. It would be recommended to implement the droop control in the DO layer and determine what improvements its management of the frequency characteristics could offer.

**PARAMETRIZATION** The author would like to point to the added value of accurate component parametrization and sizing. A scaled plant model with constraints of all components will likely influence the set of feasible solutions.

Similar adjustments of parameters, such as the prediction horizon length and objective function weights, can significantly change the control output.

**APPROXIMATION** With multiple approximation techniques used to implement equations, the accuracy of the results is expected to suffer. It would be beneficial to investigate the effective loss in optimality.

**3-STAGE** Simulation of the GNO and DO layers would be of tremendous value. Their functioning and interaction with the SSTO layer can be investigated.

Lastly, the feasibility and effectiveness of the then-simulated concept would profit from validation using real-world data as part of a case study. It would be a major step towards bridging the gap between theory and practice.

# A

# APPENDIX 1

## A.1 LITERATURE RESEARCH

### A.1.1 *Grid stability issues*

*Nominal grid frequency*

The European electricity grid has been agreed to operate at a nominal frequency of 50Hz at all times. Normally, this frequency is generated by electric motors that rotate at exactly 50Hz. They are large synchronous generators. Because deviations could damage sensitive electrical loads, margins are very tight. Therefore, compensatory action is taken starting at deviations of 10mHz, with allowable long-term deviations of 180mHz. At fluctuations of 800mHz or more, the grid risks failure operation causing blackouts. The fluctuations are initiated by changes in grid loading. Adding a load to the grid will strain an electric motor, briefly causing it to spin slower, dropping its frequency. Conversely, if a load is removed, the grid frequency will spike as the electric motor's speed increases. Significant load changes can cause massive frequency fluctuations.

Historically, it has been discovered that fluctuations have a non-Gaussian distribution around the nominal frequency. Apparently, it is more likely to have more extreme fluctuations, aggravating the grid stability issue. [5, 66]

*Ancillary services*

To guarantee the stable operation of the electricity grid, grid operators provide uncompensated ancillary services. They entail the provision of passive inertia that facilitates control aiming to maintain the prescribed grid frequency after load changes.

Usually, it is achieved with these synchronous generators which often convert energy from burned coal or gas to electricity. They are often referred to as slack buses. They dictate the grid frequency which is used as reference for grid-following components. Due to their massive associated inertia, the stored energy in the mass can temporarily compensate load changes. The grid operator gains valuable time to steer the frequency back to its nominal value. It is especially important as the primary frequency response largely relies on mechanical systems which are quite slow to respond. [16, 67]

GRID STABILITY CONTRIBUTION In general, the transmission system operator (TSO) is responsible for the stability of the energy grid. They must balance production and demand.

The TSO manages the demand side and balances the anticipated demand by procuring energy from the producer. To guarantee stability and supply, it is crucially important for the producer to deliver the demanded energy. As the management of this critical piece of infrastructure is highly delicate, large-scale producers must obtain an energy license. Before acquiring such a license, the producer must show that they are able to reliably deliver energy to anyone who requests it. Additionally, due to the dwindling grid inertia, energy producers are required to contribute to the stability of the energy grid. According to recent lawmaking, they must contribute to maintaining frequency and voltage margins on the grid. Thus, for RES to succeed on the market, a steady energy supply and grid stability contributions are of utmost importance. [68]

### A.1.2 *Geographical expansion*

One way to introduce more flexibility into an energy distribution system is through geographical expansion. First and foremost, when only considering a single type of energy source, geographical expansion allows the inclusion of multiple regions with different weather conditions. In the example of wind power production, distributed areas have a higher statistical chance that one location is able to produce power. Building interconnected transmission networks then permits power sharing. [14, 15, 31]

FLEXIBLE TRANSMISSION NETWORKS Geographical expansion as means to increasing system flexibility is not solely important for local power-sharing in an islanded grid but also on an international grid scale. With distributed production, the installation of flexible transmission networks is vital in balancing a large-scale energy grid. It would immensely expand geographical access to weather-diverse locations. [13, 31]

CONSUMER CENTERS One issue in the renewable energy production is the large coastal population density in Europe. High building density and environmental restrictions disallow the installation of large-scale renewable energy production resources. Such lack of space is especially prevalent in the Netherlands. According to Eurostat ([69]), 95% of the population lives within 50km of the shore. Simultaneously, they are the locations with the highest on-shore wind speeds and the most potential for wind energy production. [70, 71] Thus, to maintain proximity to consumers centers, the Rijksoverheid ([17]) looks to produce renewable energy off the shore.

OFFSHORE WIND POWER A very promising means of energy production is achieved through the installation of offshore wind farms. With this technology, coastal countries like the Netherlands are able to generate green energy, making up a significant share of their energy mix. The Rijksoverheid ([17]) estimates that by 2030, 75% of all the current electricity consumption in the Netherlands will come from offshore wind turbines. This circumstance is incredibly consequential as Dutch renewable energy production's operational flexibility will be strikingly low. That is because production and geographical diversification are

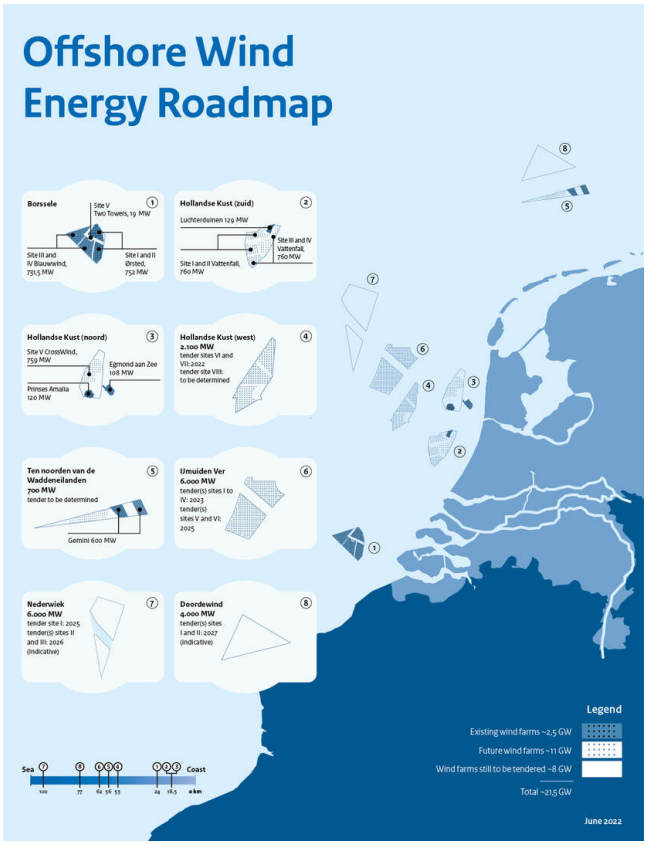


Figure A.1: Existing and future offshore wind farms in the Netherlands. [17]

shallow. This can be verified in Fig. A.1 where almost all present and planned production sites are concentrated in great proximity to each other in the North Sea.

Heterogeneous production in the Dutch energy mix creates a dire need for grid-aware technology that provides stability and a balance between production and demand.

CONTEXT The designed application in the following chapters is presented in the context of a current location-specific issue. More precisely, challenges in the energy transition faced in the Netherlands are used as an example to to quantify the magnitude of the issue in context. Such understanding is non-trivial.

### A.1.3 *Battery challenges*

NONLINEAR DYNAMICS Oftentimes, the dynamics of many storage systems (especially battery systems) are highly nonlinear. Such nonlinearities are inherent to internal electrochemical reactions. Perfect knowledge of their internal processes would be ideal for control. Thus, in the effort to accurately capture their dynamics, models can become almost arbitrarily complex. However, such a high degree of accuracy sacrifices valuable computation time. Therefore, to limit the increase computation time, some dynamics are linearized. In the process, accuracy concessions are made as discrepancies between the component and its model can be expected. [34, 72]

PARAMETER UNCERTAINTY The accuracy loss due to the approximations of internal processes has collateral effects. Inaccurately estimated system states can result in scenarios where control action is taken based on erroneous information. Here, the event of uncertain losses is one major reason. Next to that, some crucial parameters like the state of charge (SOC) are immeasurable *in operando*. Potential consequences from constraint violations and sub-optimal operation are diminishing components' longevity and potential harm to the safety of the system and its environment. [73]

### A.1.4 *Grid variables*

ACTIVE POWER This component of the apparent power is the power that is able to perform productive work. A load will consume this energy to operate. This true power is measured in kilowatt (kW). [28]

REACTIVE POWER This power component flows back and forth in the AC circuit. It is unable to perform work and is the result of inductive and capacitive loads in a circuit. For example, any electrical component that functions using a coil or electric motor is an inductive load. Due to the loads' respective properties of opposing change in current and voltage, switching them off causes a spike in voltage. Respectively, inductive and capacitive loads produce either a phase lag or lead.

In principle, the ideal capacitor is defined as $i = C\frac{dV}{dt}$. When charge accumulates on the capacitor plates, a difference in voltage potential across the plates is built up (fig. A.2). As the potential difference is a result of current flow, the current leads the voltage. In the ideal case, the phase difference is $-90°$ if the voltage sine wave is established as reference. It originates from the fact that the current peaks where the change in voltage is maximum. Figure A.3 shows this interaction for an ideal capacitor. Clearly, the current leads the capacitor voltage. Inductive loads are complementary to this behavior.

The power reflected by a reactive load as a result of a phase difference is the reactive power (Q). Such a reactive power component is often undesired as it strains the grid without performing work. Accordingly, it is profitable to reduce the phase difference between voltage and current. It minimizes the reactive power occupying grid capacities. Finally, using phasor representation, figure A.4 depicts how the phase angle is determined in the inductive and capacitive scenarios. [28, 74]

THE POWER FACTOR The apparent power $S = \sqrt{P^2 + Q^2}$ (kVA), relates the active and reactive power. Due to the presence of inductive and capacitive loads, some power is reflected back into the grid. The power factor quantifies the share of apparent power as $pf = P/S$ with values between 0 and 1. It is a different representation of the phase angle.

In terms of energy generation and the infeed into the grid, meeting the demand of both complements is vital for grid stability. Especially because these parameters also influence the grid voltage and frequency. GFMIs with active power and voltage control are able to

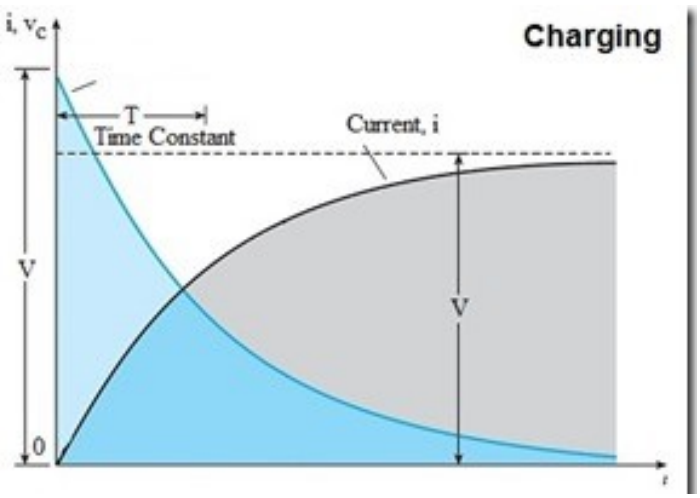


Figure A.2: Voltage and current relationship in a charging capacitor. [75]

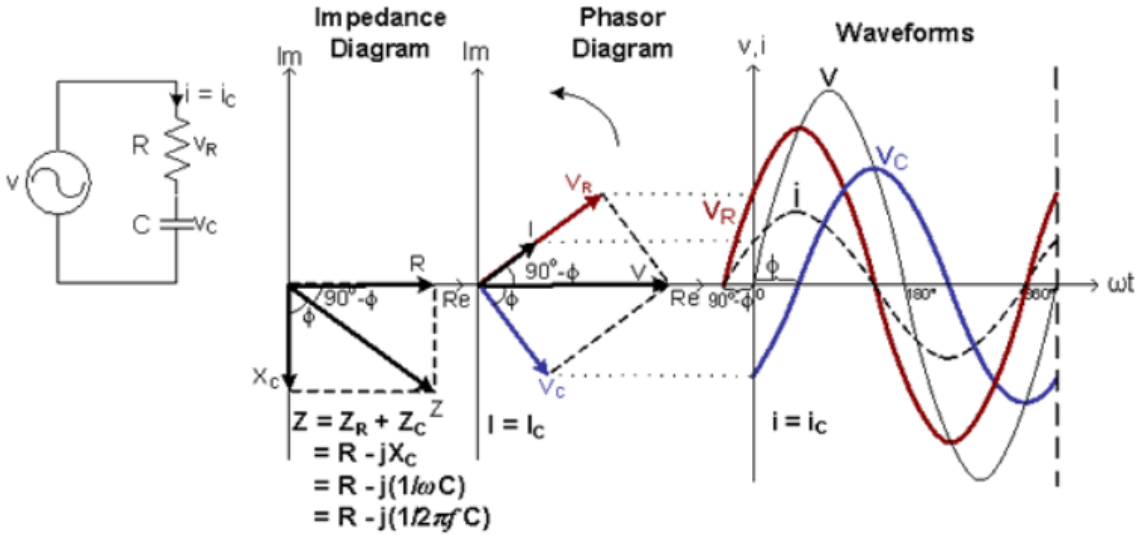


Figure A.3: Visualization of how a capacitor affects the current-voltage relationship in a simple AC circuit. The current waveform leads the voltage. [76]

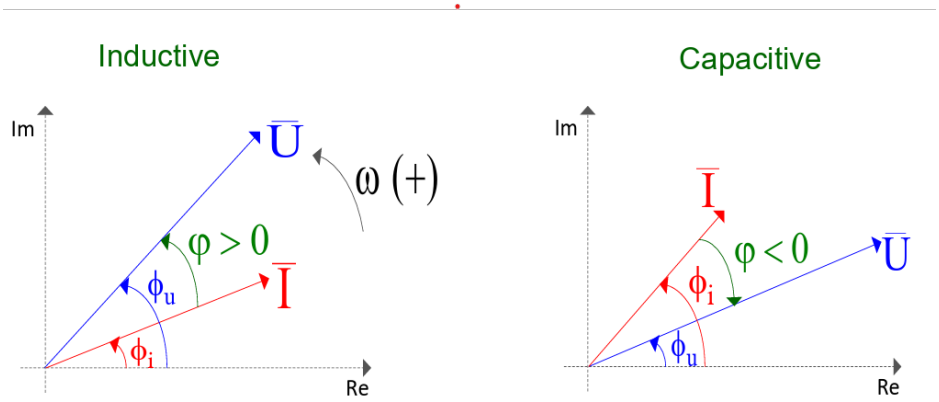


Figure A.4: Voltage and current phasors showing the phase angles for inductive and capacitive loads. [77]

control these parameters. Thereby, they would be able to greatly facilitate the successful management of a European power grid.

### A.1.5 *Piecewise linear approximation*

An intriguing point of contention is the interaction between the GNO and the SSTO layer. The former aims to determine an operating point from a nonlinear model which is passed to a linear optimization layer. Here, the piecewise linear approximation aims to correct the operating point (the GNO control step) with linear model segments to ensure feasibility. On this basis it estimates system parameters to be passed to the SSTO layer. In the identification of such an operating point, it is crucial that the GNO adheres to stability and stationarity criteria. Linear approximation is only permitted under their consideration. The feasibility space of the linearized segment as well as optimality depend on the formulation of the SSTO layer. For the latter, it is desirable to find an operating point close to the plant optimum. [48, 54, 78]

### A.1.6 *Linearization*

LINEAR MODELS One common approach is to linearize the plant model. It greatly reduces the model's complexity and enables the use of much more computationally efficient linear solvers. They can respond to dynamic changes on the grid in the required time. However, such linearization trades off model accuracy. Obviously, a linearized model does not accurately represent the dynamics of the real system.Thus, uncertainty not only results in a potential loss in optimality but can also result in losses in optimality and feasibility issues. [79]

OPTIMALITY When solving a for linearized model, the true optimum becomes unknown. That can be attributed to the plant-model mismatch. Chachuat *et al.* ([56]) claims that identified parameters from a well matched plant can achieve optimality in a single iteration. Unfortunately, due to the necessary reduction in computational cost through linearization, such ideal is not attainable and optimality is lost. Accounting for model uncertainty, the true plant optimum can only be approached. [56, 78]

FEASIBILITY The consequence of a greater plant-model mismatch is a different operation space. As linearized dynamics alter the model on which the controller calculates the reference signal, desired system states may be infeasible to reach for the true plant. [80]

### A.1.7 *State observer*

Some (e.g. [41, 44]) implement variations of the Kalman Filter to estimate system parameters. They consecutively update the optimization function with these new estimates, aiming to minimize losses in optimality. Here, some have shown the implementation on two

timescales, updating the DO layer in an online manner and the SSTO layer offline with a run-to-run cycle. The latter is also referred to as batch optimization where estimations are performed on chunks of data. Srinivasan *et al.* ([43]) utilize them to model parametric uncertainty and disturbances in their system. The combination seems necessary since the offline updating alone is insufficient in accounting for disturbances with fast dynamics. Yet, the batch optimization improves parameter estimates.

Frequently, the observer is implemented in a two-step. After obtaining measurement data from sensors, the first step estimates uncertain variables and the second step provides the control layer with the predicted states.

In the estimation step, desired state variables are reconstructed from observable outputs and their derivatives. [43] Some authors made use of the the extended Kalman filter and the unscented Kalman filter to estimate the desired states. [41, 44] Important in the energy hub application is the handling of unmeasured disturbances for which Muske and Badgwell ([81]) presents an augmented disturbance model. Due to the model used in the estimation, this approach becomes difficult when high plant-model mismatch is expected. The disturbance model becomes subject to uncertainty. [57, 82] This problem can be addressed by using measurements to refine the plant model. They reduce conservatism in the optimization by increasing the model accuracy. [56] To estimate parameters that optimize the model, they must be persistently excited. Simultaneously, constant excitation of the inputs significantly impacts the calculation of optimal inputs. This conundrum is known as the dual control problem. [78]

### A.1.8 *Task sequence*

The main task of the MPC is to track some predicted future trajectory based on available data. The problem this feat poses is that the controller must make a prediction of future system states based on uncertain information and track the same trajectory, adjusting for unmeasured disturbances while minimizing computation time. To visualize the working of the MPC's purpose, Qin and Badgwell ([44]) summarized the procedure in three questions: 1) Where is the process now? 2) Where should the process go? 3) How do we get there? With these questions in mind, the integrated task can be decomposed into layers that are distinct from each other. In the first part, state feedback based on sensor data can give insight into the current system state. Next, one MPC component determines discrete system setpoints that describe future system states. These setpoints are then passed to another controller that is tasked with following the synthesized setpoints. With this basic functional and temporal division, it is possible to design a symphony of singularly perturbed systems. They are further characterized in the following and ascribed tasks congruent with the functional and temporal decomposition principle. [37, 41, 48, 83]

## A.2 CONCEPT

### A.2.1 *Objective function*

A generalized approach to the design of the SSTO control layer is taken by Marchetti *et al.* ([54]). They formulate the quadratic problem dependent on the information passed by the GNO layer. Following their proofs, a feasible, offset-free SSTO problem of quadratic form can be designed from a nonlinear optimization layer under presence of uncertainty. It takes the following form:

$$\min_{\mathbf{u}_s,\mathbf{y}_s} \left\| \mathbf{z}_s - \mathbf{z}^{\mathrm{S}}_{k+1} \right\|^2_{\mathrm{a}_s} + \left\| \mathbf{u}_s - \mathbf{u}^{\star}_{k+1} \right\|^2_{\mathrm{R}_s}$$

s.t.

$$\begin{aligned}
&\mathbf{y}_s = \mathrm{A}_s \left( \mathbf{u}_s - \mathbf{u}_0 \right) + \mathbf{y}_0 + \hat{\mathbf{d}}(t \mid t), \\
&\mathbf{y}^{\mathrm{eq}}_s = \mathbf{y}^{\mathrm{s}}, \\
&\mathbf{y}^{\mathrm{L}}_k \leq \mathbf{y}^{\mathrm{in}}_s \leq \mathbf{y}^{\mathrm{U}}_k, \\
&\mathbf{u}^{\mathrm{L}}_k \leq \mathbf{u}_s \leq \mathbf{u}^{\mathrm{U}}_k,
\end{aligned}$$

They describe this solution approach in great detail and provide insight into the constants and variables used. Important here is the application of equality and inequality constraints, disturbance estimate $\hat{\mathbf{d}}(t \mid t)$, and setpoint target values of the format $\mathbf{x}_s, x \in [z, u, y]$. This approach requires knowledge of the set of active constraints.

### A.2.2 *Moving-average filter*

Embedded in literature is the idea to utilize a moving-average filter around which power fluctuations can be determined. A sliding window with a simple forward Euler implementation could be of the form [84]:

$$\bar{P}_{RES} = \frac{1}{T} \int_{t-T}^{T} P_{RES} d\tau \tag{A.1}$$

where T is the given timer interval and $\bar{P_{RES}}$ the moving average of P. The fluctuations relative to the moving average constitute the ramp-rate (RR):

$$RR = \left| \frac{dP_{RES}(t)}{dt} \right| \tag{A.2}$$

where the ramp-rate $RR \leq RR_{lim}$. Now it is possible to constrain the fluctuations in power setpoint and permits the application of a low-pass filter (LPF). Park *et al.* ([12]) utilize a first-order LPF to split the power setpoint between a BESS and a SC. They perform compensatory action when $RR_{lim}$ is exceeded and smoothen the power output, minimizing the power fluctuations on the grid and SOC fluctuations of the BESS. The limit is intended to mimic the plant's inertia, essentially acting as a pre-filter for high frequency fluctuations. Differently, Kakimoto *et al.* ([84]) apply a form of voltage control in conjunction with a SC to stabilize the DC link voltage.

It is crucial for the proper operation of the inverter that the DC link voltage remains constant. Large voltage fluctuations result in efficiency losses in the inverter.

*Filter design*

Beginning at the ramping limit, $RR_{lim}$ is chosen to provide virtual impedance to the grid. Below the limit, and relative to the moving average power point, a LPF is applied to split the RR, changing the SC's power setpoint for values above the cutoff-frequency. The SC is responsible for voltage stabilization. The values below are passed to a second LPF with a different cutoff-frequency to split the RR between the BESS and $H_2$ system. Values above initiate change in power of the former system and values below of the latter. In the process, it should be possible to weave the design of the virtual impedance from eq. 3.1 into one of the LPFs. Adjusting the impedance balances the power flow and enhances power sharing.

### A.2.3 *Ramp-rate objective function*

LINEAR CONTROL The requirement for a short response time necessitates linear operation. This way, rapidly fluctuating disturbances can be adequately addressed. It is relevant for the DC link voltage control where tight margins (~0.94 - 1.04 pu [32] ) are expected to be maintained. It is essential for stable and efficient inverter operation.

MIXED INTEGER CONTROL As it is possible to turn the $H_2$ components on and off, they require a binary variable that accounts for their operational state and allows attaching a startup and shutdown cost. It is thus recommended to use a MILP routine. Simply enough, the production levels of the fuel cell and electrolyzer are multiplied with a respective binary, e.g. $z_{FC} \in [0,1]$ and $z_{El} \in [0,1]$. Similarly to Bischi *et al.* ([72]), one could add startup and shutdown cost to the objective function with an extra element of the form

$$C_{on/off}(k) = C_{FC,start} * state_{FC}(k) + C_{El,start} * state_{El}(k)$$

where the binary state keeps track of whether the unit has been turned on or off in period k. Whenever a state is changed, the cost is added to the general cost function. By adding a penalization term to the state change, they can be limited. This is especially relevant in cases of temporary over-/underproduction where it could be more efficient to reroute power and keep these components running.

POWER FLOW Next to the SOC values, the DO gets passed a combined power setpoint from the SSTO with which it must manage the power flow of three storage elements. The power setpoint is established and optimized as follows:

$$\min_{\mathbf{P},\mathbf{SOC}} w_1 \left\| \mathbf{P}_{ESS}(k+1) - \mathbf{P}_{ESS}(k) \right\| + w_2 \left\| \mathbf{SOC}_{ESS}(k+1) - \mathbf{SOC}_{ESS}(k) \right\|$$

s.t.

$$\begin{aligned}
&\mathbf{P}_{ESS} = \mathrm{P}_{SC} + \mathrm{P}_{BESS} + \mathrm{P}_{H2},\\
&\mathbf{P}_{H2} = z_{FC} * \mathrm{P}_{FC} - z_{El} * \mathrm{P}_{El},\\
&\mathbf{SOC}_{ESS} = \mathrm{SOC}_{SC} + \mathrm{SOC}_{BESS} + \mathrm{SOC}_{H2},\\
&\mathbf{P}^{\mathrm{L}}_{ESS} \leq \mathbf{P}^{\mathrm{in}}_{ESS} \leq \mathbf{P}^{\mathrm{U}}_{ESS},\\
&\mathbf{SOC}^{\mathrm{L}}_{ESS} \leq \mathbf{SOC}_{ESS} \leq \mathbf{SOC}^{\mathrm{U}}_{ESS},
\end{aligned}$$

In this case, the objective function is composed of the power reference trajectory and the ramp-rate. The former can be characterized with the difference equation $P_{ESS} = SOC(k+1) - SOC(k)$, and the latter, $RR = P(k+1) - P(k)$, is the ramp rate, discretely implemented in the objective function. This general form translates into the equations below.

### A.2.4 *DO objective function*

Simultaneously, the objective function of the DO should be able to penalize two things. Firstly, a change in $H_2$ production rates, and secondly, fluctuations in SOC of the BESS. Both are critical economically because drastic changes (steep ramping) rapidly degrades the components. Staggering the ramp-rates of three storage systems with the double LPF specifically aims at minimizing power and SOC fluctuation. Properly tuned filters allow such action. Translated into an objective function, the RR is defined by

$$\|\mathbf{P}_{ESS}(k+1) - \mathbf{P}_{ESS}(k)\|$$

where $P_{ESS}(k+1)$ is derived from the power balance equation of the SSTO layer and is passed down as a setpoint to the DO.

The determination of the SOC setpoints by the GNO and SSTO for the respective $H_2$ and BESS are implemented in this objective function as well. They are the future setpoints SOC(k+1) that the DO is designed to follow, making the setpoint a dynamic variable. Estimating SOC(k) with the state observer provides the necessary difference equation that can be minimized in the objective function.

Further, the extension to solving an MILP routine to permit the addition of startup and shutdown costs of the fuel cell and electrolyzer is hugely beneficial in terms of economy. It can be added to the formulation.

The objective function and constraints of the DO take this form:

$$\begin{aligned}
\min_{\mathbf{P},\mathbf{SOC}} \quad & w_1 \|\mathbf{P}_{ESS}(k+1) - \mathbf{P}_{ESS}(k)\| \\
& + w_2 \|\mathbf{SOC}_{BESS}(k+1) - \mathbf{SOC}_{BESS}(k)\| \\
& + w_3 \|\mathbf{SOC}_{H2}(k+1) - \mathbf{SOC}_{H2}(k)\|
\end{aligned}$$

$$
\begin{aligned}
s.t. \quad & \mathbf{P}_{ESS} = \mathbf{P}_{H2} + \mathbf{P}_{BESS} + \mathbf{P}_{SC}, \\
& \|\mathbf{P}_{ESS}(k+1) - \mathbf{P}_{ESS}(k)\| \leq RR_{max} \\
& \|\mathbf{SOC}_{BESS}(k+1) - \mathbf{SOC}_{BESS}(k)\| = \mathbf{P}_{BESS}(k), \\
& \|\mathbf{SOC}_{H2}(k+1) - \mathbf{SOC}_{H2}(k)\| = \mathbf{P}_{H2}(k), \\
& \mathbf{P}^{\mathrm{L}}_{ESS} \leq \mathbf{P}^{\mathrm{in}}_{ESS} \leq \mathbf{P}^{\mathrm{U}}_{ESS}, \\
& \mathbf{P}^{\mathrm{L}}_{SC} \leq \mathbf{P}_{SC} \leq \mathbf{P}^{\mathrm{U}}_{SC}, \\
& \mathbf{P}^{\mathrm{L}}_{BESS} \leq \mathbf{P}_{BESS} \leq \mathbf{P}^{\mathrm{U}}_{BESS}, \\
& \mathbf{P}^{\mathrm{L}}_{H2} \leq \mathbf{P}_{H2} \leq \mathbf{P}^{\mathrm{U}}_{H2},
\end{aligned}
$$

where next steps SOC(k+1) are provided by the SSTO (for BESS) and GNO (for $H_2$) layers above and current SOC is a measurement variable, estimated by the state observer. The difference composes the power reference trajectory but is preferably passed from the other two layers.

The RR is manifested with the difference equation $P(k+1) - P(k)$ and can be explicitly constrained with a maximum ramp-rate. Its value is passed through the two filters, inducing a change in power reference in each storage component. Tuning the weights on the respective setpoints allows to assign priority to the response of the fast acting ESSs. Their deployment can be staggered and costly ramping of the $H_2$ system can be minimized.

To avoid feasibility issues, the SOCs are not explicitly constrained. They are already constrained in the other layers.

### A.2.5 *Layer synchronicity*

The GNO's goal is the determination of operating point around which further optimization can be performed. The synchronization with the layer below is thus of great importance. The operating point, determined by long-term optimization, is the control step of the MPC-GNO. It could for example take a value of around 24 hours. This value spans the prediction horizon of the next layer. Due to this synchronized temporal decomposition, the GNO layer does not need to be computed as frequently as the lower layers. One can thus afford to design it with higher complexity and allocate more time to solving a nonlinear optimization problem with increased computational cost.

Its prediction horizon has a maximum length of the the control step of the GNO layer. Along the same lines, the control step of the SSTO layer should congruent with the prediction horizon of the layer below. In line with the singular perturbation approach, it enables the decomposition of hybrid plant dynamics as well as handling disturbances and uncertain parameters developing on similar a timescale.

The MPC-DO's control step can then be adjusted to execute as frequently as needed, adapting to hardware constraints in a possible real-time implementation. Here, the controller operates with a limited time budget to not exceed scheduled runtime. It implies that a solution must be found within a single cycle, underlining the focus on computational efficiency.

Due to the simplicity of this direct control layer, the SSTO does not need to compute new setpoints as frequently. Thus, with slower execution rates of the two layers above, the setpoint determination can be computationally more expensive. It allows higher complexity in the problem formulation. Additionally, the DO can explicitly handle its own set of constraints. In process control, this feature can be quite advantageous over other simple control implementations like the PID.

### A.2.6 *Integration in a real-world application*

Today, Siemens Gamsea is working on the control of $H_2$ electrolysis from a single offshore wind turbine. Their design can be seen in fig. A.5, storing six containers with electrolyzers on a platform. Simultaneously, companies like VDL Energy System are developing a hydrogen power unit (h-PU) (fig. A.6) and BESS systems in container form. Combined with a supercap container, all three can be integrated to form the conceptualized plant that underlies the hierarchical control system. Regarding the $H_2$ storage, engineers have made use of the turbine tower of on-shore wind turbines to install large storage tanks.

Figure A.5: Offshore wind turbine invented by Siemens Gamsea. [85]


Figure A.6: Hydrogen power unit developed by VDL Energy Systems. [86]

*Plant parametrization*

One challenging aspect in the design of the RES is sizing the components. The size of the prime mover dictates the size of all the other components. In this case, the wind turbine acts as the prime mover, generating power to be fed into the electricity grid. Thereafter, the grid inverter is sized. Its maximum power rating must be slightly larger than the nominal power delivered by the prime mover.

STORAGE The storage elements must then maintain the main bus voltage and bridge production valleys to guarantee a stable power supply. To size them, a good estimate of the length of production peaks and valleys is crucial. For example, it has been shown that statistically one of two winters experiences a wind drought of a week or more. The hydrogen infrastructure would tend to the lack of long-term adaptability, meeting seasonal demand and weather changes. The $H_2$ system must be sized accordingly. Similarly, the rapid and large production changes must be compensated for by the BESS and SC.

The advantage of the RR control is that the storage size of each component can be reduced. It is also an important consideration in the plant design.

TRANSMISSION An important element in off-shore wind energy production is the energy transmission to the shore. Brief investigation into the design revealed that its consideration is not straightforward.

For example, Huang *et al.* show the line's short circuit capacity must be considered in the design. A low short circuit ratio ($SCR = \frac{S_{AC}}{P_{wf}}$<1.2) can result in significant voltage oscillations in HVDC line.

## A.3 MATH MODEL

### A.3.1 *Variable types*

DECISION VARIABLES The first type of variables are the decision or input variables. Those variables can be altered to influence the behavior of a given system and steer it to a desired state.

Here, control over the power P by charging and discharging an ESS aims to balance the power production from the wind turbine and the demand on the grid.

STATE VARIABLES These variables describe the state that a system is currently in. In absence of external influence, a system stays in a given state. Knowledge of the current system state is essential to determine how inputs will influence the states to make predictions about future system states.

Integrating the power flow, the SOC can be changed. In itself, it provides information about the energy level inside an ESS.

MEASUREMENT VARIABLES Often, it is impossible to directly measure the state variables, and one cannot gain such insight. The measurement or output variables are quantities that can be tracked over time. They can then be used to make educated guesses about how inputs influence the unobservable system states.

Measurements of the terminal voltage and current of the ESS allow the reconstruction of the SOC.

### A.3.2 *Elimination process*

Bridging the gap between the theoretical concept and the simulation model, control elements had to be removed. It seemed most important to identify core control elements that would validate the essence of the concept without becoming too expansive. The decision was approached by process of elimination.

GNO First of all, the GNO was removed from the implementation as some regard it as an economic decision layer. Its modeling and simulation would fundamentally shift the focus of this work. Along these lines, elaborate forecasting with stochastic prediction models would be a similar shift of focus.

OPERATING POINT Since no operating point is determined as part of the simulation, its piecewise linearization remains a theoretical exploration. In that manner, the dynamic updating of the SSTO by provision of different operating points was not realized in the simulation part.

OBSERVER As a further control component, the state observer was eliminated from implementation. In this application, one of its function is to update existing control structures so its added value seemed hard to prove without initial control. Further, it aids in reducing the level of uncertainty through measurements and parameter estimation. Similarly, its deployment augments the approximation of the optimal control.

DO Deciding between the SSTO and DO layers, the former synthesizing a setpoint and the latter following it, the setpoint generation appeared to be more fundamental, integrating the plant components on a control level. The DO was regarded to be geared towards storage management, less crucial in the power flow optimization. Hence, the resolution to implement the SSTO layer.

### A.3.3 *Wind turbine*

In this RES, the wind turbine acts as the prime mover. Its nominal power output is guiding for the sizing of all the other components.

As first step, requirements for the wind turbine are set. Generally, wind turbines are classified by wind zones. These zones can be used as a foundation for sizing the turbine. The

offshore wind construction roadmap in section A.1 depicted all planned wind farms in the North Sea. The Rijksoverheid ([17]) provides wind zone ratings between I-IV (Deutsches Institut für Bautechnik (DIBt)) for each site. Among the eight planned sites, half were identified to require DIBt wind zone III rated wind turbines.

*Parameters*

Given the wind turbine class, it is possible to choose a fitting turbine model. The Enercon E126-EP8 is a DIBt III wind turbine and rated at 7580kW. The turbine can be characterized with the parameters presented in table A.1.

In the selection process, one important criterion is test data availability. The reason is that the turbine model was linearized under consideration of the performance coefficient. Because this coefficient is often found empirically, sufficient measurement data should be available for its determination. Therefore, the Enercon prototype seemed like a reasonable choice.

| Parameter | Variable | Value | Unit |
|---|---|---|---|
| Rated Power | $P_r$ | 7580 | kW |
| Swept area | $A$ | 12668 | $m^2$ |
| Cut in speed | $V_{c,in}$ | 3 | $m/s$ |
| Rated speed | $V_r$ | 16.5 | $m/s$ |
| Cut out speed | $V_{c,out}$ | 28 | $m/s$ |

Table A.1: Parameters of the Enercon E126-EP8 wind turbine. [87, 88]

*Equations*

The goal in characterizing the turbine is to find a set of linear functions that relate the wind speed to the power output of the wind turbine. Here, the goal is the mapping measured or predicted wind speed to the power output $P_w(v)$. This power output is captured with equations in A.3 ([89]). They can be used to calculate the power generated for different wind speeds.

$$E(t) = \begin{cases} 0 & v < V_{c,in} \\ P_w = 0.5\rho A C_p v^3 & V_{c,in} \leq v < V_r \\ P_w = P_r & V_r \leq v < V_{c,out} \\ 0 & V_{c,out} \leq v \end{cases} \tag{A.3}$$

where $\rho$ is the air density and considered constant. A is the rotor area, $C_p$ is the coefficient of performance, and V is the linear wind speed. Differently from the other parameters, it is not straightforward to determine the $C_p$ of a wind turbine. The following paragraph elaborates on its derivation.

COEFFICIENT OF PERFORMANCE Generally, the coefficient of performance is calculated as the ratio between the produced power and the kinetic power available in the wind: $C_p = P/P_r$. Many parameters, such as blade size, shape, and material, influence the power output. It means that each turbine type has its own $C_p$. Therefore, to determine the coefficient of performance, empirical data is necessary. In most cases, it is very easy to find visual data of wind turbines' $C_p$s but data points are rarely provided. Libii ([87]) showed measurement data from which the performance curve for the E126 was plotted. It is visualized in fig. A.7a. The data can now be used in conjunction with equations A.3 to find the relationship between wind speed and power output. The result is shown in fig. A.7b.

Typically, a wind turbine can be controlled by the pitch angle of its blades. At high wind speeds the turbine's blades can be turned out of the wind to adhere to operational limits. It should be noted that active pitch control is assumed since only the in- and outputs are relevant to this project. No further investigation into wind turbine control was done. However, such control can easily be interfaced with the MPC structure.

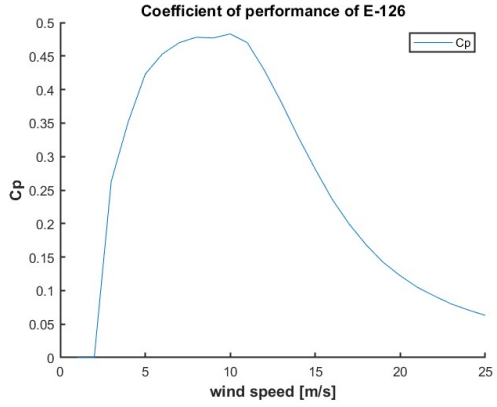


(a) Coefficient of performance at different wind speeds. [87]

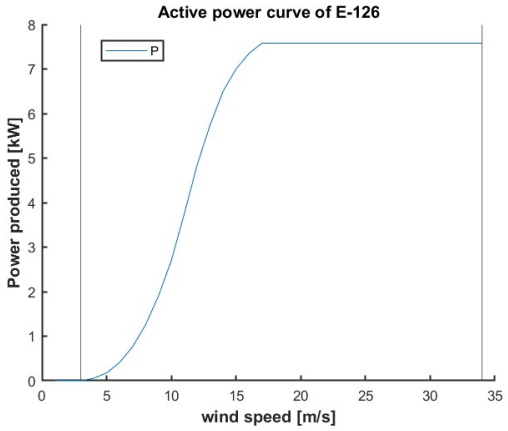


(b) Power curve data with active pitch control. [88]

Figure A.7: Visualization of the wind turbine E-126' performance characteristics

*Linearization*

Fig. A.7 shows that the power output of the under-rated section, i.e. when the turbine is in partial load condition, has a cube relationship with the wind speed. Linearization of this relationship is approximated with a linear polynomial function as shown in fig. A.8. The new relation between power generation and wind is implemented as given in eq. A.4.

$$P = 619.6 * v - 2910, \tag{A.4}$$

where v is the wind speed and P the power produced by the turbine. With it, measured or anticipated weather events can be translated into power flow into the hub.

The result of the linearization can be observed in fig. A.8. It simplifies the expression of eq. A.3 in partial load condition.

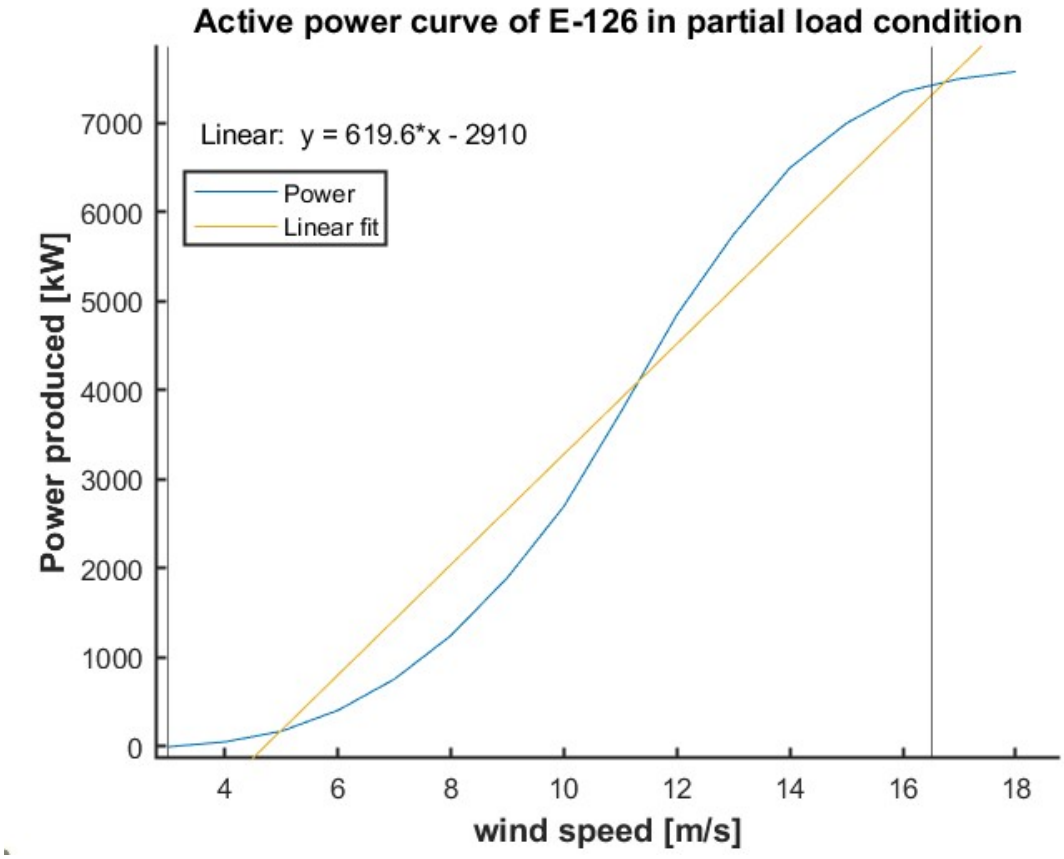


Figure A.8: Linear fit of partial load curve of fig. A.7b

### A.3.4 *Energy storage systems*

Similarly to the wind turbine model, the dynamics of the ESS must be simple enough to be optimized by the linear MPC-DO. Therefore, it is important to capture them in linear mathematical equations. This feat is particularly challenging for two reasons. Firstly, the dynamics of a battery are highly nonlinear, and secondly, the dynamics vary strongly by type depending on the material composition and even between each individual ESS of the same kind. This circumstance insinuates the necessity of data acquisition through empirical tests.

The goal is to capture the ESS dynamics with a set of linear equations. The mathematical description should be framed in a model and underpinned by a fundament of empirical tests. On this basis, a storage loss function is determined.

**EQUIVALENT CIRCUIT MODEL** The nonlinearity of any BESS can be attributed to the electrochemical nature of the component. The charge-storing and -releasing reactions introduce temporal delay. Further, electrochemical reactions suffer from efficiency losses due to heat development. They also require initiation energy, some threshold energy level, before a reaction begins.

Often, these processes are captured with a so-called equivalent circuit model (ECM), consisting of electrical resistor and capacitor elements. In-depth research on this was done

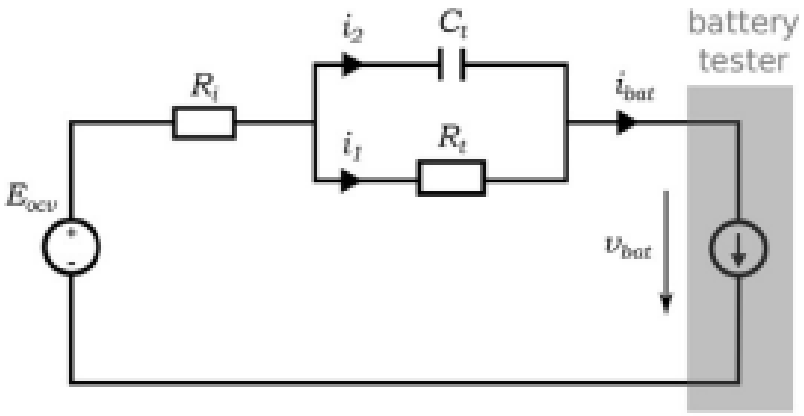


Figure A.9: First order Thevenin model used as ECM. [91]

in [90], exploring all the various energy barriers and detailing how they are modeled using electrical equivalent components in an ECM. To trade accuracy for simplicity, a classical first-order Thevenin model was chosen (fig. A.9). The models consists of a lumped series resistance $R_i$ and one RC element. The former lumps the heat related losses from all processes and the latter models the charge transfer resistance $R_ct$ and temporal delay $C_ct$. For simplicity sake, the influence of further processes is neglected.

PERFORMANCE CURVE Bischi *et al.* ([72]) capture (nonelectrical) storage components' operating conditions via their performance curve. They postulate the necessity for the piecewise linearization of these curves to enable their implementation in linear optimization algorithms. On this motive, a linear performance curve for the BESS is devised. Herein, a challenging aspect is the equivalent components' dependence on temperature, SOC, and current rate. In the context of this project, this is especially relevant with respect to the ohmic losses experienced by the component. It introduces great nonlinearity in the efficiency function.

To mathematically describe the storage loss term, the ESS must first be modeled using equivalent circuit components. To do this, empirical tests are evaluated, determining losses with respect to influential variables. This formulation is then linearized to be able to directly determine power losses based on current rate, temperature, and state of charge.

A detailed derivation of the performance curve characterization and its relation to the OCV is shown in app. A.3.5.

*OCV linearization*

The polynomial function of eq.A.6 was approximated with three linear components. Essentially, the first and last 10% SOC were defined with their respective linear function, and the middle 80% with the third function. The mathematical characterization is shown in equation A.5.

$$OCV = \begin{cases} 2.516 * \text{SOC} + 1.024 & 0\% \leq SOC < 10\% \\ -0.1934 * \text{SOC} + 3.282 & 10\% \leq SOC < 80\% \\ 1.767 * \text{SOC} + 3.096 & 80\% \leq SOC < 100\% \end{cases} \tag{A.5}$$

The linearization is visualized in fig. A.10, showing the piecewise linear fit. It should be mentioned that the loss in accuracy is expected to be minimal because the operating range of the ESS in incentivized to remain between 10-90% SOC. Functionally, the edge cases are a bit redundant but were included for completeness. Further, it can be seen that the middle region is quasi-linear and approaches a constant voltage potential, driven by a Gibbs free energy gradient. [90, 91]

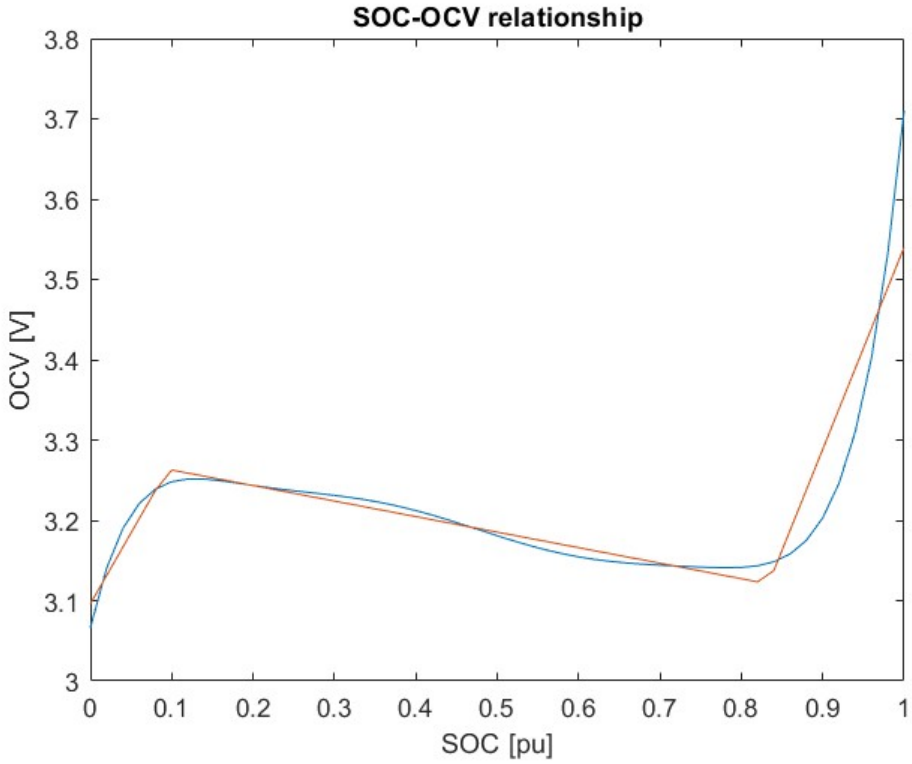


Figure A.10: SOC-OCV relationship, comparing the piecewise linearization (orange) to the polynomial function (blue).

*Storage efficiency*

To quantify the storage efficiency of the ESS, the power losses associated with changes in SOC and C-rate must be determined. To ease implementation these two loss terms were decoupled and calculated independently of each other. Furthermore, the tests that characterize the ESS were performed in temperature controlled chambers. Thus, the assumption of isotherm conditions is made.

### A.3.5 *Battery linearization*

*State of charge estimation*

Most crucial about an ESS is knowledge about its current SOC. The efficiency of its operation strongly depends on it. However, the SOC of an ESS cannot be measured *in operando*. Therefore, the next best thing to do is to measure the terminal voltage and the current flowing in and out of the component. The measured values are then used to estimate the component's SOC.

Another issue is the determination of the OCV of an ESS. It is a necessary quantity in determining the internal resistances. Similarly, it is impossible to measure *in operando* and can hardly be reconstructed due to varying internal resistance. Thus, it is most commonly estimated by establishing an SOC-OCV relationship where the OCV is determined from the SOC based on low current test measurements.

It should be mentioned that no single comprehensive test series could be found that was deemed sufficient to fully characterize the dynamics of such an ESS. Instead, various tests of batteries with similar electrochemical composition were integrated to model the efficiency function. It is speculated that the loss of accuracy from linearization would diminish the effect of this circumstance. Also, if such tests are indeed performed, they should be easily implementable following this approach.

*Parameter selection*

Comparing different model selection criteria, Suárez-García *et al.* ([91]) capture the electrodynamics of a $LiFePO_4$ battery. They characterize the battery with a first-order Thevenin model, consisting of an ohmic resistor $(R_0)$, a charge transfer resistance $(R_{ct})$, and the according capacitance $(C_{ct})$. Their study aimed at parameterizing the battery with respect to accuracy and computational speed. Using the Akaike Information Criterion (AIC), the model had a $> 1\%$ error compared to the measured test. Resulting were the values of equation A.6, relating the SOC to parameter functions.

$$\begin{aligned} OCV &= 156.4 * SOC^7 - 522.7 * SOC^6 + 707.3 * SOC^5 - 496.4 * SOC^4 + 193.2 * SOC^3 \\ &\quad - 41.64 * SOC^2 + 4.484 * SOC + 3.066 \\ R_0 &= 0.0003188 * SOC + 0.01136 \\ R_{ct} &= 0.004006 * SOC - 0.001034 \\ C_{ct} &= 2.643 * 10^{-8} * e^{12.48 * SOC} \end{aligned} \tag{A.6}$$

Incidentally, two equations were found to have the best fit when characterized by a linear model. Perfectly in line with the linearization objective, readily implementable in the optimization algorithm. The two other equations are not linear so they had to be modified. Fortunately, the result from the Bayes Information Criterion (BIC) test found a linear equation for the charge transfer capacitance: $C_{ct} = -45870 * SOC + 69260$. This equation was applied, at the expense of around 0.2% accuracy relative to the test in Suárez-

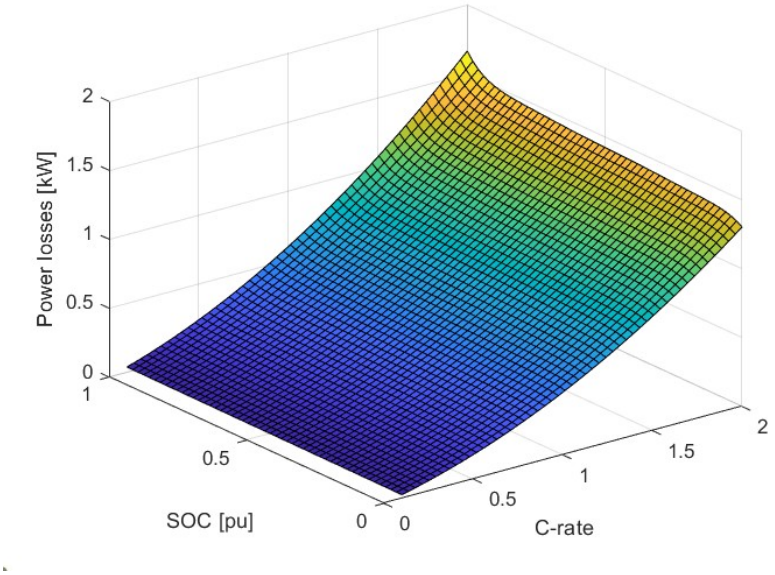


Figure A.11: 3D plot of the battery losses.

García *et al.* ([91]). The last component, the SOC-OCV equation, was approximated with a piecewise linearization.

### A.3.6 *Battery loss term*

SOC LOSSES The dynamic power losses suffered due to a change in SOC were calculated from equations A.6 where the determined series and charge transfer resistances are multiplied twice with the measured current, such that the associated power can be determined. The resulting power loss due to change in SOC is given in equation A.7. [92]

$$P_{loss,SOC} = I^2 * (R_0(SOC) + R_{ct}(SOC)) \tag{A.7}$$

CURRENT RATE LOSSES Schimpe *et al.* ([93]) is one of the few authors that evaluates the energy efficiency of Li-ion ESS containers accounting for losses due to the rate of current drawn from the unit. They quantified percentage losses as a function of C-rate between values of 0.1-2C. Their function was linearly approximated with $I_{loss,\%} = 12.1/1.9 * C - Rate + 1.76$. Since this equation provides a percentage value of the total current, the power lost was calculated with eq. A.8 from the power at the source of the ESS. [92–94]

$$P_{loss,I} = OCV(SOC) * I * I_{loss,\%} \tag{A.8}$$

The losses are visualized in fig. A.11. It is not only a significant element to accurately track the power flow but also to perform the optimization under consideration of losses.

Hysteresis effects are disregarded in this model. To account for this, Liu *et al.* ([92]) present a method where they add a correction factor K.

LOSS TERM In the optimization, the combined loss term is accounted for in the power balance equation as $P_{loss} = P_{loss,I} + P_{loss,SOC}$.

*Dynamic equation*

The battery dynamics were modeled based on the first-order Thevenin model. Using the electrical equivalent components and Mussi *et al.* ([95]), the dynamics can be represented as

$$\dot{V}_T(t) - \dot{V}_{OCV} + R_0\dot{I}(t) + \frac{T(t)}{C_{ct}} - \frac{V_{OCV}(t) - V_T(t) - R_0 I(t)}{Cct * R_{ct}} = 0 \tag{A.9}$$

Using this equation and the linearized resistance and capacitance functions from eq. A.6, one can find the terminal battery voltage that is applied to the RES bus.

### A.3.7 *Reactive power equation*

Here, the relation $V_{AC} = \eta * m * V_{DC}$ is established by Jago ([96]). As no charge is lost, $\eta$ is taken to be the same as for the active power relationship with m=1 for simplicity. Furthermore, stiff voltage ratings on the main DC bus seem like a realistic constraint. [27] The relationship between the voltage and reactive power thus becomes

$$\begin{aligned} min \quad & w_3 * |V_{inv,des} - V_{inv}| + w_4 * (V_{inv,des} - V_{inv})^2 \\ s.t. \quad & V_{inv,des} = \lambda * V_{inv,meas} + (1-\lambda) * V_{inv,pred} \\ & V_{inv,pred} = V_{load,pred} + \Delta V \end{aligned} \tag{A.10}$$

where $V_{load,pred} = V_{nom}$ and $\Delta V$ being the voltage variation due to reactive power flow. The same droop control law for the reactive power is implemented with

$$\Delta V = m_Q * (Q_{pred} - Q_{meas})$$

where

$$Q_{pred} = \frac{V_{inv}(V_{inv} - V_{load})}{X_L}$$

The predicted reactive power is added with a reactance term to anticipate voltage changes at the inverter due to variations in reactive power.

The result is a catch 21 where the inverter voltage is required to find the reactive power, which is used to calculate the same inverter voltage. This issue was not solved within the scope of this thesis. Perhaps, it could be possible to use some external prediction of the voltage. To simplify the equation, it can be assumed that there is no desired reactive power and take $Q_{pred} = Q_{des} = 0$, such that

$$\Delta V = -m_Q Q_{meas}$$

### A.3.8 *McCormick envelope*

$$\begin{aligned} P >= & \ V_{min} * I + V * I_{min} - V_{min} * I_{min} \\ P >= & V_{max} * I + V * I_{max} - V_{max} * I_{max} \\ P <= & \ V_{max} * I + V * I_{min} - V_{max} * I_{min} \\ P <= & \ V_{min} * I + V * I_{max} - V_{min} * I_{max} \end{aligned} \tag{A.11}$$

This approximate relationship between current, voltage, and power enables the inclusion of voltage and current terms in the objective function. With it, the reactive droop control and voltage fluctuation terms can be related to the power flow.

# B

# APPENDIX 2

## B.1 SIMULATION MODEL

### B.1.1 *Matpower model*

Limiting the scope of this model is the absence of the full $H_2$ setup. The cycle was left out because the toolbox does not feature a hydrogen cycle. Ideally, the electrolyzer has a downstream storage and a fuel cell. Here, the fuel cell reconnects with the main DC bus as a source. Integrating the hydrogen flow with replacement components proved difficult due to the interaction between the impedance, capacitance, and controlled source. Particularly, where the source must act with regard to $H_2$ storage levels which were to be filled by the power dissipation of simple impedance component. Thus, it was chosen to only include the electrolyzer as energy sink. It was simplified to a fixed load with the potential to be augmented.

The composed model was solved by a Quadratic Programming (QP) routine, optimizing the power flow over a 24h prediction horizon. During the optimization, it is possible to modify the cost function and constraints with custom user functions using Matpower's MP-OPT extension. Herein, the goal was to open the door for the integration of other components, such as the state observer, striving for automatic modification of cost and constraints.

In this process, two shortcomings of the Matpower toolbox regarding the goal of this project were detected. They all pertain to the dynamic behavior of the grid. Firstly, the optimization does not explicitly consider the frequency dynamics and its effect on the power flow. The inventor M.C. Murillo-Sanchez confirmed that this feature was not yet implemented, mainly due to the short timescale complicating optimization.

The other limitation is a direct consequence. Due to the absence of frequency dynamics, no grid-forming technology can be integrated. Thus, no droop control could be implemented into the plant model. Similarly, the slack bus (fig. 5.2) acts as the reference bus for the voltage angle and real power, complicating the connection of a GFMI to the grid side.

## B.2 OPTIMIZATION MODEL RESULTS

Whenever insightful, different weight settings are explored for the formulated objective function and constraints. Regarding the constraints, it should be mentioned that this part

of the simulation was performed using the power relationship $P = VI$. It was included to enable the explicit penalization of voltage fluctuations. As explored in section 2.3, it is an important consideration for GFMIs. Effectively, this meant that the optimization routine was solved with Matlab's fmincon, a nonlinear solver. Later on, this constraint requires the introduction of the McCormick envelope (eqs. A.11) to the problem formulation. With it, it is possible to approximate P=VI and solve a quadratic (or linear) problem.

### B.2.1 *Initial formulation*

The first approach refined from the mathematical model sets up a simple optimization routine (from equations 4.2, 4.3, 4.4). They are defined with the following equations:

$$\begin{aligned} min \quad & w_1 * |P_{RES,des} - P_{RES}| + w_2 * (P_{RES,des} - P_{RES})^2 \\ & + w_{SOC} * (SOC_{ESS} - SOC_{ESS,des})^2 \\ & + w_{SOC,final} * (SOC_{ESS}(K) - SOC_{ESS,init})^2 \\ & + w_{V,fluc} * (V_{RES} - V_{nom})^2 \end{aligned} \tag{B.1}$$

$$\begin{aligned} s.t. \quad & SOC_{ESS}(k+1) = SOC_{ESS}(k) + P_{ESS}(k) \\ & P_w - P_{ESS} - P_{loss} - P_{inv} = P_{RES} \\ & P_{RES} = V_{RES} * I_{RES} \end{aligned}$$

EXPECTATION In this optimization routine, the production and consumption quantities, $P_w$ and $P_{inv}$ respectively, are prediction values. As the implementation is purely optimization based and the in- and outputs are known, the solver is expected to find an optimal solution by adjusting $P_{ESS}$ such that $P_{RES}$ can follow its reference, stabilizing the voltage in the process.

COMPARISON Four relevant scenarios were investigated. First, the "certain" case where the prediction and the true demand were the same (fig. B.1 left side). In the other, the "uncertain" case, the desired setpoint $P_{RES,des}$ was introduced as a different quantity mismatching the true demand (fig. B.1 right side).

Two further scenarios were investigated where some baseline power was either predicted or consumed (fig. B.2). These two columns directly compare how the ESS is affected.

Next to visual inspection, the absolute function values as well as the NCO are tracked. They can aid in comparing the scenarios, also to determine the effect of weight adjustments.

RESULTS Constrained by the power balance equation, the power flow in- and out of the ESS acted as the decision variable. Its result is plotted in fig. B.1c. The battery update law details the relationship between power and SOC, where negative flow towards the inverter discharges the battery.

By constraining the RES power with P=VI, the voltage penalization term could be added to eq. B.1. Its value is mostly maintained as the nominal voltage and power changes are handled by adjusting the current flow.

In each case, before t=5h, demand is larger than production and the battery discharges accordingly. As production out scales demand, the power flow is reveres and the battery is recharged.

Examining fig. B.1, the overlap in demand results in the same ESS discharge curve. Differences in storage management become clearer once the desired consumption deviates from the real consumption.

A larger square weight effectively resulted in more drastic control action, i.e. steeper battery (dis-)charging as well as a much larger absolute function value. Raising the SOC weight had the opposite effect such that the SOC was maintained more closely at the desired target value.

An interesting observation was made in the baseline comparison (fig. B.2). Here, interchanging the desired and actual demand resulted in different power flow on the RES bus but the behavior of the ESS was the same.

FUNCTION VALUES Next to the visual inspection, the absolute function and NCO values were tracked. With absence of an explicit process model, tracking the NCO provides gradient information based on measurements.

Here, the control action taken based on anticipated consumption increases the absolute objective function value and doubles the NCO value. These values also differed strongly between the investigated scenarios. Some almost doubled that of the "certain" case.

In the baseline comparison of fig. B.2, where the baseline is used as prediction and as consumption value in the respective case, the power flow in the ESS and the function values are the same, also when changing the function weights.

*Discussion*

In the "certain" case, the problem is solved by a deterministic solver which finds a reference trajectory for the ESS power. Its output complements the power generated by the wind turbine. Together, they are able to meet the simulated demand.

Further, the optimization is performed within the prescribed SOC limits and can be adapted by changing its weight to prioritize the health and longevity of the ESS. Its value is determined as a necessary variable to be passed down to the DO layer for RR control.

ELECTRIC POWER A general remark about the optimization should be made on the current and voltage relationship. Due to the penalty term on the voltage, it is possible to maintain it close to its nominal value and incentivize current changes. Enabling is the addition of the nonlinear relationship P=VI. It was deemed necessary as it allows explicit constraining and creates a basis for feedback from the plant later on. Overall, this element in implementation showed expected results because no sacrifice in optimality had to be made.

To pick up on the voltage constraint in conjunction with the fixed quantities, it was also discovered that the ability to determine feasible solutions greatly suffered when enforcing hard constraints on the current or power on the RES bus. They would marginalize the solution space to a degree of infeasibility. Thus, adding soft constraints to such variables is particularly important with respect to feasibility.

POWER BALANCE On the other hand, contrary to expectations, the initial power balance equation (eq. B.1) resulted in challenges with feasibility. The reason were the fixed time series data used as in- and output. Herein, $P_{ESS}$ was the only optimization variable present in the formulation.

Along these lines, it was discovered that the feasibility issues depend on the prediction. They originate from large discrepancies between prediction and true demand. This circumstance was highlighted by the investigation of the baseline scenario. Here, the power output of the ESS remained exactly the same when switching the predicted and actual power output to the inverter. An error between two fixed quantities is minimized, so little space for an optimal solution is left.

Essentially, addressing the issue much depends on the size of the ESS where a small battery quickly experiences power curtailment issues and a larger battery increases the decision space. Tying the result back to the concept, the decision space of the SSTO layer can be much increased through the integration with the $H_2$ cycle. Here, the latter is able to provide energy to the BESS, vastly increasing the total storage capacity.

WEIGHT CHANGES Similarly, adjusting the optimization weights $w_1$ and $w_2$ showed changes in the SOC fluctuations. However, only the magnitude is affected. It is speculated that this interaction is caused by the shift in relative weighing of the errors. It is confirmed by the fact that no change is observable if all weights are increased.

The observed results left little room for optimization. Large values of the objective function and the NCO were confirmatory. Adjusting the weights was insufficient to address this issue. It mediated adaption of the problem formulation and lead to the introduction of further decision variables.

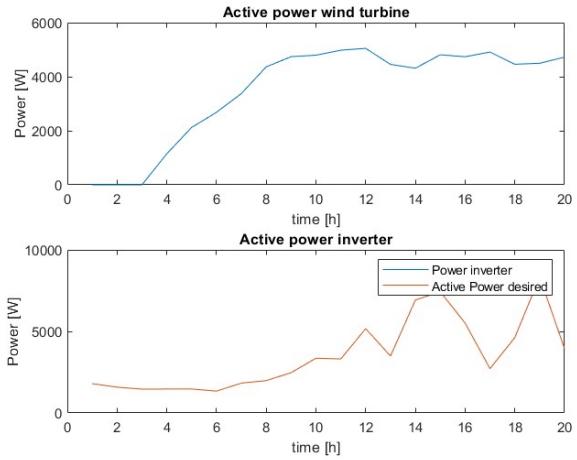


(a) Production and consumption values. Prediction and the actual consumption are the same.

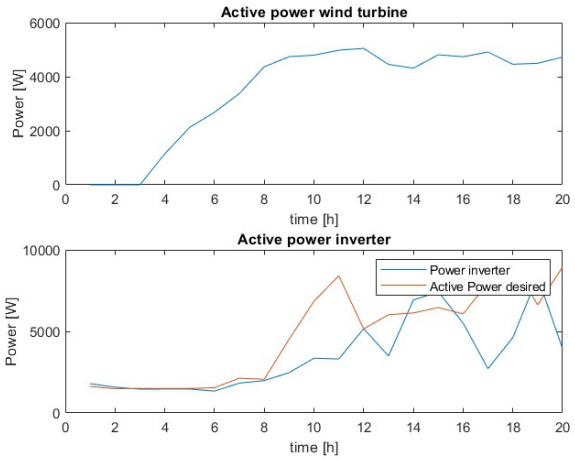


(b) Production and consumption values with consumption mismatch.

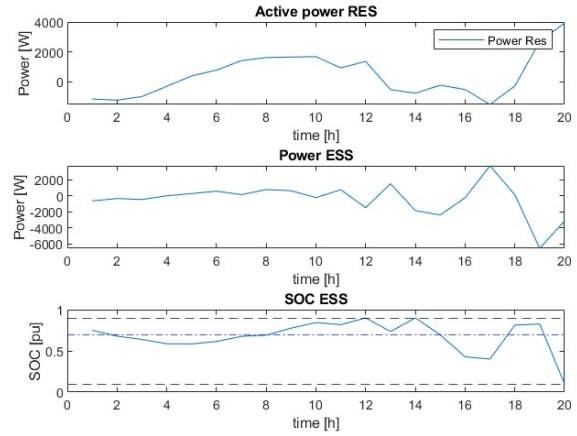


(c) State and optimization variables of the optimization routine.

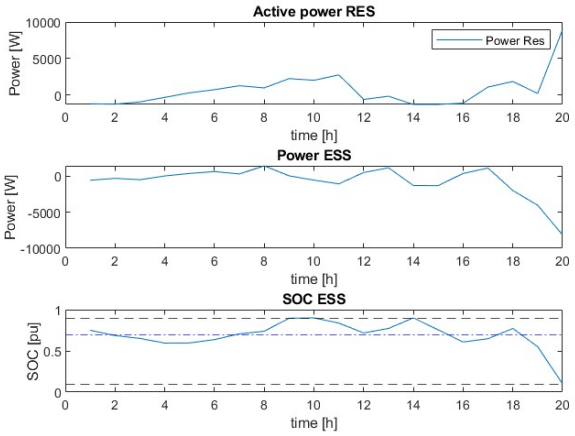


(d) State and optimization variables of the optimization routine.

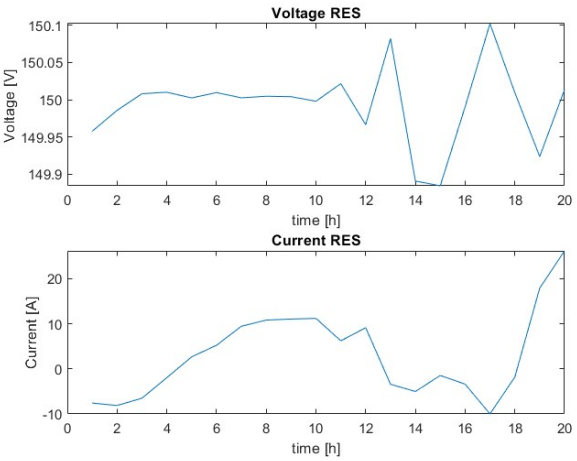


(e) Voltage and current plots.

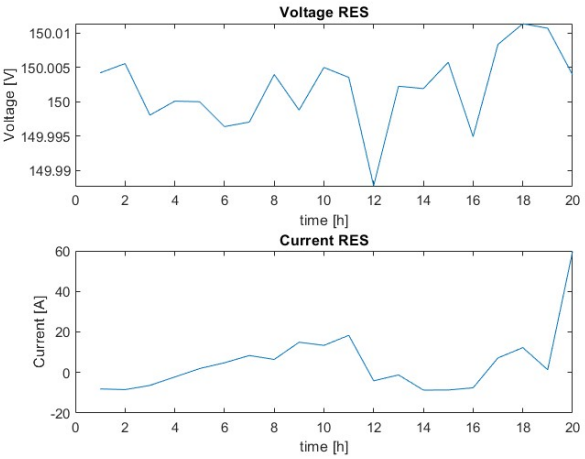


(f) Voltage and current plots.

Figure B.1: Comparison of optimization with a certain scenario (left) and uncertainty in the prediction and real consumption (right).

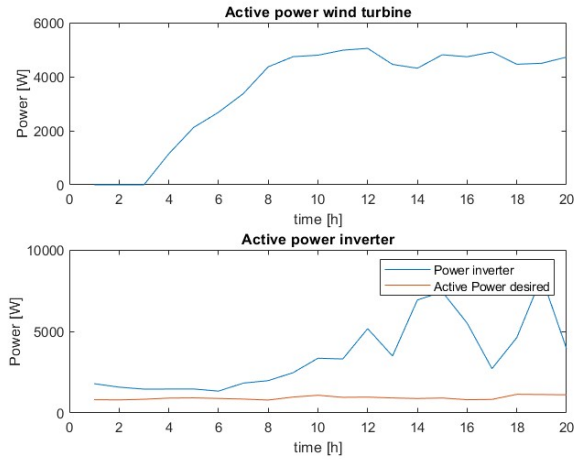


(a) Production and consumption values with consumption mismatch, baseline prediction.

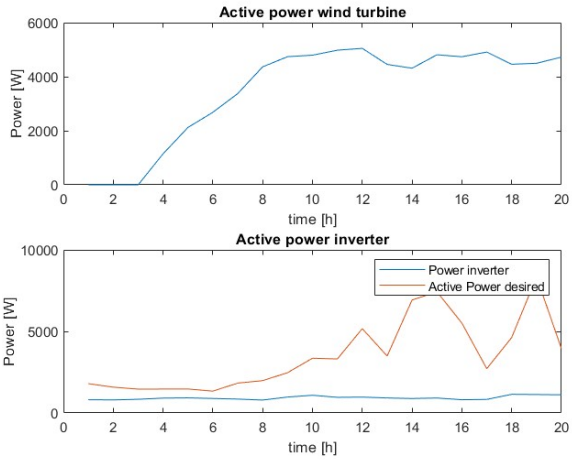


(b) Production and consumption values with consumption mismatch, baseline consumption.

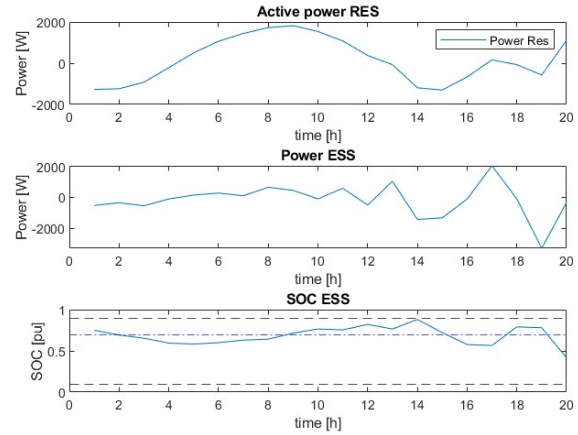


(c) State and optimization variables of the optimization routine.

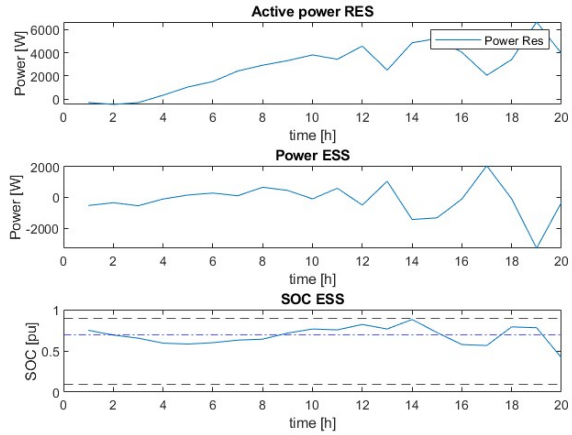


(d) State and optimization variables of the optimization routine.

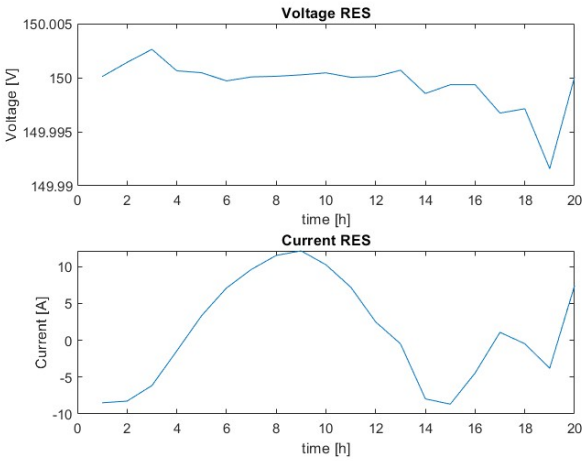


(e) Voltage and current plots.

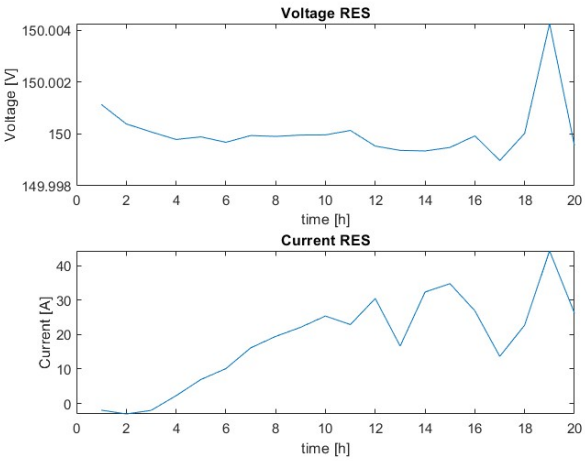


(f) Voltage and current plots.

Figure B.2: Depicted are the two scenarios comparing a baseline value used in the prediction term (left) and as the true consumption (right).

### B.2.2 *Power setpoint shift*

The following modification of the problem formulation was done for two reasons. Firstly, to enable the setpoint placement on the grid side. And secondly, to increase the decision space of the controller where introduction of the adjustment variable aimed to loosen the relationship between the fixed quantities and the decision variable $P_{ESS}$.

$$
\begin{aligned}
min \quad & w_1 * |P_{inv,des} - P_{inv}| + w_2 * (P_{inv,des} - P_{inv})^2 \\
& + w_{SOC} * (SOC_{ESS} - SOC_{ESS,des})^2 \\
& + w_{SOC,final} * (SOC_{ESS}(K) - SOC_{ESS,init})^2 \\
& + w_{V,fluc} * (V_{RES} - V_{nom})^2 \\
& + w_{adj} * (P_{inv,des} - P_{inv} + P_{adj})^2 \\
s.t. \quad & P_{inv,des} = \lambda * P_{inv,meas} + (1 - \lambda) P_{inv,pred} \\
& SOC_{ESS}(k+1) = SOC_{ESS}(k) + P_{ESS}(k) \\
& P_w - P_{ESS} - P_{loss} = P_{RES} - P_{adj} \\
& P_{inv} = -\eta * (P_{RES} - P_{adj}) \\
& P_{RES} = V_{RES} * I_{RES}
\end{aligned}
\tag{B.2}
$$

Hereby, the power on the AC and DC sides of the inverter were related with the efficiency term $\eta$, shifting the setpoint.

EXPECTATION The the introduction of the adjustment variable $P_{adj}$ in eq. B.2 intended to anticipate power peaks and preemptively penalize them, incentivizing the controller to shift the power output to a more constant power profile. It is approached by distributing anticipated demand mismatches and adjusting the output of the ESS accordingly. The inclusion of $P_{adj}$ in the objective function intends to penalize those scenarios.

Furthermore, $P_{inv,des}$ creates the reference from measured and anticipated values, balancing their relative importance with $\lambda$, depending on their reliability. The intention is the admittance of plant feedback in the form of measurement values to improve the performance of the optimization. In the simulation, the predicted and "measured" values are kept the same.

RESULTS Building on the previous results, the two baseline scenarios were compared to each other in the frame of the varied problem formulation.

From visual inspection, it appears that the power flow (fig. B.3) can be altered by changing $\lambda$. They show how the ESS power flow as well as the adjusted power respond to changes in $\lambda$. The shape of the adjusted power seems to weakly trace the ESS power, resembling its outline.

This observation is corroborated by fig. B.4, with $\lambda \in [0,1]$ chosen at its boundaries. In the "certain" case (left), $P_{RES}$ and $P_{adj}$ look much alike. The other case (right) reveals that the adjustment power seems to complement the inverter power, summing them to the desired value.

Interestingly, alterations of $w_{adj}$ did not change the simulation results. In comparison to the "certain" case of the previous iteration, it was not possible to remove the offset between the desired and actual inverter power.

FUNCTION VALUES The absolute function value and the NCO value have shrunk with a factor of more than five compared to their respective case of the initial formulation.

Noteworthy is that the results from the baseline comparison do not reciprocate anymore, showing different values depending on what data is used for the prediction and consumption.

*Discussion*

To tackle this problem, the adjustment variable $P_{adj}$ was introduced which aimed at increasing the decision space. The addition of a second optimization variable was intended to smoothen power output. With the square penalty, large deviations from the reference are penalized more heavily. Thus, shifting deviating peaks would lower the overall cost.

The results of this optimization show that the storage management is indeed facilitated. It was possible to offload a share of the power flow. However, it didn't adjust the storage based on anticipated peaks. Part of the reason could be that the adjustment variable could not be sufficiently constrained by attributing it a physical meaning.

During excess production, the addition of a loosely constrained power sink, namely the adjustment variable, should be able address the issue. Hence, it was expected that, in those cases, the error at the inverter would approach zero. Especially, because the results confirmed that the ESS was mostly limited by its maximum capacity. In hindsight, it could be possible that $P_{adj}$ was introduced as a relief to $P_{RES}$ but added in the objective function in addition to the error minimization at the inverter, changing the prioritization.

With increase of $w_{SOC}$, it was possible to keep the charge level almost constant and the discharge was mainly handled through $P_{adj}$.

It appeared necessary to increase the decision space of the formulated problem to minimize feasibility issues while enabling the addition of operational constraints.

At first instance, the setpoint shift with a constant efficiency was straightforward and the nature of the optimization remained unchanged. Yet, its introduction enabled the addition of an inverter efficiency function. Its effect would be accounted for in the optimization.

WEIGHT CHANGES Simultaneously, the expectation of improved control was defied, as shown by the weight variations $w_1$ and $w_2$. Where the error magnitude between the desired and actual inverter output was expected to change according to the weight, differences were observed in the SOC but not in the inverter power flow. It is possible that the

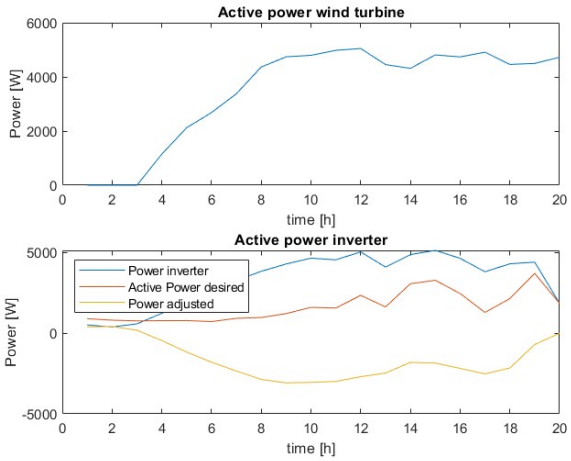


(a) Power flow out of the wind turbine and to the inverter. Setpoint and optimization values are shown.

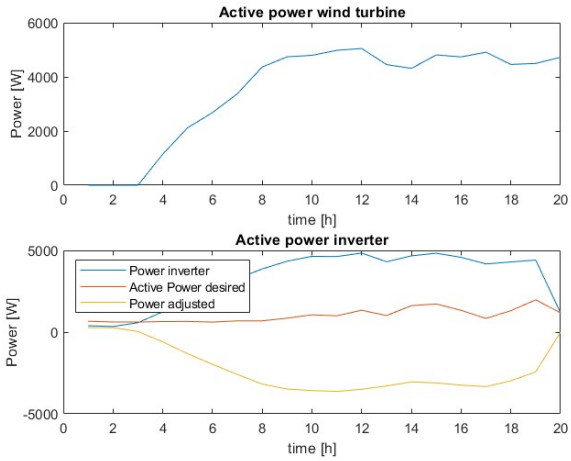


(b) Power flow out of the wind turbine and to the inverter. Setpoint and optimization values are shown.

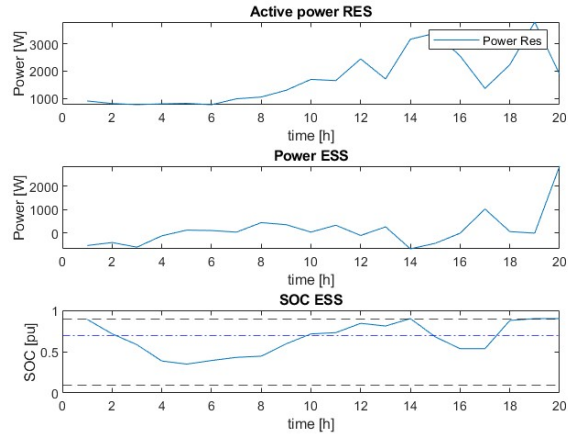


(c) RES and ESS power flow is plotted along with the SOC.

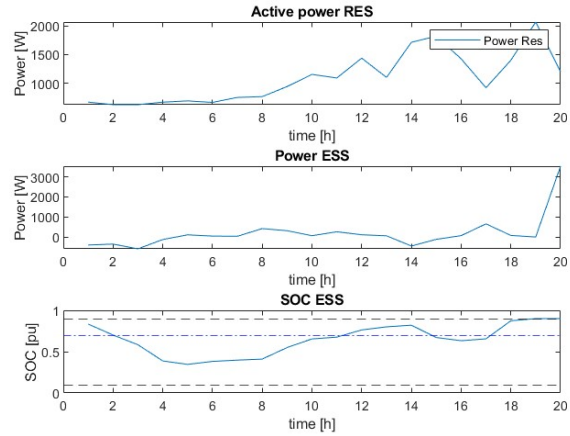


(d) RES and ESS power flow is plotted along with the SOC.

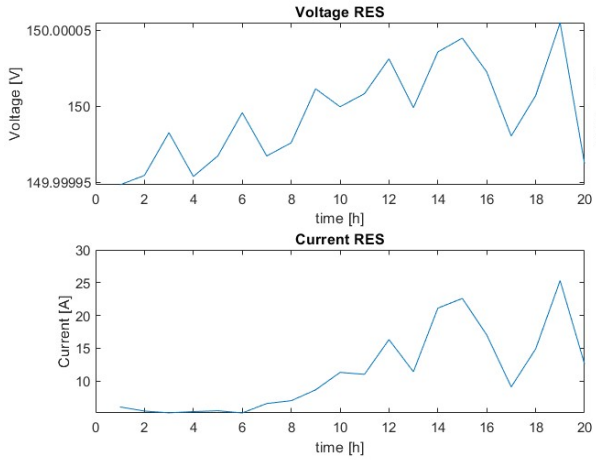


(e) Voltage and current plots.

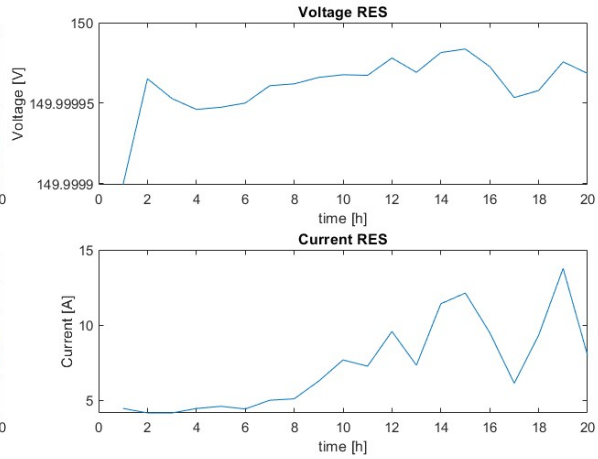


(f) Voltage and current plots.

Figure B.3: Simulation results with the baseline prediction. Plots on the left are taken with $\lambda = 0.3$ and on the right $\lambda = 0.7$.

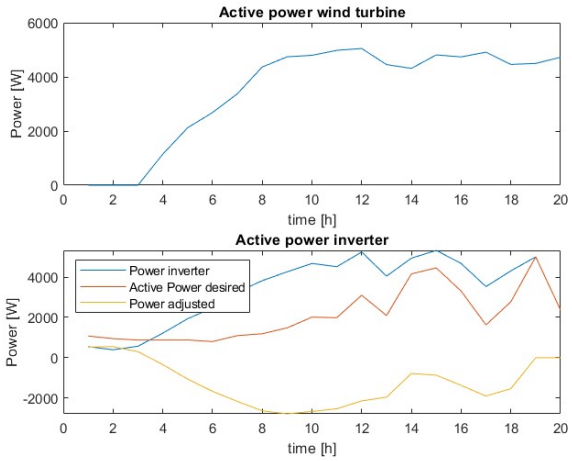


(a) Power flow out of the wind turbine and to the inverter. Setpoint and optimization values are shown.

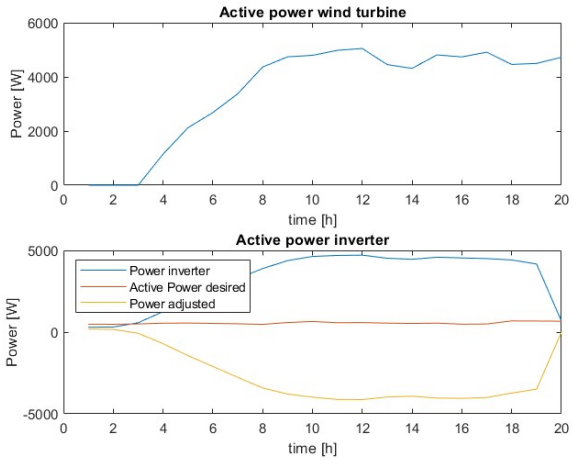


(b) Power flow out of the wind turbine and to the inverter. Setpoint and optimization values are shown.

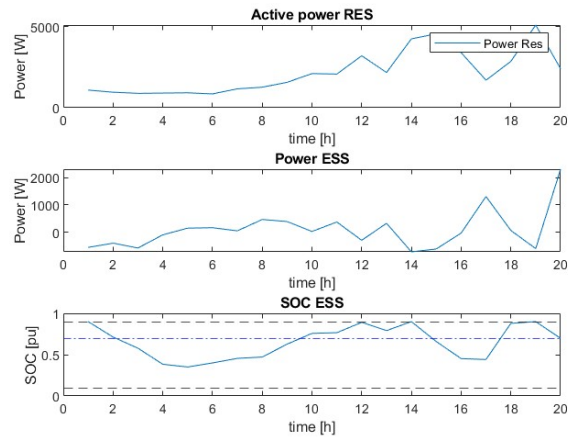


(c) RES and ESS power flow is plotted along with the SOC.

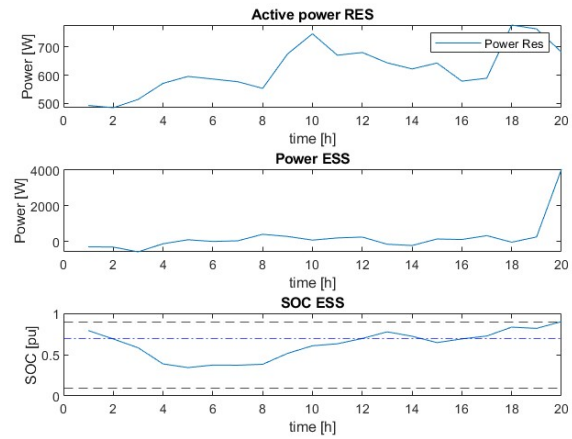


(d) RES and ESS power flow is plotted along with the SOC.

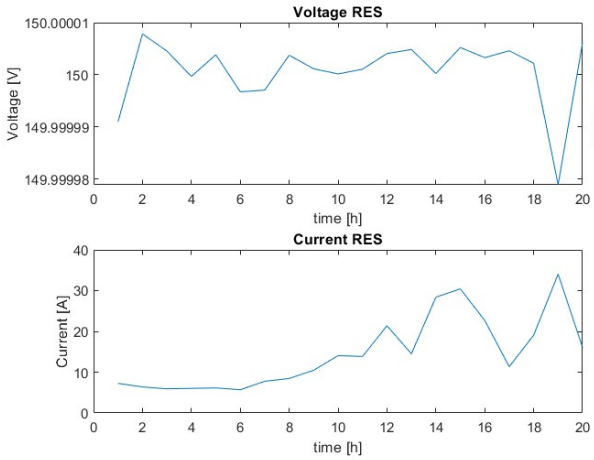


(e) Voltage and current plots.

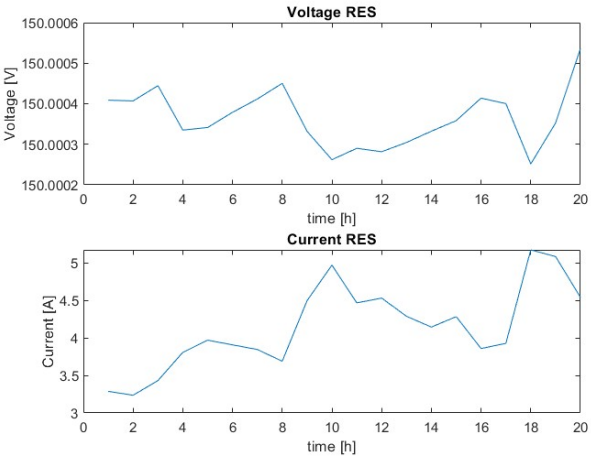


(f) Voltage and current plots.

Figure B.4: These figures plot the "certain" scenario (left) and the baseline prediction case (right).

weighted sum of the inverter error was much larger than the SOC, upon which the latter was adjusted by the algorithm.

Generally, it proved challenging to interpret the effect of $P_{adj}$ as it could only be attributed with a limited physical relevance to the system. Maintaining the idea of loosening the problem's constraints and increasing the decision space, the reactance term was introduced. Here, the frequency, voltage magnitude, and angle can be changed to influence the power output from the inverter. It is also expected to ease analysis as its parameters can be attributed to physical quantities in the model. With this knowledge, it should be possible to properly constrain the variables in the problem formulation.

WEIGHT CHANGES Due to the frequency variable, management of the ESS's SOC was much facilitated. Adjustments of $w_{SOC}$ alter the SOC with minor losses in tracking accuracy at the inverter. Increases in $w_1$ and $w_2$ eradicated the offset through slight changes in voltage and frequency. Lastly, increasing the voltage weight $w_V$, increases the offset of the inverter power. Interesting to note is that compensation through frequency adjustment can be observed. This interaction between voltage and frequency is necessary to balance the active power output. It is promising because active droop control makes use of these two variables. Their interplay can already be controlled here by adjusting the optimization function weights.

### B.2.3 *Reactance term*

In this variation, the adjustment variable $P_{adj}$ was replaced with $\Delta P$ (eq. 4.6). Hereby, the desired power setpoint at the inverter is altered to react to power adjustments due to frequency changes.

It is furthermore desired to penalize frequency deviations from the nominal value. Thus, the frequency term in eq. B.3 is added along with the weight $w_f$. Both, the reactance and penalty terms are added to incorporate feedback from the plant in the model optimization later on. Its introduction intends to lay the foundation for the reactance component and the associated droop control.

$$
\begin{aligned}
min \quad & +w_f * (f_{inv} - f_{nom}) \\
s.t. \quad & P_{inv,des} = \lambda * P_{inv,meas} + (1-\lambda) P_{inv,pred} \\
& P_{inv,pred} = P_{load,pred} + \Delta P \\
& \Delta P = \frac{(V_{RES} * \eta) * V_{grid}}{X_L} * 2\pi * (f_{inv} - f_{nom})
\end{aligned}
\tag{B.3}
$$

The small-signal variation $\Delta P$ from eq. 4.6 is added to the prediction term.

Due to the absence of plant feedback in the optimization implementation, it is attempted to utilize the forecast to anticipate changes in power $\Delta P$ due to changes in frequency.

Enabling is the coupling reactance model which relates the voltage and power on the RES side to the power and frequency on the grid side.

EXPECTATION The addition of the reactance term is expected to induce a shift in the ESS power flow. The reason is the introduction of the frequency term which is directly related to the power setpoint at the inverter. The same equation also relates the inverter with RES voltage. Thus, the latter is expected to experience larger fluctuations.

RESULTS Some of the results of the adapted problem formulation were condensed into fig. B.5. They show a much closer similarity between the desired and actual power output. In direct comparison, their shape seems to resemble that of the frequency as well as the predicted grid power.

The introduction of the reactance term shows the interaction between the frequency component and the power flow of the ESS as well as the predicted load on the grid. Buffering the difference between the prediction and consumption under consideration of $\Delta P$ is the ESS. It can best be observed in fig. B.6, as the interaction is accentuated with a lower weight on the SOC. The altered power flow also slightly shifts the frequency and power setpoints on the inverter, the former to a larger and the latter to a smaller value.

Frequency changes can best be observed after t=14h in the "certain" case (fig. B.5 left). As the predicted load on the grid rises, the frequency falls, and vice versa. The frequency changes in accordance with $\Delta P$. This relationship can also be seen in the baseline comparison of fig. B.5 (right).

Lastly, investigating the influence of $\lambda$ on the absolute function value as well as the NCO shows a decrease in both with increasing $\lambda \in [0, 1]$. To keep the measurements relevant and stay in line with the previous implementation for comparison's sake, $\lambda = 0.7$ has been chosen.

Similarly to the previous VI-plots, the voltage and current relationship (fig. B.7) was largely unaffected. Increasing the weight of the voltage term altered voltage magnitude itself without changing the shape of the trajectory and the SOC only minimally.

*Discussion*

Compared to the adjustment variable, the location at which the reactance term was added in this implementation is very different. The reactance now modulates the inverter setpoint based on predicted changes in the coupling reactance. The predictions are based on dynamic changes induced by the grid.

With the introduction of the coupling reactance, two major changes were performed. Namely, the addition of the inverter frequency as an optimization variable and the incorporation of the voltage term into other constraints.

FREQUENCY VARIABLE As the frequency optimization variable is proportional to $\Delta P$, it is logical that the frequency rises with increasing output from the inverter. As dictated by the grid inertia law, when supply increases, as does the frequency. Similarly, as the ESS

discharges, it provides power to the RES, increasing inverter output and frequency in the process.

VOLTAGE VARIABLE In line with the expectations, changes in voltage are much more pronounced. As the variable is present in the reactance, its value affects the power flow to the grid. In accordance with eq. 2.3, a rise in voltage magnitude mediates an increase in active power flow.

LIMITATION The main limitation of the optimization approach also affects the results of this simulation, namely the absence of the grid dynamics. In this case, the frequency is largely unconstrained, governed by its own error term in the objective function. Beneficial is that its presence circumvents feasibility issues. Simultaneously, it is able to buffer any overproduction, facilitating power flow and ESS storage management. However, in the application, this scenario is highly undesirable because major frequency changes have the potential to vastly destabilize the grid. This circumstance shows the necessity for active power and frequency control.

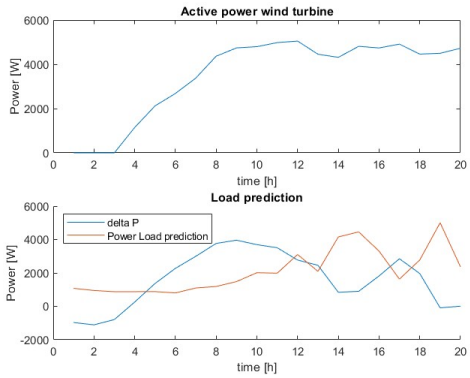


(a) "Certain" case: Power production and prediction of the load as well as the adjustment due to the reactance.

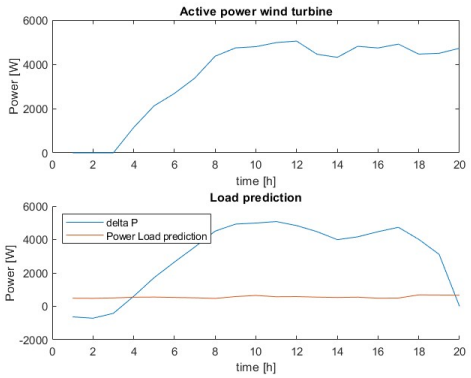


(b) Baseline case: Power production and prediction of the load as well as the adjustment due to the reactance.

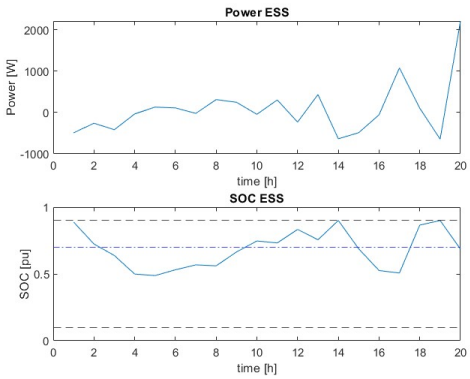


(c) Power flow and SOC of the ESS.

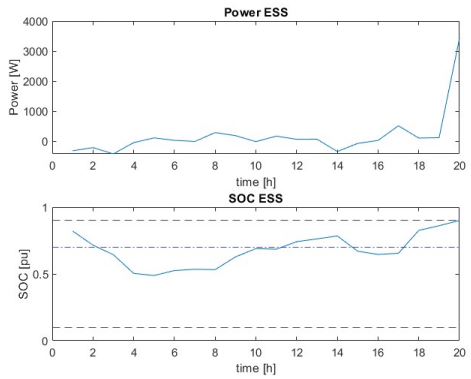


(d) Power flow and SOC of the ESS.

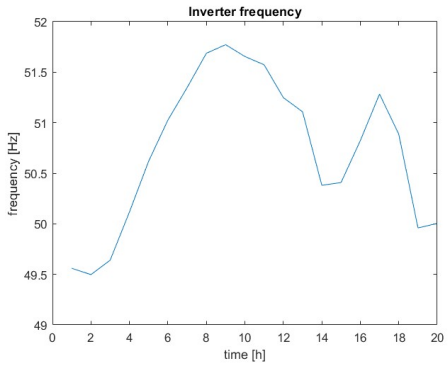


(e) Frequency at the inverter.

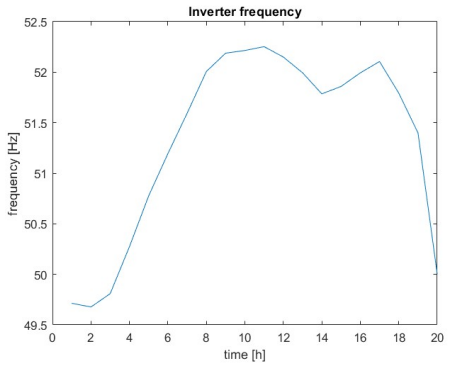


(f) Frequency at the inverter.

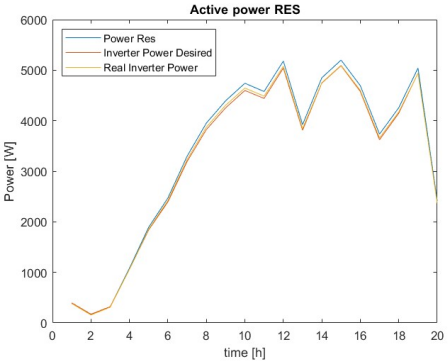


(g) Active power flow on the RES and inverter along with the setpoint at the inverter.

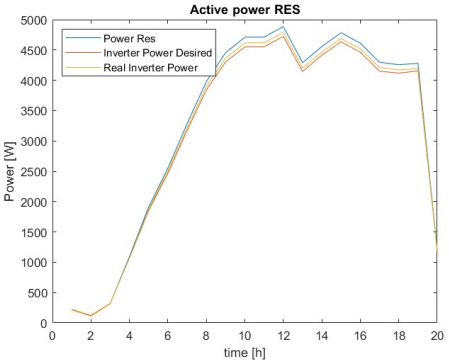


(h) Active power flow on the RES and inverter along with the setpoint at the inverter.

Figure B.5: Comparison of the "certain" scenario (left) and the baseline prediction (right).

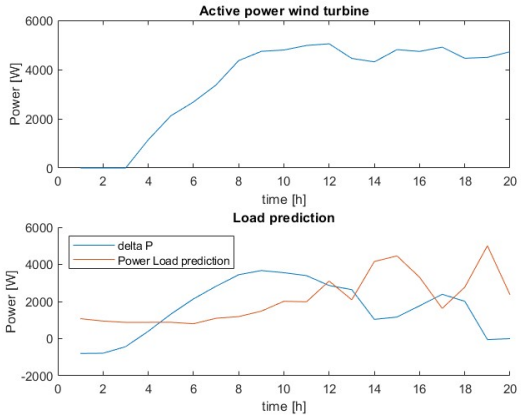


(a) "Certain" case: Power production and prediction of the load as well as the adjustment due to the reactance.

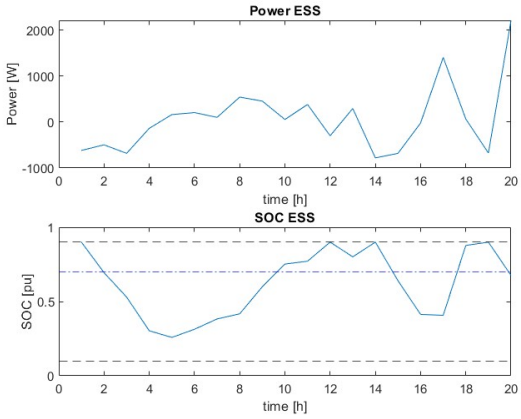


(b) Power flow and SOC of the ESS.

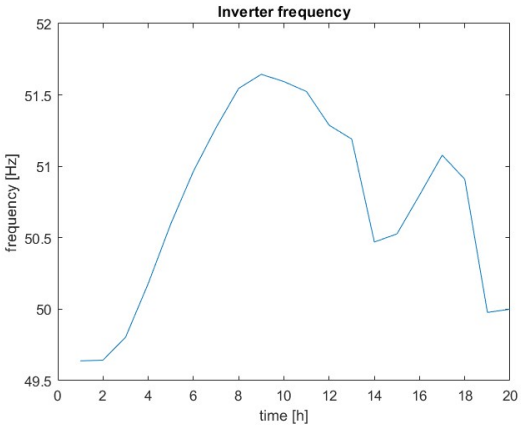


(c) Frequency at the inverter.

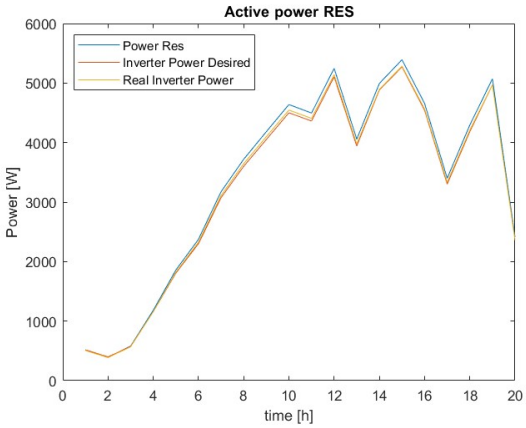


(d) Active power flow on the RES and inverter along with the setpoint at the inverter.

Figure B.6: Shown are the results of the "certain" case simulation, varied by reducing the weight $w_{SOC}$.

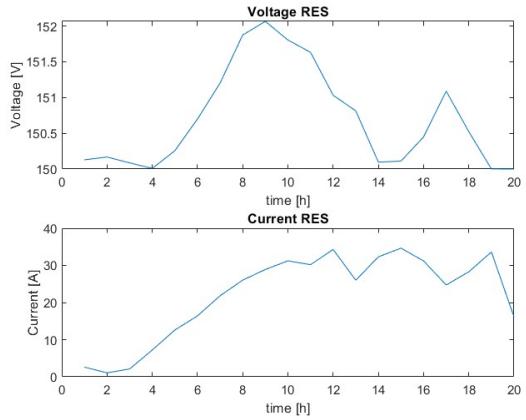


(a) Voltage and current plots.

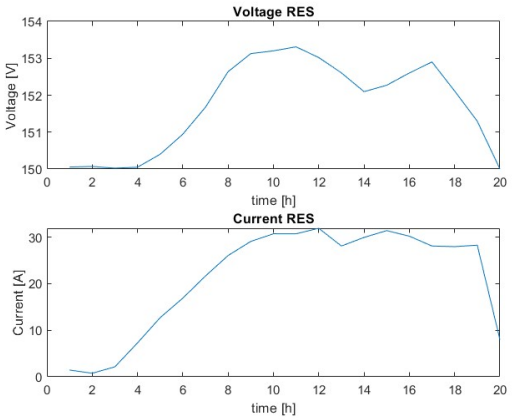


(b) Voltage and current plots.

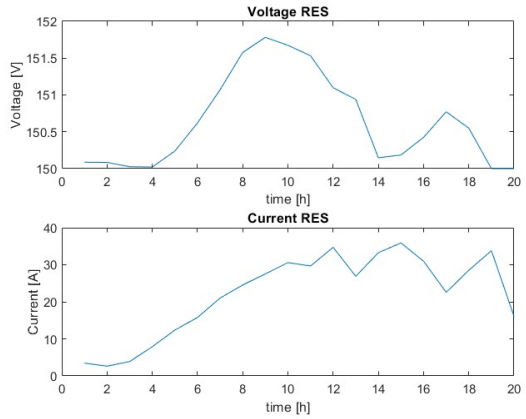


(c) Voltage and current plots.

Figure B.7: Power decomposition plots with the certain case on the left and the baseline prediction case on the right.

### B.2.4 *Optimization with frequency*

The following adaption of the constraints aimed at incorporating some form of droop control into the optimization routine. Here, the goal is establishing a relation between the power on the RES side and the inverter. The former should not only match the active power setpoint but also provide means to adjust for frequency changes through the reactance. The equations are implemented as constraints following the derivation in chapter 4, utilizing eq. 4.7. They are added to the initial formulation as an extension to the constraints:

$$
\begin{aligned}
&s.t. \\
&P_{inv,des} = \lambda * P_{inv,meas} + (1-\lambda) P_{inv,pred} \\
&P_{inv,pred} = P_{load,pred} + \Delta P \\
&\Delta P = \frac{V_{inv} * V_{grid}}{X_L} * \Delta\delta \\
&\Delta\delta = \omega_0 - \omega_{grid} + m_p * (P_{load,pred} - P_{load,meas})
\end{aligned}
\tag{B.4}
$$

EXPECTATION With the inverter frequency removed as optimization variable and the addition of the reactance equations, it is expected that the consumption becomes less accurate to trace as the unconstrained frequency variable is removed as power buffer.

FUNCTION VALUES The baseline scenario with the true consumption produces smaller absolute function values by factor 100 and the NCO is reduced by factor $10^5$. With such disparate values, this scenario was further investigated with the weight changes shown in the section here.

RESULTS Inclusion of the reactance equations into the optimization function had significant impact on the power flow in the hub. Fig. B.4 displays some results of the investigation.

Interesting behavior is shown in "certain" scenario by the reactance power (fig. B.8e). It appears to have large spikes compared to the other power plots and previous cases. A similar observation was made in case where the prediction was changed to baseline. Contrary, the reactance power of the opposite baseline scenario (fig. B.8f) appears to have a high correlation with the other power flows, i.e. $P_{RES}$ and $P_{inv}$. The reactance power seems to be an amplified signal of the latter two.

Noteworthy is the Frequency power graph (figs. B.8e and B.8f). The associated variable adjusts the inverter power flow due to frequency fluctuations. It essentially consists of the error between the desired and "measured" frequency with a gain attached, implementing the droop gain of eq. 2.3. Increasing the gain assimilates the shapes of the reactance power and inverter power more (fig. B.9. It changes the prediction value on the inverter as well.

Raising the optimization weight $w_2$ on the error of the inverter setpoint lowers the fluctuations in the reactance power. It simultaneously increases the fluctuations of power flow

of the ESS and the SOC. Although no investigated scenarios yielded significant changes in the power curve of the ESS.

*Discussion*

In this final adaption, the frequency variable was removed as an optimization variable. It was replaced by the reactance and droop formulation, aiming to constrain the variables. With their addition, it was expected that the tracking accuracy decreased due to the removal of the unconstrained variable that buffered the power mismatch between the supply and demand.

POWER ANGLE The focus point of this implementation is the formulation of the power angle as part of the coupling reactance. This element was intended to change the inverter power setpoint by leveraging predictions of power fluctuations on the grid and their effect on the reactance behavior.

A few observations were made in the process that all pointed to the same issue, the absence of measurements from a plant. This situation was circumvented at first with the utilization of time series data, implementing the equations as a purely predictive component.

Determination of the relative voltage angle still proved difficult due to the correlation between the grid variables. Herein, it was necessary to provide data on the grid's power and load, voltage, and frequency. With them, it was expected to be able to calculate the reactance power and voltage angle at the inverter terminal. However, because the grid dynamics are not modeled, the grid's voltage angle and magnitude are unconstrained. Their effect on the active power flow was uncertain.

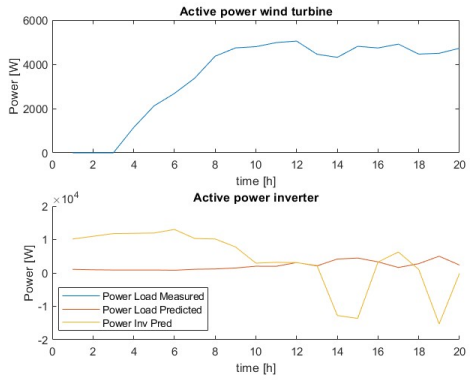


(a) Produced power (top) and predicted vs "measured" quantities on the grid side (bottom).

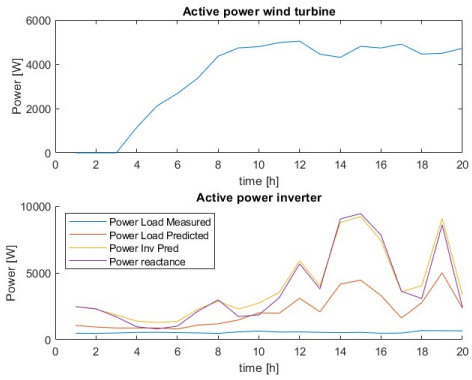


(b) Produced power (top) and predicted vs "measured" quantities on the grid side (bottom).

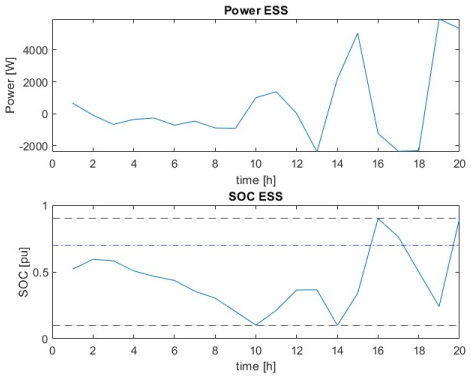


(c) Power flow and SOC of the ESS.

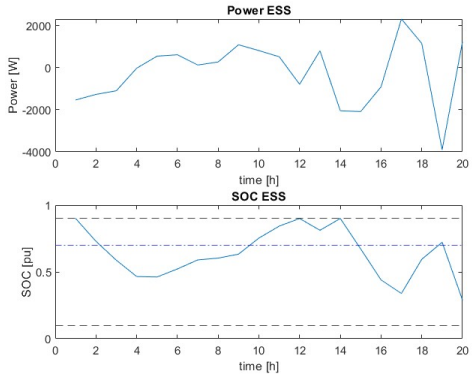


(d) Power flow and SOC of the ESS.

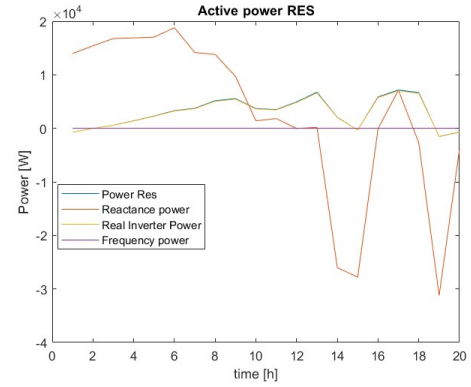


(e) Comparison of the true power flow on the RES and through the inverter.

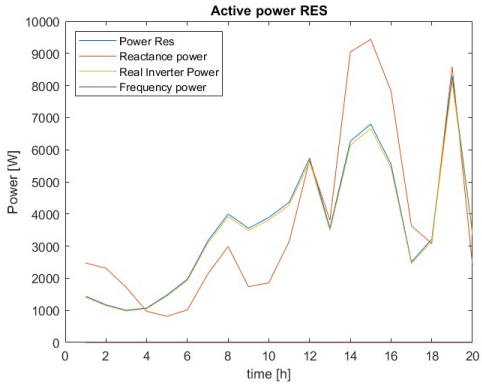


(f) Comparison of the true power flow on the RES and through the inverter.

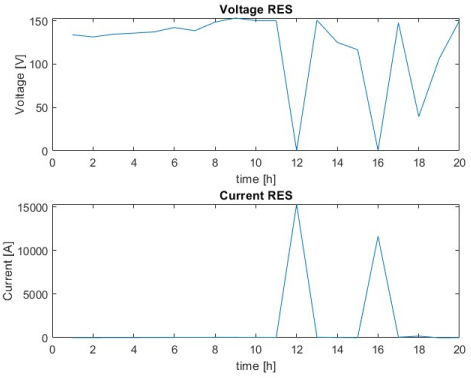


(g) Current and voltage plots on the RES side.

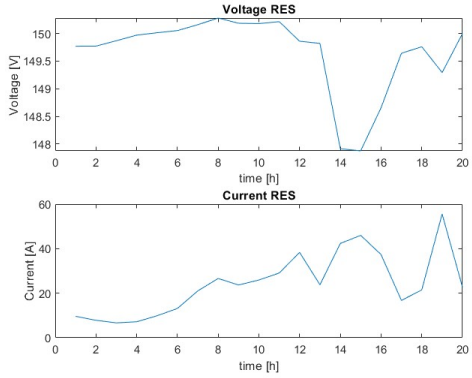


(h) Current and voltage plots on the RES side.

Figure B.8: The left side presents the "certain" case where the predicted and true consumption on the grid are the same. The right side depicts a baseline scenario where the true consumption is almost constant.

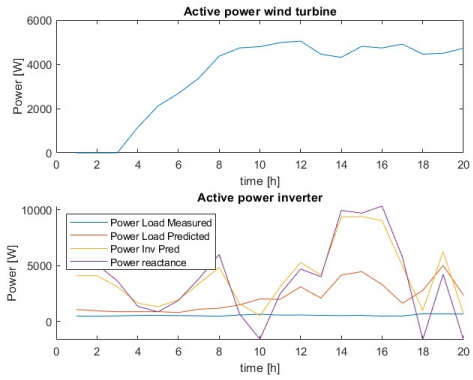


(a) Produced power (top) and predicted vs "measured" quantities on the grid side (bottom).

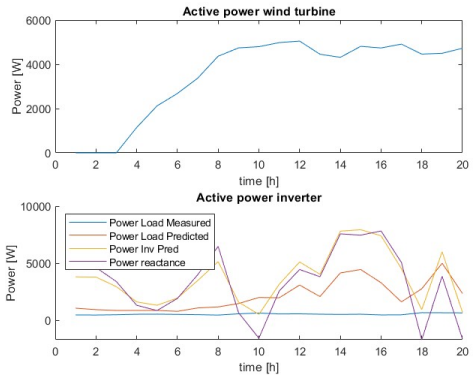


(b) Produced power (top) and predicted vs "measured" quantities on the grid side (bottom).

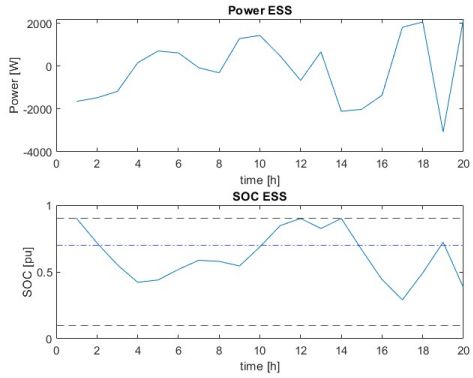


(c) Power flow and SOC of the ESS.

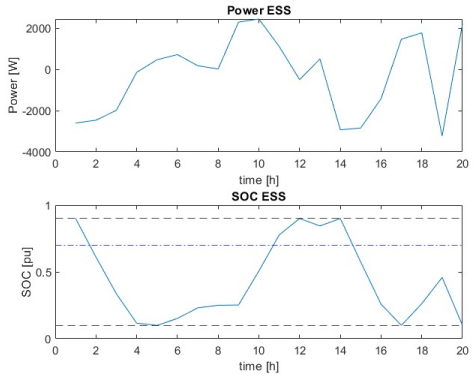


(d) Power flow and SOC of the ESS.

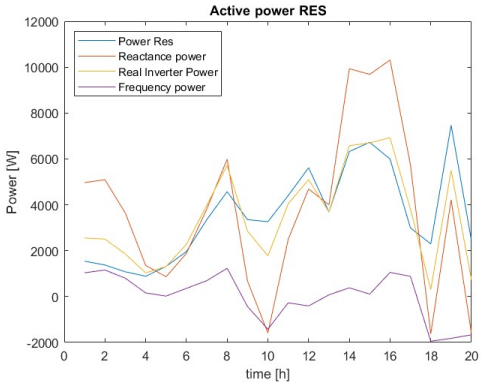


(e) Comparison of the true power flow on the RES and through the inverter.

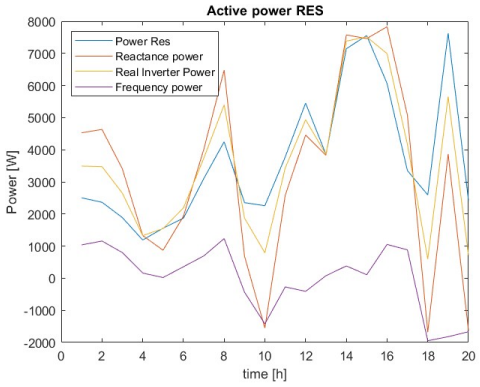


(f) Comparison of the true power flow on the RES and through the inverter.

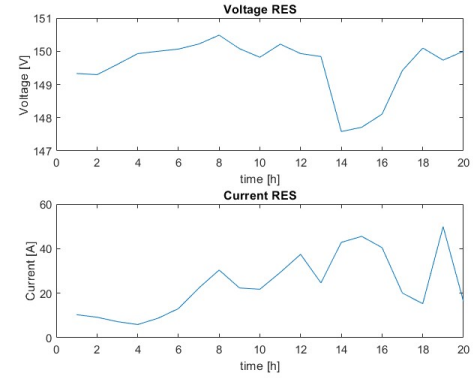


(g) Current and voltage plots on the RES side.

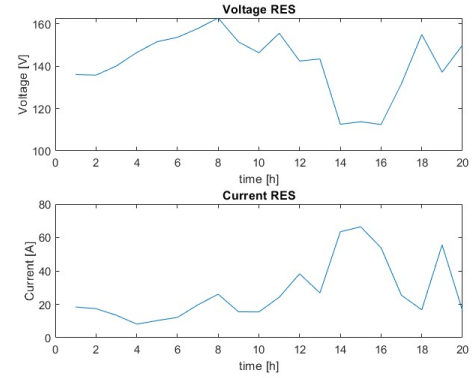


(h) Current and voltage plots on the RES side.

Figure B.9: The left side presents a baseline scenario where the true consumption is almost constant and an increased droop ratio. The right side depicts the same scenario with a large $w_2$ weight.

## B.3 PLANT MODEL RESULTS

Implementing the optimization algorithm on the designed plant, it is investigated if the power flow of the ESS can be leveraged to control the power flow on the grid. The algorithm should respond to demand changes while providing stability. With droop control, it aims to minimize frequency and voltage deviations. It is determined whether an inverter setpoint can be followed under consideration of future production and consumption. Herein, the forecast of production and demand is a sliding window over expected quantities.

### B.3.1 *Initial Optimization*

In the following section, a first implementation of the optimization routine on the modeled plant is undertaken. The mathematical formulation presented as the "first approach" of the optimization model section (sec. B.2.1) is now tested to interact with the dynamics of the plant.

Most important aspects in this analysis were the in- and outputs of the optimization routine. namely $P_{ESS}$ and the SOC. The former acts as the reference signal for the ESS and effectively manages the power flow. The latter is a measurement variable that updates its value in the optimization routine.

**FIGURE PLOTS** The results according to this simulation are presented in figs. B.10, B.11. Here, the effects of the setpoint optimization can be observed. First of all, it is apparent that the power on the RES and the grid closely follow the setpoint changes induced by the battery. Furthermore, as consumption exceeds production, the battery is discharged and the SOC decreases accordingly.

From the load curve, it can also be seen that the power output varies with change in load. The highest rate of change can be seen at t=2.5h. Here, the load increases and the power setpoint is raised to adjust. At t=4h, the production briefly exceeds the demand and the SOC increases.

Notably, at t=6.4h, the ESS reaches its lower SOC limit and is prevented from discharging any further. Here, the power flow out of the ESS ceases and with it the flow into the RES and the grid. The latter two are now following production values of the wind turbine.

This incident has cascading effects on the frequency and voltage measured on the grid. The plots in fig. B.11 visualize the drop in voltage as well as negative frequency spike occurring at the same instant.

**WEIGHT VARIATIONS** Lastly, the weight $w_1$ on the square term in the objective function were changed to analyze their influence on the grid dynamics. The results are plotted in fig. B.12.

When emphasizing the weight of the square term in the objective function, the control action taken (setpoint changes) by the control are much more drastic. Associated are larger fluctuations of the SOC and much bigger level changes on the grid.

*Discussion*

Similar to the model-free setup, part of the investigation should assess whether or not parameters behave as expected.

As the ESS power flow is the decision variable, it should be determined if it can be manipulated to control RES and grid parameters. First of all, the battery discharges at a rate consistent with the power flow. Furthermore, the RES and grid follow setpoint changes induced by the ESS, showing that it is possible to control the active power on the grid. Importantly, as the SOC of the ESS reaches its lower limit, the power flow ceases and the grid experiences a drop in supply. The output levels are now equal to the production.

Equally spaced frequency spikes can be observed at every setpoint change of the ESS. Here, the same equational relation as in the model-free approach holds where these changes in frequency are expected because, in accordance with the grid inertia equation (eq. 2.1), a sudden decrease in power supply (from the ESS) induces a negative change in frequency.

At this point, the electrical power P=VI does not need to be modeled explicitly. The dynamics are captured by the model where the voltage is changed along with changes in power flow. It is an important aspect because, in the optimization, this nonlinear constraint poses numerical issues for a quadratic solver. It also necessitates adaptions in the problem formulation as, due to the absent constraint, the voltage cannot be explicitly penalized.

Reviewing the voltage and frequency dynamics, it appears that the RES- and grid-side are strongly coupled to each other. Every shift in power has cascading effects on the grid. Therefore, in the next step, the coupling reactance was introduced to weaken the coupling between the two sides. This component seems to be especially important in weak grid scenarios where changes in output can have drastic impact on the grid dynamics.

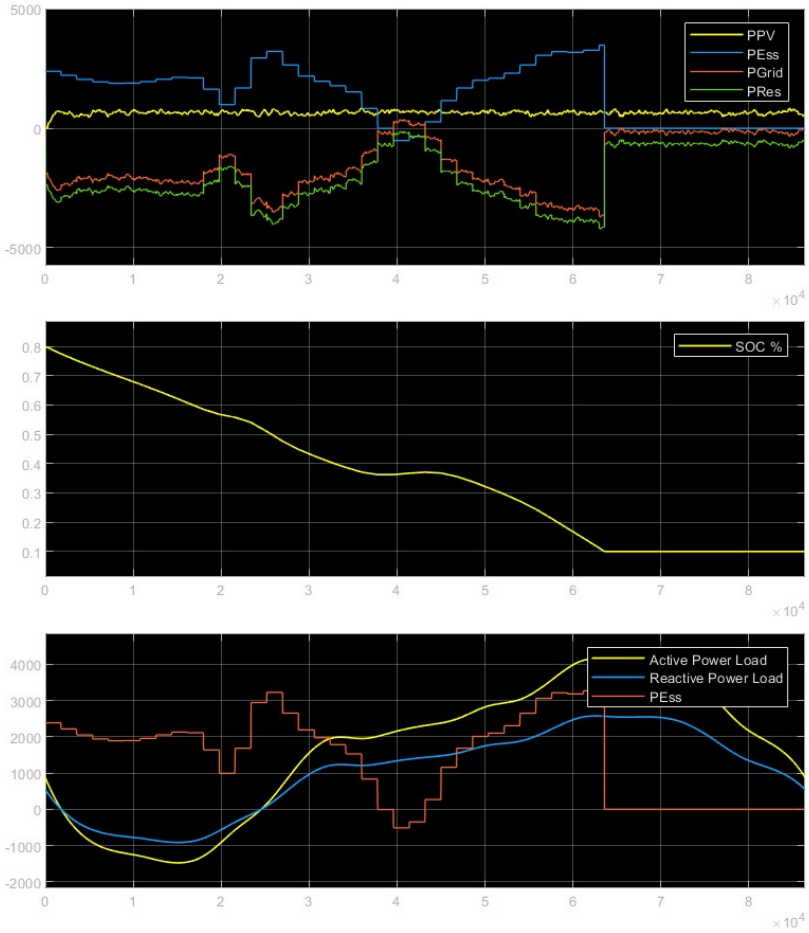


Figure B.10: Top: Phasor power flow, measured at four different instances, namely at the turbine and ESS terminals, and before and after the inverter. Middle: SOC of the ESS. Bottom: Variable load applied to the grid

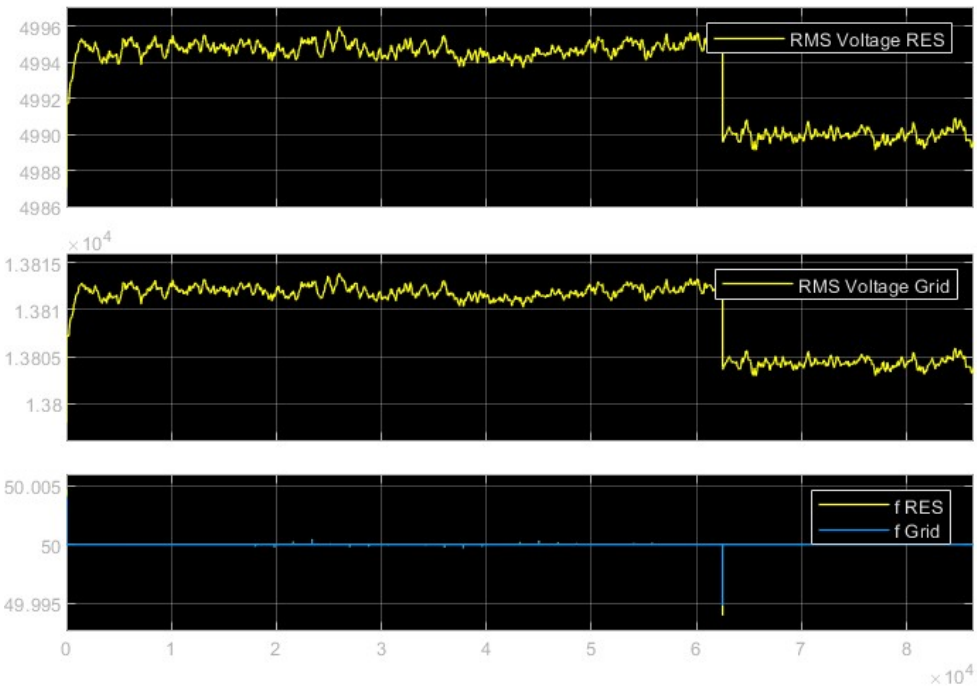


Figure B.11: Voltage and frequency plots of the RES and grid.

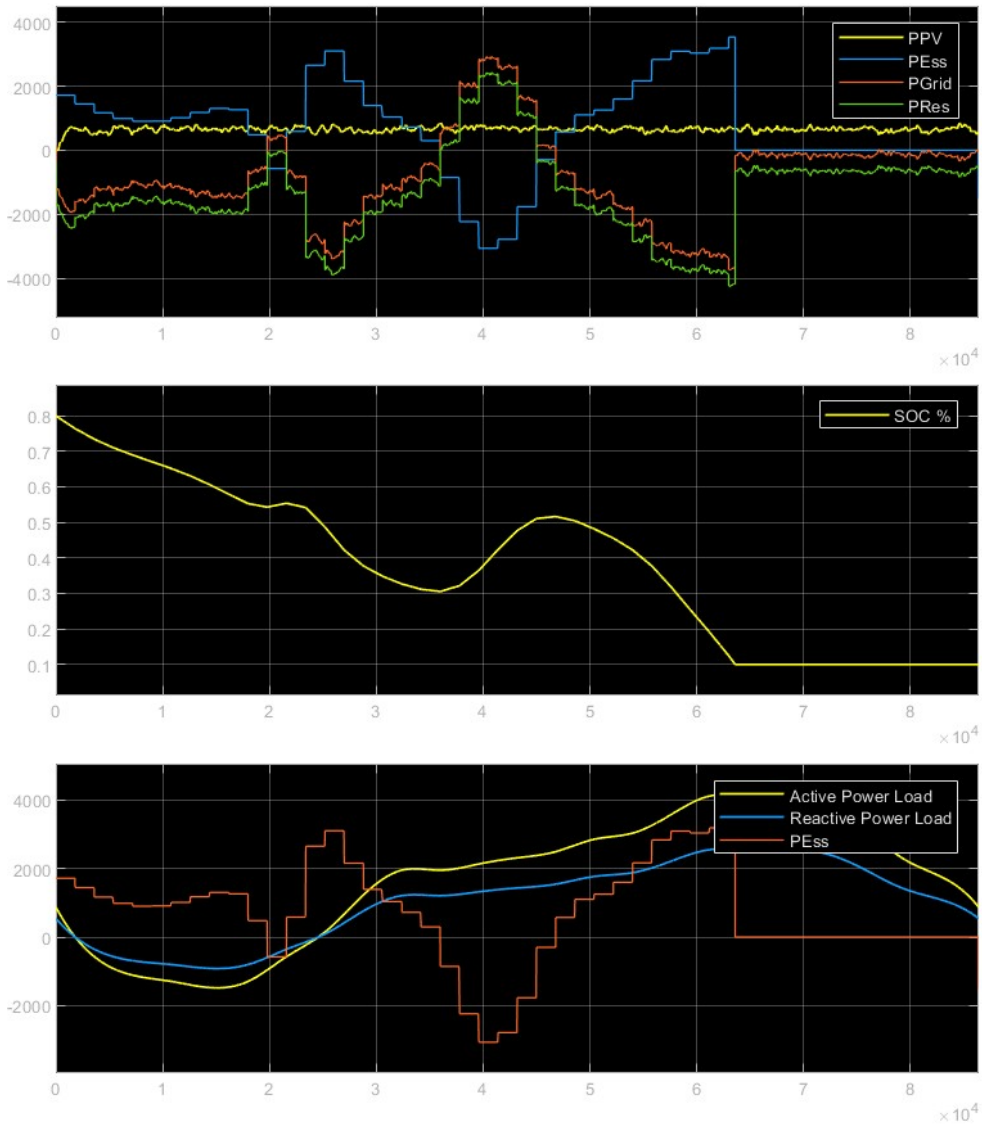


Figure B.12: Power flow, SOC, and grid load with an increased weight of the square inverter setpoint error.

### B.3.2 *Coupling reactance*

In this step, the coupling reactance is introduced after the inverter. Thus, the adaption is briefly investigated to determine the reactance's influence on the dynamics observed previously.

Adaptions in the controller comprise two elements. The power setpoint shift to the grid-side of the inverter and the reintroduction of the power relationship P=VI. The former aims to determine an inverter setpoint that can be translated into a setpoint for the ESS on the RES side. The latter is achieved with approximation using the McCormick envelope.

EXPECTATION Incorporation of the coupling reactance component is expected to aid in decoupling the dynamics of the grid and the RES.

With the addition of the electrical power equation, it is expected that the voltage stability can be improved. Herein, the deviations from the nominal voltage can be explicitly penalized, minimizing fluctuations.

COUPLING REACTANCE The dynamic coupling between the RES and the grid is undertaken by varying the reactance inductance value L. The results are shown in fig. B.13, portraying the voltage and frequency relative to the inverter-reactance couple. Here, the RES measurement is taken before the inverter, "inverter" between the inverter and reactance, and grid after the reactance.

Displayed in fig. B.13a are the frequency and voltage on the either side of the coupling reactance for the smallest reactance value (L = 0.0002H). Here, both parameters behave very similarly to each other with the small difference that the voltage on the grid is slightly higher and the frequency deviations marginally smaller.

Increasing the reactance value also increases the difference in magnitude between the voltages on either side of the reactance (fig. B.13b). Simultaneously, about half of the magnitude of the frequency spikes is transmitted to the grid. Furthermore, small voltage fluctuations are more attenuated in comparison to the smaller inductance value. The result is a smoother voltage curve on the grid side.

The same trend can be observed for values for L=0.02H (fig. B.13c). Here, the large negative spike is barely transferred to the grid and frequency changes appear to have minor influence. Differently, the voltage on the RES side begins to sag and fluctuates much more in comparison to smaller reactance values.

Lastly, the largest inductance value (L=0.2H) ran into convergence issues due to large spikes in power and frequency which Simulink was unable to resolve.

Generally, it is possible to observe some frequency spike at regularly spaced instances. They seem to occur at every ESS setpoint change.

Investigation of the voltage term in the objective function revealed that changing the associated weight does not exert control over the magnitude or shape of the voltage curve on the RES or grid.

POWER FLOW The measured current and power, as well as the ESS parameters are captured by plots shown in fig. B.14.

With respect to the changing reactance values, only very minimal changes in power and current magnitude were observed. Each current measurement assimilates the shape of the power profile of the ESS. The current before and after the coupling reactance are identical.

*Discussion*

In the comparison of different reactance values, an important aspect is the power continuity. From the plots, it can be obtained that the inductance only minimally influences the power flow. Essentially, the only difference is the amount of charge that can be stored in the magnetic field of the inductor.

FREQUENCY After the introduction of the coupling reactance, the frequency behaves as intended. With increasing reactance value, the coupling between the grid and the RES decreases, dampening frequency spikes experienced on the grid. Because the stored charge is released when the current changes, the damping occurs at the expense of a larger voltage spike. Simultaneously, the voltage drop across the inverter increases as confirmed by the graphs. Small inductance values achieve insufficient decoupling of the dynamics, where similar frequency changes are experienced on the grid as on the RES. As large inductance appears to negatively affect the RES voltage, inhibiting most dynamic interaction, a mean value of L=0.002H was chosen, balancing coupling and control. It is expected that some dynamic coupling is required to enable the droop control.

VOLTAGE Regarding the implementation of the electric power law into the optimization algorithm, the McCormick envelope (eq. A.11) was chosen to approximate the equation. Herein, the goal was to reestablish the explicit power law to reintegrate the voltage term into the objective function. Its idea to penalize voltage fluctuations and incentivize the maintenance of a constant voltage.

Upon adjusting the weight $w_V$, no change could be observed in the behavior of the ESS. It is speculated that the approximation may be too general. That is because it utilizes the upper and lower voltage and current limits which have not been investigated in-depth in this project. Conversely, stricter boundary conditions would result in an infeasible solution. More research into the exact value and impact of these boundary conditions on the problem is required to improve the estimation.

FLUCTUATIONS Within the power profile, it was possible to observe significant fluctuations between setpoint changes in the SSTO. Some of these fluctuations were near instantaneous and of large magnitude. They would become extremely problematic for the ESS when component limitations, such as maximum power or SOC, are violated. They highlight the necessity for the $H_2$ storage to maintain a desirable battery SOC as well as for the DO to respond to such short-term fluctuations. Especially the RR control can integrate the three ESSs while minimizing deviations from the setpoint synthesized by the SSTO. It should be able to provide the integrated ESS with the means to compensate for fluctuations in the power production of the wind turbine.

FEEDBACK Until this point, the algorithm does not receive any feedback from the sensors placed on the plant. Thus, the optimization is performed irrespective of the grid's response. Feedback on the frequency, voltage, and power flow should alter the optimization such that its response can adjust to the changes observed on the grid.

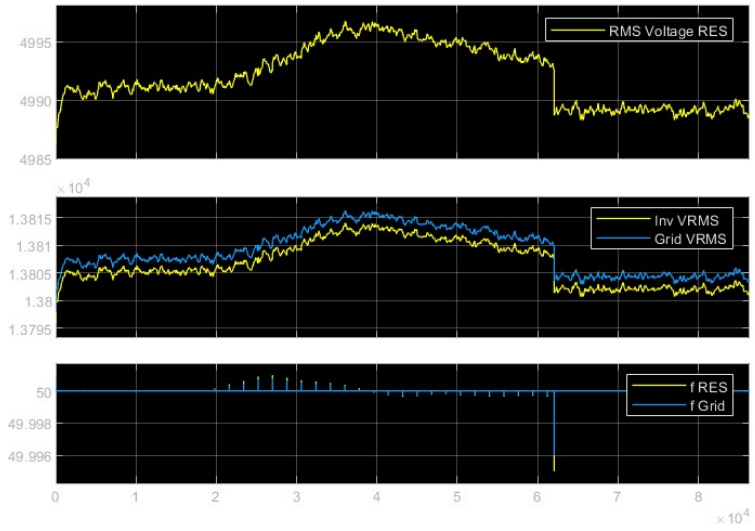


(a) Inductance value L=0.0002

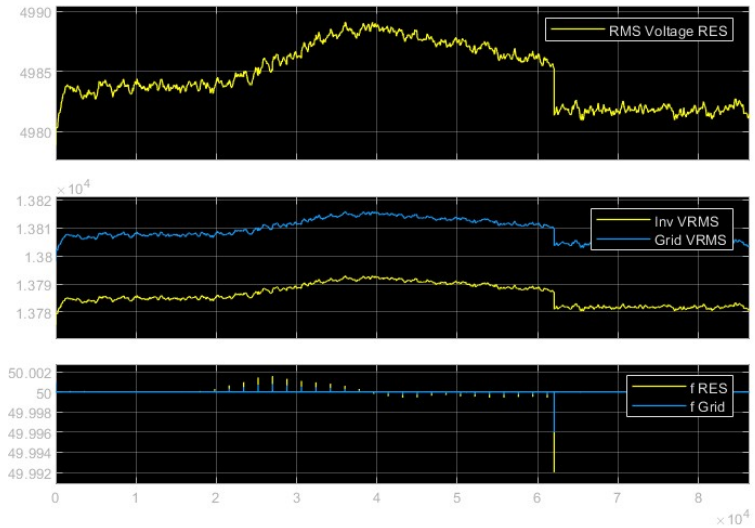


(b) Inductance value L=0.002

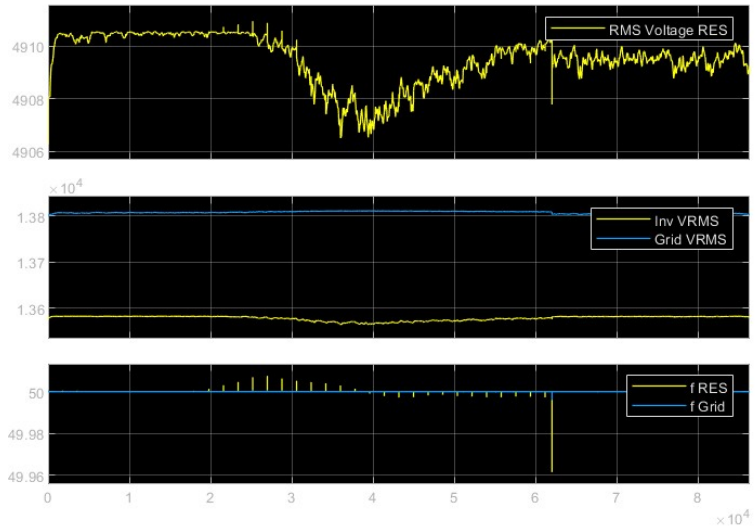


(c) Inductance value L=0.02

Figure B.13: Voltage and frequency plots for variations of the coupling reactance's inductance value.

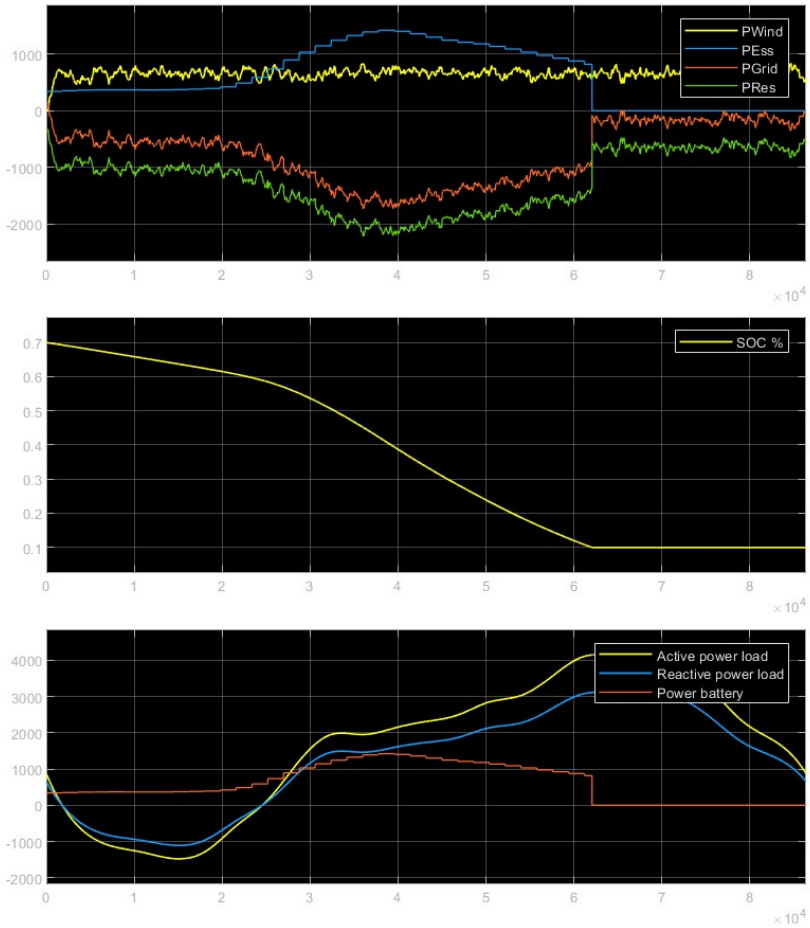


(a) Phasor power flow at the top, SOC of the ESS in the middle, and load applied to the grid at the bottom.

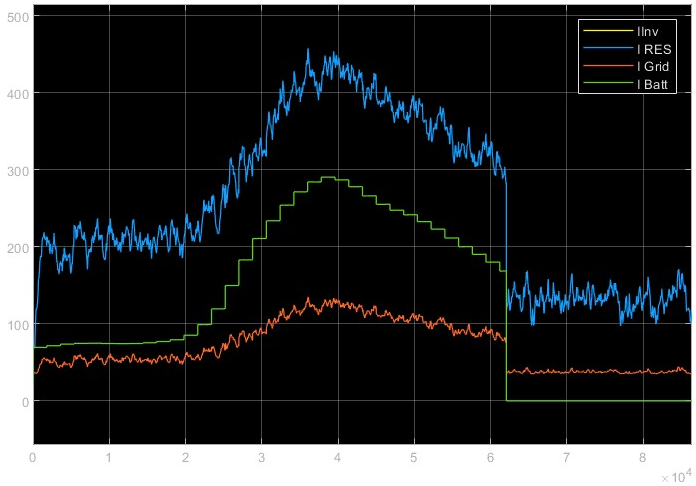


(b) Current flow, measured at different instances of the simulation.

Figure B.14: Power and current plots for the final choice coupling reactance's inductance value L=0.002.

### B.3.3 *Measurement*

Following the procedures from the optimization based implementation and the previous results, it appeared necessary to introduce further feedback. In first instance, the optimization algorithm is provided with an active power measurement from at the inverter, complementary to the setpoint. The implementation of this step is congruent with eq. B.3, balancing prediction and measurements terms.

The results of the simulation show various exemplary plots for values between 0.1 and 0.9, favoring the measurement in the former case and the prediction in the latter. A direct comparison reveals interesting differences between these scenarios. They can be observed in figs. B.16, B.15, B.17, varying the weight $\lambda$. For each case, they portray the power flow, SOC, grid load, voltage, frequency, and currents.

**POWER FLOW** With measurement focus (fig. B.16a, $\lambda = 0.1$), the ESS is discharged at an almost constant rate. Overall, the ESS power flow is much lower than the consumed power.

Contrary the power output in the "estimation" case (fig. B.16d, $\lambda = 0.9$) is larger than the consumption. It outlines the consumption curve, peaking after the largest increase in consumption. Finally, the SOC reaches its lower limit at the power flow is cut off.

Balancing between prediction and measurement (figs. B.16b, B.16c, $\lambda = 0.4, \lambda = 0.65$) improve the tracking of the load curve. Particularly the latter has been found to be the best relative fit. It increases with the load peaks and takes a similar shape. Interestingly, the power setpoint in both cases fluctuates much more as in the extrema. They are especially severe in the initial hours, indicating drastic control action.

**VOLTAGE AND FREQUENCY** Comparing the plots in fig. B.15, it appears that the voltage remains largely unaffected by the ESS power flow. Its variations are antagonistic to the reactive power flow, as the power increases the voltage falls, and vice versa.

Frequency spikes can be observed to occur at ESS setpoint changes. Negative setpoint changes cause positive frequency spikes, scaling proportionally with magnitude. Hence, frequency spikes for $\lambda = 0.4$ and $\lambda = 0.65$ are much more numerous. Noteworthy is their location. They were measured between the inverter and the coupling reactance but do not appear on the grid-side after the coupling reactance.

**CURRENT** Complementary to the other plots is fig. B.17, displaying the various currents flowing in the model. Their shape has great resemblance of the power flows where the largest currents are applied on the RES due to its lower voltage relative to the grid. The currents before and after the reactance are identical.

It can be observed that the $\lambda = 0.4$ case (fig. B.17b) traces the grid current better than the others.

A current peak develops with increasing $\lambda$. It can be attributed to the ESS, and is reflected in the RES and grid currents.

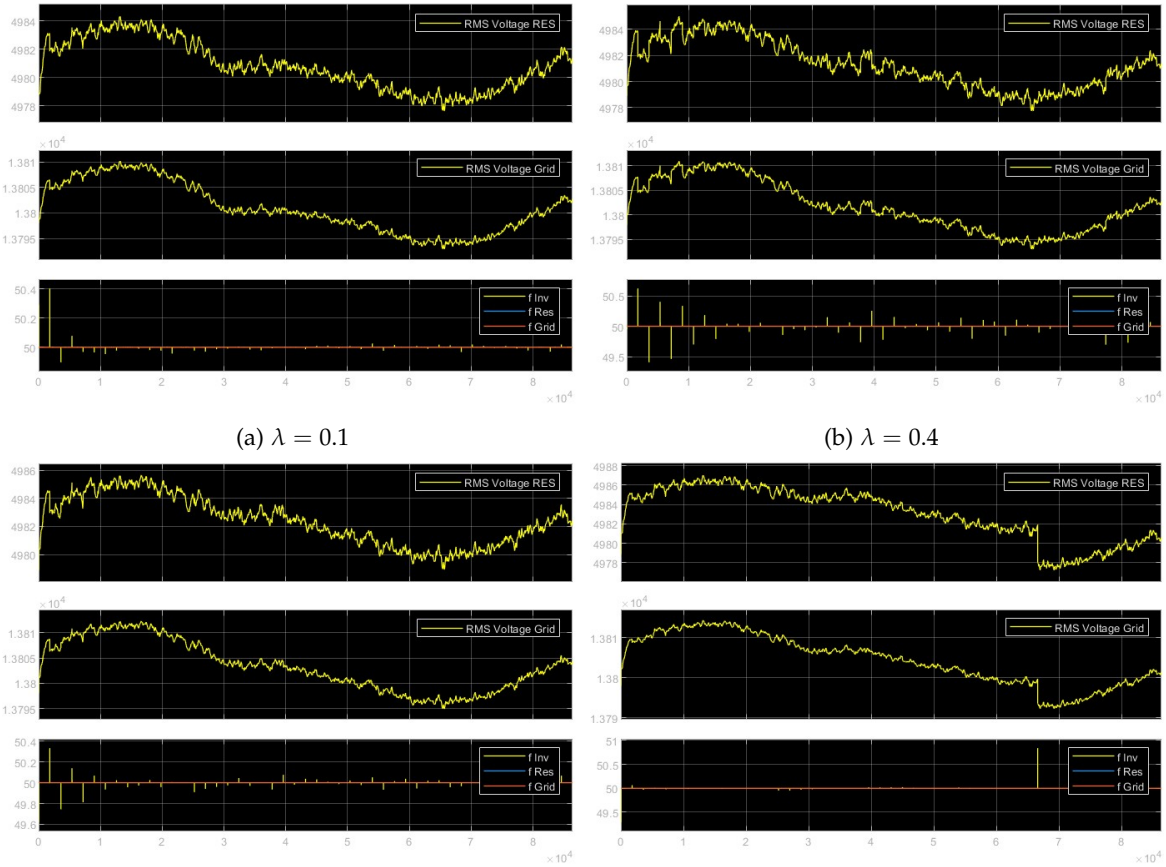


(a) $\lambda = 0.1$ (b) $\lambda = 0.4$

(c) $\lambda = 0.65$ (d) $\lambda = 0.9$

Figure B.15: Voltage and frequency plots for different values of $\lambda$, weighing between prediction and measurement.

*Discussion*

This augmentation of the optimization investigates what influence a measurement of the active power at the inverter terminal has.

Compared to the implementation without feedback, increasing reliance on the measured component raised the total power drawn from the ESS. However, either extreme had little variation in the power drawn. More balanced consideration of both parts (i.e. $\lambda = 0.4$ and $\lambda = 0.65$) showed large fluctuations in the power setpoint determined by the algorithm. It almost appears as if it bounces between the measured and predicted terms.

These variations are accompanied by frequency spikes on the grid. They are due to the drastic changes in grid load and come as expected. However, they are undesirable as they would destabilize a power grid.

It should also be mentioned that the reliance on the measurements for the SSTO optimization is not ideal. By omitting the modeling of the observer, measurements are instantaneous, i.e. the last sample before the optimization is reiterated. It implies that any of those last samples can contain a significant measurement error which is not considered in the optimization. The presence of batch measurements would minimize such situations.

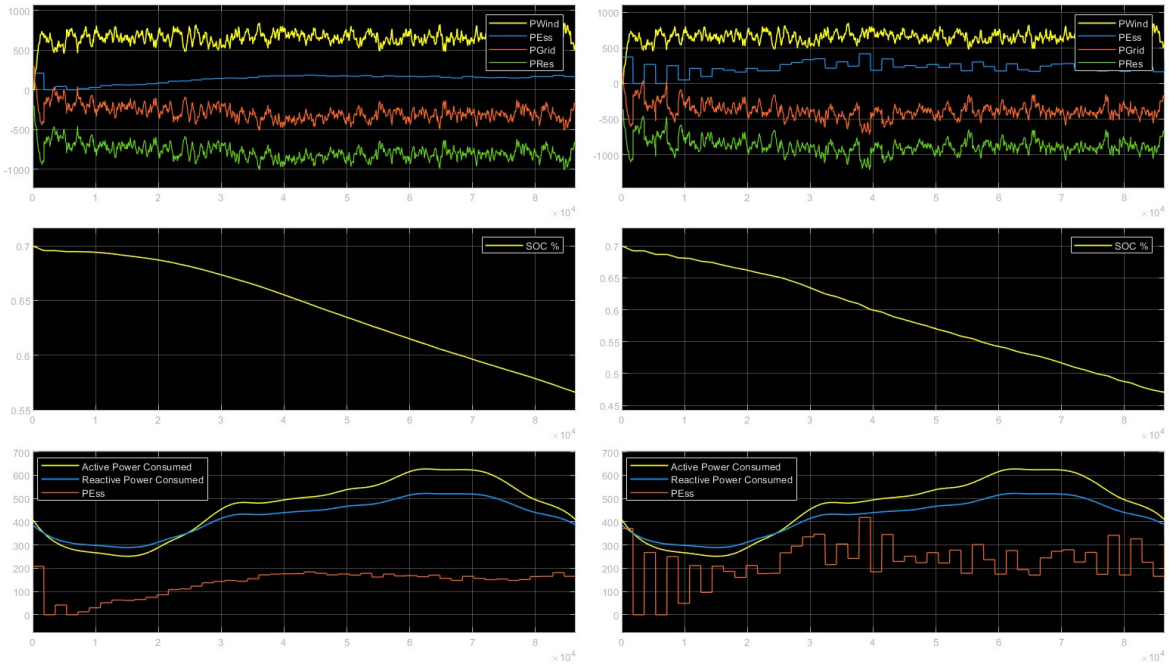


(a) $\lambda = 0.1$




(b) $\lambda = 0.4$

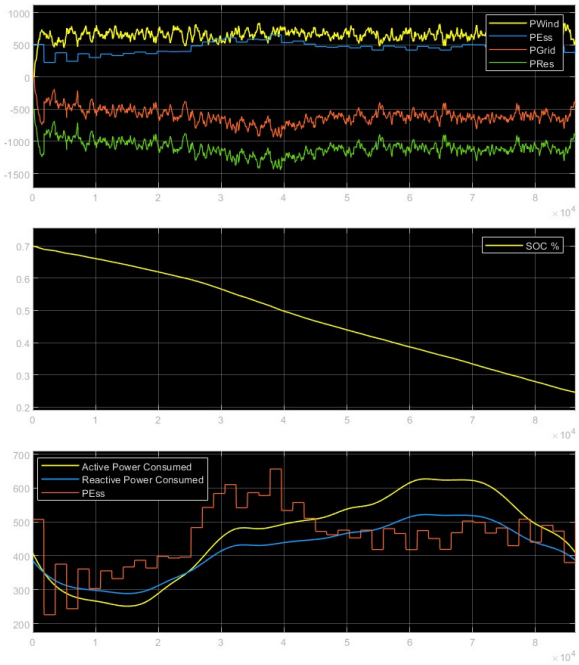


(c) $\lambda = 0.65$

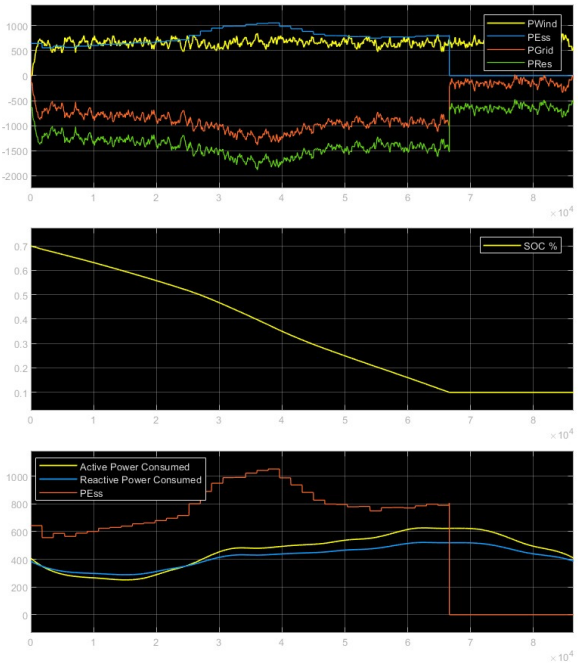


(d) $\lambda = 0.9$

Figure B.16: Phasor plots for different values of $\lambda$, weighing between prediction and measurement.

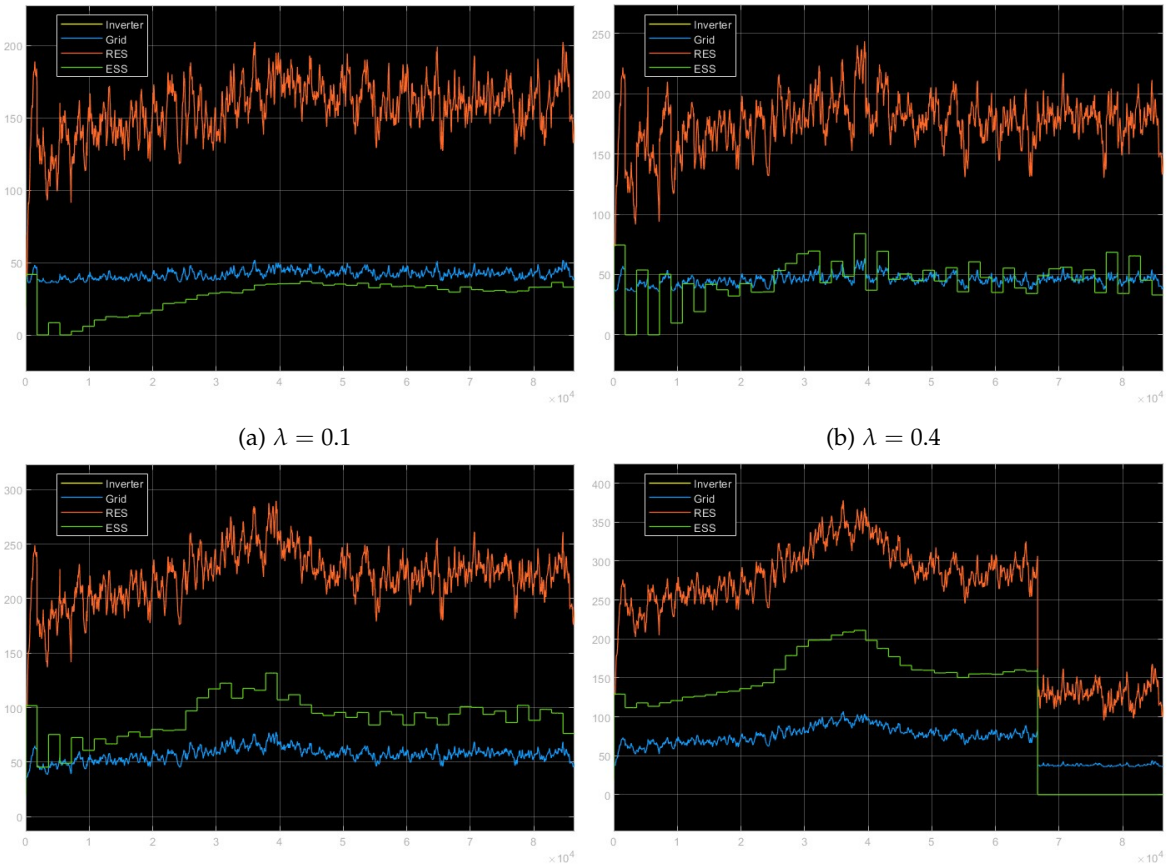


(a) $\lambda = 0.1$ (b) $\lambda = 0.4$

(c) $\lambda = 0.65$ (d) $\lambda = 0.9$

Figure B.17: Current plots for different values of $\lambda$, weighing between prediction and measurement.

### B.3.4 *Small angle approximation*

In this final step, the linearized form of the coupling reactance equation (eq. 4.7) was implemented. The equation uses the small angle approximation of the droop control to calculate variations in the power flow across the reactance.

The goal of the implementation is twofold.Firstly, testing the derived equation, and secondly, comparison of the implementation between the optimization- and model-based simulations.

EXPECTATION With its addition, droop control of the active power and frequency should be possible. The MPC leverages measurements of frequency, voltage, and active power as well as time series predictions to determine power flow variations. It is expected that the regulation of power and voltage on the RES side can be improved to minimize frequency fluctuations and deviations from the active power reference on the grid side.

RESULTS The graphs depicting the plant behavior are plotted in fig. B.18. They present the measured quantities induced by the ESS power setpoint change as calculated by the optimization.

Worth mentioning is the frequency measurement. The small spikes disappeared and merely five large spikes remained. These spikes are congruent with variations in the output of the ESS. Consequence of negative supply changes are positive frequency spikes and vice versa.

The ESS discharge curve is rather constant with a steadily declining SOC. The total discharge is rather low with the SOC dropping 12%.

The voltage plots remain similar to previous implementations, varying mainly due to the reactive power flow.

*Discussion*

This adaption intends to solve the problems that arose from the implementation of the coupling reactance. Due to the variable multiplications, the equation is nonlinear and could not be solved by the quadratic solver. Hence, the small angle approximation was sought out to tend to the issue.

The approximation did not fully prevent numerical issues. They were observed in the ESS power profile. Whenever the reference signal would crash to zero, no solution was found in this particular iteration. It was found out that the McCormick envelope caused issues in the solution finding. Its use was particularly difficult without proper plant sizing and parametrization.

As devised in the math model, the implementation of the reactance with the droop control is a final element to investigate whether some conclusions can be drawn from its comparison with the model-free version.

Examination of the optimization variables showed that the calculated reactance values were mainly contributing to the nature of the $P_{ESS}$ setpoint.

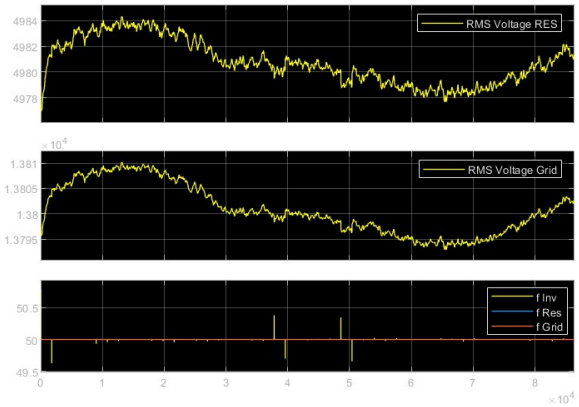


(a) Voltage and frequency plots.

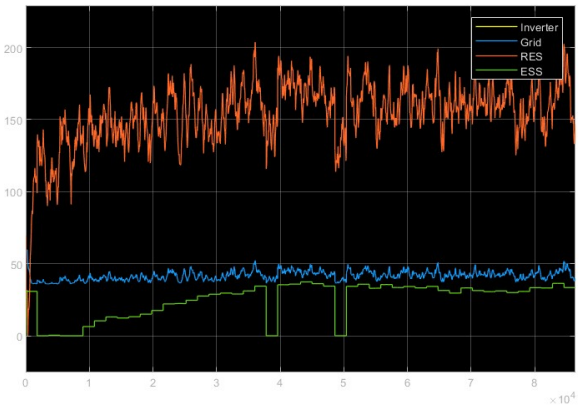


(b) Current plots

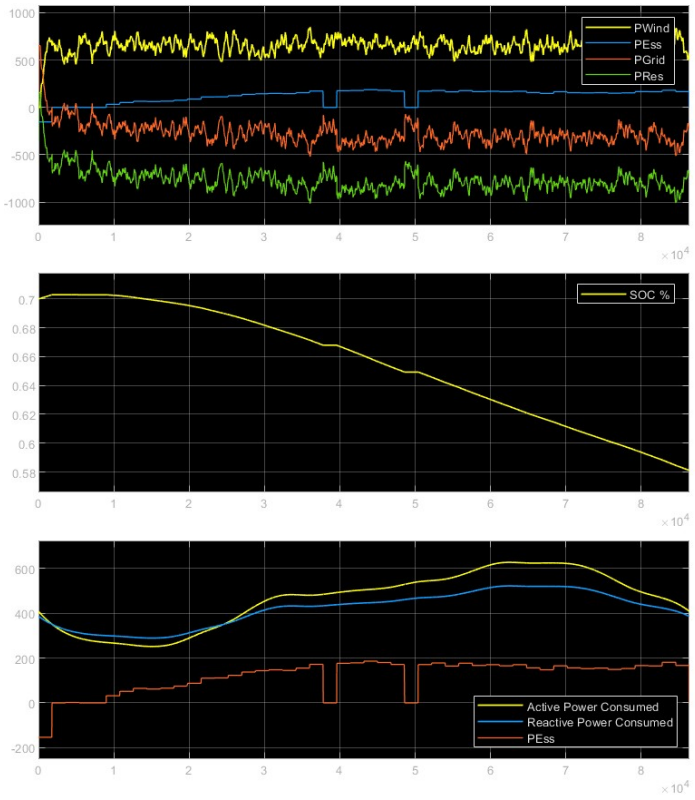


(c) Power flow and load on the grid.

Figure B.18: Plots resulting from the optimization with small angle approximation using measurements on the RES and grid side of the inverter.

# BIBLIOGRAPHY


[1] M. Geidl, G. Koeppel, P. Favre-Perrod, B. Klöckl, G. Andersson, and K.-J. D.-I. Fröhlich, "The energy hub: A powerful concept for future energy systems," *IEEE Power and Energy Magazine*, vol. 5, no. 1, pp. 24–30, 2007. DOI: 10.1109/MPAE.2007.264850.

[2] K. Abnett, "Europe's power industry warns ageing grids risk green goals | reuters," Reuters, Sep. 2023. [Online]. Available: https://www.reuters.com/world/europe/europes-power-industry-warns-ageing-grids-risk-green-goals-2023-09-20/.

[3] P. W. Parfomak, "Energy storage for power grids and electric transportation: A technology assessment," US Congressional Research Service, Mar. 2012. [Online]. Available: https://crsreports.congress.gov/product/pdf/R/R42455.

[4] B. Steman, P. Nieuwesteeg, M. Plantema, and K. Friele, "Verbeteren netinpassing zonne-energieprojecten," HASKONINGDHV NEDERLAND B.V., 2021. [Online]. Available: https://capaciteitskaart.netbeheernederland.nl/.

[5] Forschungszentrum Jülich, "Diverse causes behind frequency fluctuations in power grids," *phys.org*, Jan. 2018. [Online]. Available: https://phys.org/news/2018-01-diverse-frequency-fluctuations-power-grids.html.

[6] FEDERAL MINISTRY FOR ECONOMIC AFFAIRS AND CLIMATE ACTION, "Grids and infrastructure," Die Bundesregierung, 2023. [Online]. Available: https://www.bmwk.de/Redaktion/EN/Artikel/Energy/electricity-grids-of-the-future-01.html.

[7] M. Schülde, X. Veillard, and A. Weiss, "Four themes shaping the future of the stormy european power market," McKinsey & Company, Jan. 2023. [Online]. Available: https://www.mckinsey.com/industries/electric-power-and-natural-gas/our-insights/four-themes-shaping-the-future-of-the-stormy-european-power-market.

[8] enelgreenpower, "Prosumers: When energy consumers become energy producers," *Gigawhat*, Mar. 2023. [Online]. Available: https://www.enelgreenpower.com/learning-hub/gigawhat/search-articles/articles/2023/03/prosumers-energy.

[9] J. H. Eto, R. H. Lasseter, D. Klapp, A. S. Khalsa, B. Schenkman, M. Illindala, and S. Baktiono, "The certs microgrid concept, as demonstrated at the certs/aep microgrid test bed," 2018. [Online]. Available: https://api.semanticscholar.org/CorpusID:173172513.

[10] A. A. Kebede, T. Kalogiannis, J. V. Mierlo, and M. Berecibar, *A comprehensive review of stationary energy storage devices for large scale renewable energy sources grid integration*, May 2022. DOI: 10.1016/j.rser.2022.112213.

[11] R. R. Negenborn, A. G. Beccuti, T. Demiray, S. Leirens, G. Damm, B. D. Schutter, and M. Morari, "Supervisory hybrid model predictive control for voltage stability of power networks," *American Control Conference*, May 2007. DOI: 10.1109/ACC.2007.4282264. [Online]. Available: http://psdyn.ece.wisc.edu/IEEEbenchmarks/.

[12] S.-S. Park, J.-S. Lee, D.-H. Park, and R.-Y. Kim, "Hierarchical structure-based ramp rate control of renewable energy sources for hub-station," in *2021 24th International Conference on Electrical Machines and Systems (ICEMS)*, Hanyang University, Gyeongiu, Korea: IEEE, 2021, pp. 808–811, ISBN: 9788986510218. DOI: 10.23919/ICEMS52562.2021.9634341.

[13] J. Katz, J. Cochran, and M. Miller, "Methods for procuring power system flexibility," National Renewable Energy Laboratory, May 2015.

[14] J. Katz and J. Cochnan, "Integrating variable renewable energy into the grid: Key issues," National Renewable Energy Laboratory, May 2015.

[15] S. S., S. Mekhilef, H. Mokhlis, and M. Karimi, "Mitigating methods of power fluctuation of photovoltaic (pv) sources – a review," *Renewable and Sustainable Energy Reviews*, vol. 59, pp. 1170–1184, 2016, ISSN: 1364-0321. DOI: https://doi.org/10.1016/j.rser.2016.01.059. [Online]. Available: https://www.sciencedirect.com/science/article/pii/S1364032116000897.

[16] P. Denholm, T. Mai, R. W. Kenyon, B. Kroposki, and M. O'Malley, "Inertia and the power grid: A guide without the spin," May 2020. [Online]. Available: https://www.osti.gov/biblio/1659891.

[17] Rijksoverheid, "Offshore wind energy," Rijksoverheid, 2023. [Online]. Available: https://www.government.nl/topics/renewable-energy/offshore-wind-energy.

[18] D. B. Rathnayake, M. Akrami, C. Phurailatpam, S. P. Me, S. Hadavi, G. Jayasinghe, S. Zabihi, and B. Bahrani, "Grid forming inverter modeling, control, and applications," *IEEE Access*, vol. 9, pp. 114 781–114 807, 2021, ISSN: 21693536. DOI: 10.1109/ACCESS.2021.3104617.

[19] A. Johnson, *Grid code frequency response working group system inertia*. [Online]. Available: https://www.nationalgrid.com/sites/default/files/documents/16890-Meeting%208%20-%20Inertia%20presentation.pdf.

[20] J. Xu, T. B. Soeiro, F. Gao, H. Tang, and P. Bauer, "A simplified modulated model predictive control for a grid-tied three-level t-type inverter," in *2020 IEEE 29th International Symposium on Industrial Electronics (ISIE)*, 2020, pp. 618–623. DOI: 10.1109/ISIE45063.2020.9152376.

[21] J. Xu, T. B. Soeiro, F. Gao, L. Chen, H. Tang, P. Bauer, and T. Dragicevic, "Carrier-based modulated model predictive control strategy for three-phase two-level vsis," *IEEE Transactions on Energy Conversion*, vol. 36, pp. 1673–1687, 3 Sep. 2021, ISSN: 15580059. DOI: 10.1109/TEC.2021.3073110.

[22] S. Roy, P. K. Sahu, S. Jena, and A. K. Acharya, "Modeling and control of dc/ac converters for photovoltaic grid-tie micro-inverter application," vol. 39, 2021, pp. 2027–2036. DOI: https://doi.org/10.1016/j.matpr.2020.09.330..

[23] Y. Geng, L. Zhu, X. Song, K. Wang, and X. Li, "A modified droop control for grid-connected inverters with improved stability in the fluctuation of grid frequency and voltage magnitude," *IEEE Access*, vol. 7, pp. 75 658–75 669, 2019. DOI: 10.1109/ACCESS.2019.2920312.

[24] Y. Xue and L. Chang, "Closed-loop spwm control for grid-connected buck-boost inverters," in *2004 IEEE 35th Annual Power Electronics Specialists Conference (IEEE Cat. No.04CH37551)*, vol. 5, 2004, 3366–3371 Vol.5. DOI: 10.1109/PESC.2004.1355070.

[25] Y. Huang, D. Wang, L. Shang, G. Zhu, H. Tang, and Y. Li, "Modeling and stability analysis of dc-link voltage control in multi-vscs with integrated to weak grid," *IEEE Transactions on Energy Conversion*, vol. 32, no. 3, pp. 1127–1138, 2017. DOI: 10.1109/TEC.2017.2700949.

[26] M. J. Erickson and R. H. Lasseter, "Integration of battery energy storage element in a certs microgrid," in *2010 IEEE Energy Conversion Congress and Exposition*, 2010, pp. 2570–2577. DOI: 10.1109/ECCE.2010.5617986.

[27] R. H. Lasseter and P. Piagi, "Control and design of microgrid components," University of Wisconsin, Jan. 2006, p. 257.

[28] E. Muljadi, C. P. Butterfield, R. Yinger, and H. Romanowitz, "Energy storage and reactive power compensator in a large wind farm: Preprint," Jan. 2004. DOI: https://doi.org/10.2514/6.2004-352. [Online]. Available: http://www.osti.gov/bridge.

[29] M. Moritz, T. Heins, S. K. Gurumurthy, M. Joševski, I. Jahn, and A. Monti, "Distributed model predictive frequency control of inverter-based power systems," *IEEE Access*, vol. 12, pp. 53 250–53 265, 2024. DOI: 10.1109/ACCESS.2024.3387369.

[30] T. Tian and I. Chernyakhovskiy, "Forecasting wind and solar generation: Improving system operations," National Renewable Energy Laboratory, Jan. 2016.

[31] P. Denholm and J. Cochran, "Wind and solar on the power grid: Myths and misperceptions," National Renewable Energy Laboratory, May 2015.

[32] W. Hu, Z. Chen, Y. Wang, and Z. Wang, "Wind power fluctuations mitigation by dc-link voltage control of variable speed wind turbines," in *2008 43rd International Universities Power Engineering Conference*, 2008, pp. 1–5. DOI: 10.1109/UPEC.2008.4651600.

[33] G. Kay, N. J. Dunstone, A. Maidens, A. A. Scaife, D. M. Smith, H. E. Thornton, L. Dawkins, and S. E. Belcher, "Variability in north sea wind energy and the potential for prolonged winter wind drought," *Atmospheric Science Letters*, vol. 24, 6 Jun. 2023, ISSN: 1530261X. DOI: 10.1002/asl.1158.

[34] K. A. Rafea, M. Elsholkami, A. Elkamel, and M. Fowler, "Integration of decentralized energy systems with utility-scale energy storage through underground hydrogen-natural gas co-storage using the energy hub approach," *Industrial and Engineering Chemistry Research*, vol. 56, pp. 2310–2330, 8 Mar. 2017, ISSN: 15205045. DOI: 10.1021/acs.iecr.6b02861.

[35] X. Li, D. Hui, and X. Lai, "Battery energy storage station (bess)-based smoothing control of photovoltaic (pv) and wind power generation fluctuations," *IEEE Transactions on Sustainable Energy*, vol. 4, pp. 464–473, 2 2013, ISSN: 19493029. DOI: 10.1109/TSTE.2013.2247428.

[36] C. E. Garcia, D. M. Prett, and M. Morari, "Model predictive control: Theory and practice a survey*," vol. 25, 1989, pp. 335–338. DOI: https://doi.org/10.1016/0005-1098(89)90002-2.

[37] P. D. Christofides, R. Scattolini, D. M. de la Peña, and J. Liu, "Distributed model predictive control: A tutorial review and future research directions," *Computers and Chemical Engineering*, vol. 51, pp. 21–41, Apr. 2013, ISSN: 00981354. DOI: 10.1016/j.compchemeng.2012.05.011.

[38] D. Q. Mayne, J. B. Rawlings, C. V. Rao, and P. O. M. Scokaert, "Constrained model predictive control: Stability and optimality," *Automatica*, vol. 36, pp. 789–814, 6 2000. DOI: https://doi.org/10.1016/S0005-1098(99)00214-9.

[39] C. V. Rao and J. B. Rawlings, "Steady states and constraints in model predictive control," *AIChE Journal*, vol. 45, pp. 1266–1278, 6 1999, ISSN: 00011541. DOI: 10.1002/aic.690450612.

[40] D. Kim and J. E. Braun, "Mpc solution for optimal load shifting for buildings with on/off staged packaged units: Experimental demonstration, and lessons learned, energy and buildings," *Energy and Buildings*, vol. 266, 2022. DOI: https://doi.org/10.1016/j.enbuild.2022.112118..

[41] D. Krishnamoorthy, B. Foss, and S. Skogestad, "Steady-state real-time optimization using transient measurements," *Computers and Chemical Engineering*, vol. 115, pp. 34–45, Jul. 2018, ISSN: 00981354. DOI: 10.1016/j.compchemeng.2018.03.021.

[42] S. Cao and R. R. Rhinehart, "An efficient method for online identification of steady state," 1995, pp. 363–374. DOI: https://doi.org/10.1016/0959-1524(95)00009-F. [Online]. Available: https://www.sciencedirect.com/science/article/pii/095915249500009F.

[43] B. Srinivasan, D. Bonvin, E. Visser, and S. Palanki, "Dynamic optimization of batch processes ii. role of measurements in handling uncertainty," *Computers and Chemical Engineering*, vol. 27, pp. 27–44, 2002, ISSN: 0098-1354. DOI: https://doi.org/10.1016/S0098-1354(02)00117-5.. [Online]. Available: www.elsevier.com/locate/compchemeng.

[44] S. J. Qin and T. A. Badgwell, "A survey of industrial model predictive control technology," 2003, pp. 733–764. DOI: https://doi.org/10.1016/S0967-0661(02)00186-7.

[45] K. A. Pruitt, R. J. Braun, and A. M. Newman, "Evaluating shortfalls in mixed-integer programming approaches for the optimal design and dispatch of distributed generation systems," *Applied Energy*, vol. 102, pp. 386–398, 2013, ISSN: 03062619. DOI: 10.1016/j.apenergy.2012.07.030.

[46] M. Knechtges and A. Moser, "Impact of grid-forming control and the available energy in dc links on the system frequency after a system split," in *2022 IEEE 7th Southern Power Electronics Conference (SPEC)*, 2022, pp. 1–5. DOI: 10.1109/SPEC55080.2022.10058233.

[47] H. Lin, Q. Wang, Y. Wang, Y. Liu, N. Huang, R. Wennersten, and Q. Sun, "A multi-agent based optimization architecture for energy hub operation," *Energy Procedia*, vol. 142, pp. 2158–2164, Dec. 2017. DOI: 10.1016/j.egypro.2017.12.621.

[48] P. Tatjewski, "Advanced control and online process optimization in multilayer structures," *Annual Reviews in Control*, vol. 32, pp. 71–85, 1 Apr. 2008, ISSN: 13675788. DOI: 10.1016/j.arcontrol.2008.03.003.

[49] M. H. Holmes, *Introduction to Perturbation Methods*. Springer, 1995, ISBN: 978-0-387-94203-2.

[50] R. Scattolini, *Architectures for distributed and hierarchical model predictive control - a review*, May 2009. DOI: 10.1016/j.jprocont.2009.02.003.

[51] R. R. Negenborn, S. Leirens, B. D. Schutter, and J. Hellendoorn, "Supervisory nonlinear mpc for emergency voltage control using pattern search," *Control Engineering Practice*, vol. 17, pp. 841–848, 7 Jul. 2009, ISSN: 09670661. DOI: 10.1016/j.conengprac.2009.02.003.

[52] M. Ellis, H. Durand, and P. D. Christofides, "A tutorial review of economic model predictive control methods," *Journal of Process Control*, vol. 24, pp. 1156–1178, 8 2014, ISSN: 0959-1524. DOI: https://doi.org/10.1016/j.jprocont.2014.03.010. [Online]. Available: https://www.sciencedirect.com/science/article/pii/S0959152414000900.

[53] O. Santander, M. Baldea, and T. A. Soderstrom, "Stochastic model predictive control with closed-loop model updating," *Industrial and Engineering Chemistry Research*, Oct. 2023, ISSN: 15205045. DOI: 10.1021/acs.iecr.3c01835.

[54] A. G. Marchetti, A. Ferramosca, and A. H. González, "Steady-state target optimization designs for integrating real-time optimization and model predictive control," *Journal of Process Control*, vol. 24, pp. 129–145, 1 Jan. 2014, ISSN: 09591524. DOI: 10.1016/j.jprocont.2013.11.004.

[55] A. Jamshidnejad, G. Gomes, A. M. Bayen, and B. D. Schutter, "Integrated offline and online optimization-based control in a base-parallel architecture," Jul. 2019. [Online]. Available: http://arxiv.org/abs/1907.05464.

[56] B. Chachuat, B. Srinivasan, and D. Bonvin, "Adaptation strategies for real-time optimization," *Computers and Chemical Engineering*, vol. 33, pp. 1557–1567, 10 Oct. 2009, ISSN: 00981354. DOI: 10.1016/j.compchemeng.2009.04.014.

[57] B. Chachuat, A. Marchetti, and D. Bonvin, "Process optimization via constraints adaptation," *Journal of Process Control*, vol. 18, pp. 244–257, 3-4 Mar. 2008, ISSN: 09591524. DOI: 10.1016/j.jprocont.2007.07.001.

[58] J. Martins, S. Spataru, D. Sera, D. I. Stroe, and A. Lashab, "Comparative study of ramp-rate control algorithms for pv with energy storage systems," *Energies*, vol. 12, 7 2019, ISSN: 19961073. DOI: 10.3390/en12071342.

[59] Y. Zhang and Y. Wei Li, "Energy management strategy for supercapacitor in droop-controlled dc microgrid using virtual impedance," *IEEE Transactions on Power Electronics*, vol. 32, no. 4, pp. 2704–2716, 2017. DOI: 10.1109/TPEL.2016.2571308.

[60] DuneWorks and Netbeheer Nederland, "The end-users as starting point for designing dynamic pricing approaches to change household energy consumption behaviours," 2013. [Online]. Available: https://www.netbeheernederland.nl/sites/default/files/Dynamic_pricing_and_behaviour_change_99.pdf.

[61] P. Veers *et al.*, "Grand challenges in the design, manufacture, and operation of future wind turbine systems." DOI: 10.5194/wes-2022-32. [Online]. Available: https://doi.org/10.5194/wes-2022-32.

[62] J. LeSage, *Microgrid energy management system (ems) using optimization*, 2024. [Online]. Available: https://github.com/jonlesage/Microgrid-EMS-Optimization/releases/tag/v19.1.0.

[63] J. Bendík, "Dataset of 15-minute values of active and reactive power consumption of 1000 households during single year," *Mendeley Data*, vol. 2, 2023. DOI: 10.17632/pns69yxgrp.2.

[64] R. D. Zimmerman and C. E. Murillo-Sanchez, *Matpower (version 8.0) [software]*, 2024. DOI: 10.5281/zenodo.11212330. [Online]. Available: https://matpower.org.

[65] Mathworks, *Renewables: Wind turbine models*, 2024. [Online]. Available: https://nl.mathworks.com/help/sps/renewable-energy-relib.html?s_tid=CRUX_topnav.

[66] T. Gobmaier, "Measurement of the utility frequency," *netzfrequenzmessung.de*, 2023. [Online]. Available: https://www.mainsfrequency.com/frequ_info_en.php.

[67] nano energies, "Frequency regulation," *Knowledge base*, 2023. [Online]. Available: https://nanoenergies.eu/knowledge-base/frequency-regulation.

[68] Rijksoverheid, "Supplying gas or electricity to low-volume users," Rijksoverheid, 2024. [Online]. Available: https://business.gov.nl/regulation/supplying-gas-electricity-low-volume-users/.

[69] I. Collet and A. Englebert, *Archive:coastal regions - population statistics*, 2013. [Online]. Available: https://ec.europa.eu/eurostat/statistics-explained/index.php?title=Archive%3ACoastal_regions_-_population_statistics.

[70] J. Badger *et al.*, *Global wind atlas*, 2013. [Online]. Available: https://globalwindatlas.info/en/.

[71] M. Pierrot, *The wind power - wind energy market intelligence*. [Online]. Available: https://www.thewindpower.net/country_zones_en_10_netherlands.php.

[72] A. Bischi, L. Taccari, E. Martelli, E. Amaldi, G. Manzolini, P. Silva, S. Campanari, and E. Macchi, "A detailed milp optimization model for combined cooling, heat and power system operation planning," *Energy*, vol. 74, pp. 12–26, C 2014, ISSN: 03605442. DOI: 10.1016/j.energy.2014.02.042.

[73] P. Dini, A. Colicelli, and S. Saponara, "Review on modeling and soc/soh estimation of batteries for automotive applications," *Batteries*, vol. 10, no. 1, 2024. DOI: https://doi.org/10.3390/batteries10010034.

[74] P. Mancarella, G. Andersson, J. Peças-Lopes, and K. Bell, "Modelling of integrated multi-energy systems: Drivers, requirements, and opportunities," in *2016 Power Systems Computation Conference (PSCC)*, 2016, pp. 1–22. DOI: 10.1109/PSCC.2016.7541031.

[75] S. McFadyen, *Capacitor theory*, 2013. [Online]. Available: https://myelectrical.com/notes/entryid/221/capacitor-theory.

[76] Museu de Comunicacoes, *Ac networks - phase shift*. [Online]. Available: https://www.cmm.gov.mo/eng/exhibition/secondfloor/moreinfo/2_4_4_PhaseShift.html.

[77] J. R. Torres, *Lecture: Complex power and per unit normalization*, 2023.

[78] B. Srinivasan and D. Bonvin, "Convergence analysis of iterative identification and optimization schemes," in *Proceedings of the 2003 American Control Conference, 2003.*, vol. 3, 2003, 1956–1960 vol.3. DOI: 10.1109/ACC.2003.1243360.

[79] E. F. Camacho and C. Bordons, *Model Predictive Control*, 2nd ed. SpringerLink, 2007, ISBN: 978-1-85233-694-3. DOI: 10.1007/978-0-85729-398-5.

[80] K. R. Muske and J. B. Rawlings, "Model predictive control with linear models," *AIChE Journal*, vol. 39, 2 1993. DOI: https://doi.org/10.1002/aic.690390208.

[81] K. R. Muske and T. A. Badgwell, "Disturbance modeling for offset-free linear model predictive control," *Journal of Process Control*, vol. 12, pp. 617–632, 5 2002, ISSN: 0959-1524. DOI: https://doi.org/10.1016/S0959-1524(01)00051-8. [Online]. Available: www.elsevier.com/locate/jprocont.

[82] M. Ławryńczuk, P. M. Marusak, and P. Tatjewski, "Cooperation of model predictive control with steady-state economic optimisation," *Control and Cybernetics*, vol. 37, 1 Jan. 2008. [Online]. Available: https://www.researchgate.net/publication/228772006.

[83] J. F. Forbes and T. E. Marlin, "Model accuracy for economic optimizing controllers: The bias update case," 1994, pp. 1919–1929. [Online]. Available: https://pubs.acs.org/sharingguidelines.

[84] N. Kakimoto, H. Satoh, S. Takayama, and K. Nakamura, "Ramp-rate control of photovoltaic generator with electric double-layer capacitor," *IEEE Transactions on Energy Conversion*, vol. 24, pp. 465–473, 2 2009, ISSN: 08858969. DOI: 10.1109/TEC.2008.2001580.

[85] OE Digital. "'missing link' - thermoplastic composite pipes could transport hydrogen from offshore wind turbines." (2021), [Online]. Available: https://www.oedigital.com/news/492615-missing-link-thermoplastic-composite-pipes-could-transport-hydrogen-from-offshore-wind-turbines (visited on 05/29/2024).

[86] VDL Energy Systems. "Hydrogen solutions." (2023), [Online]. Available: https://www.vdlenergysystems.com/hydrogen (visited on 05/29/2024).

[87] J. N. Libii, "Comparing the calculated coefficients of performance of a class of wind turbines that produce power between 330 kw and 7,500 kw," *World Transactions on Engineering and Technology Education*, vol. 11, pp. 36–40, 1 Jan. 2013. [Online]. Available: https://www.researchgate.net/publication/289972454_Comparing_the_calculated_coefficients_of_performance_of_a_class_of_wind_turbines_that_produce_power_between_330_kw_and_7500_kw.

[88] L. Bauer and S. Matysik, "Enercon e-126 7.580," 2015. [Online]. Available: https://en.wind-turbine-models.com/turbines/14-enercon-e-126-7.580#:~:text=The%20rated%20power%20of%20Enercon,7.580%20is%20127%2C0%20m..

[89] M. Sharafi and T. Y. ELMekkawy, "Multi-objective optimal design of hybrid renewable energy systems using pso-simulation based approach," *Renewable Energy*, vol. 68, pp. 67–79, Aug. 2014, ISSN: 09601481. DOI: 10.1016/j.renene.2014.01.011.

[90] F. Linde, "Parametric modeling of a super-capacitor [unpublished manuscript]," M.S. thesis, University of Twente, 2023.

[91] A. Suárez-García, V. Alfonsín, S. Urréjola, and Á. Sánchez, "Optimal parametrization of electrodynamical battery model using model selection criteria," *Journal of Power Sources*, vol. 285, pp. 119–130, Jul. 2015, ISSN: 03787753. DOI: 10.1016/j.jpowsour.2015.03.076.

[92] S. Liu, A. Forsyth, and R. Todd, "Battery loss modelling using equivalent circuits," in *2019 IEEE Energy Conversion Congress and Exposition (ECCE)*, 2019, pp. 2478–2484. DOI: 10.1109/ECCE.2019.8912542.

[93] M. Schimpe, M. Naumann, N. Truong, H. C. Hesse, S. Santhanagopalan, A. Saxon, and A. Jossen, "Energy efficiency evaluation of a stationary lithium-ion battery container storage system via electro-thermal modeling and detailed component analysis," *Applied Energy*, vol. 210, pp. 211–229, Jan. 2018, ISSN: 03062619. DOI: 10.1016/j.apenergy.2017.10.129.

[94] S. Farhad and A. Nazari, "Introducing the energy efficiency map of lithium-ion batteries," *International Journal of Energy Research*, vol. 43, pp. 931–944, 2 Feb. 2019, ISSN: 1099114X. DOI: 10.1002/er.4332.

[95] M. Mussi, L. Pellegrino, M. Restelli, and F. Trovò, "A voltage dynamic-based state of charge estimation method for batteries storage systems," *Journal of Energy Storage*, vol. 44, Dec. 2021, ISSN: 2352152X. DOI: 10.1016/j.est.2021.103309.

[96] J. S. Jago, "Modeling of pv penetration in residential neighborhoods on aruba," 2013. [Online]. Available: http://resolver.tudelft.nl/uuid:748675f3-58ee-4d87-9acf-6dcb21d36908.